Telomere-Dependent Interleukin-1 Receptor Activation Promotes Immune Suppression in Triple-Negative-Breast Cancer

Ananda Kishore Mukherjee[1,2], Ankita Singh[1], Shalu Sharma[1,2], Shuvra Shekhar Roy[1,2], Antara Sengupta[1,2], Subhajit Dutta[1,2], Soujanya Vinayagamurthy[1,2], Sulochana Bagri[1,2], Divya Khanna[1], Megha Chatterjee[1], Meenakshi Verma[1], Dristhi Soni[1,2], Anshul Budharaja[3], Sagar Kailasrao Bhisade[4], Vivekanand[6], Ahmad Perwez[1], Mohammed Faruq[5,6], Ishaan Gupta[3,4], Shantanu Chowdhury[1,2,5,7*]

[1]Integrative and Functional Biology Unit, CSIR-Institute of Genomics and Integrative Biology, New Delhi 110026, India

[2]Academy of Scientific and Innovative Research (AcSIR), Ghaziabad 201002, India

[3]IIT Delhi, Hauz Khas, Delhi

[4]IISER Bhopal, Bhauri, Bhopal

[5]GNR Knowledge Centre for Genome and Informatics, CSIR-Institute of Genomics and Integrative Biology, New Delhi 110026, India

[6] Genomics and molecular medicine, CSIR-Institute of Genomics and Integrative Biology, New Delhi 110026, India

[7]Lead contact *Correspondence: shantanuc@igib.in

Abstract

The role of telomeres in sustained tumor growth is well understood. However, mechanisms of how telomeres might impact the tumor microenvironment (TME) are not clear. Upon examining tumor associated macrophages (TAMs) in 94 hormone-negative (triple-negative) breast cancer (TNBC) cases we found infiltration of TAMs to be telomere sensitive: Tumors with relatively short telomeres had higher abundance of TAM and vice versa. This observation was replicated across TNBC clinical tissue, patient-derived organoids, tumor xenografts and cancer cells with long/short telomeres. Mechanistically, we demonstrate that non-telomeric binding of TRF2, a telomere-repeat-binding-factor; at the interleukin receptor *IL1R1* promoter directly activates *IL1R1* through recruitment of the histone-acetyl-transferase p300 and consequent H3K27 acetylation. Interleukin-1signaling could be induced in TRF2-high cells through ligands IL1A/B, but not TNFα, and abrogated by the receptor antagonist IL1RA, supporting specificity of the TRF2-IL1R1axis. TRF2 binding at the *IL1R1* promoter was mediated by G-quadruplex motifs and was sensitive to telomere length – thereby establishing telomere-length-dependent regulation of *IL1R1* and IL1-mediated TAM infiltration in cancers. Our results reveal a heretofore unknown function of telomeres in interleukin signaling and anti- tumor immune response, through non-telomeric TRF2. Therefore, we propose telomere length as a novel biomarker underlying patient-specific response to cancer immunotherapy.

Introduction

Shortening of telomeres with ageing contributes to compromised immune response (Goronzy et al., 2006; Hodes et al., 2002; Pawelec et al., 2014; Sansoni et al., 2008; Weng, 2012). However, although the role of telomeres in cancer stands well-established as a hallmark (Aviv et al., 2017; Hanahan and Weinberg, 2000), whether and how telomeres influence immune response in cancer is poorly understood.

Immune response to tumor cells assist in cancer prognosis and intervention (Chew et al., 2012; Hanahan and Weinberg, 2011; Wang et al., 2017). Major advances in understanding show how infiltration of immune cells including tumor-infiltrating-lymphocytes (TIL), tumor-associated-macrophages (TAM), natural-killer and dendritic cells impact tumor progression (Fares et al., 2019; H et al., 2018; Wang et al., 2017). TAMs - typically M2 macrophage-like - play a dominant role in promoting immune-suppressive tumor-microenvironment (TME) through the secretion of anti-inflammatory cytokines like IL4 and IL13 (Burkholder et al., 2014) (H et al., 2018) (Cassetta et al., 2016; SD et al., 2020). Poor prognosis in triple-negative-breast cancers (TNBC) has been frequently associated with TAMs. Multiple reports show TAMs, predominantly M2-like, to be the most abundant monocytic immune cells in TNBC and implicate their role in invasiveness and aggressive tumor growth (Jeong et al., 2019; Medrek et al., 2012; Oner et al., 2020) (Burkholder et al., 2014; Mantovani and Locati, 2013; Shun et al., 2005; Yuan et al., 2014)

However, the mechanistic role of telomeres in cancer cells influence TAM remains poorly studied. Two observations point towards a potential role, First, the differential expression of immunity-related genes was noted depending on telomere length (Hirashima et al., 2013a) (Lopez-Doriga et al., 2018). Second, telomerase (the key enzyme responsible for telomere maintenance) and ALT (alternative lengthening of telomeres) were found to influence TAM markers like CD163 in glioblastoma (Hung et al., 2016) suggesting potential molecular links between immune-suppressive TAMs and cancer-cell telomeres.

Recently we showed telomeres influence expression of genes remote from telomeres and spread across the genome (Mukherjee et al., 2018). This was through the non-telomeric binding of TRF2 in gene promoters in a fashion that depended on telomere length. That is, relatively long telomeres sequestered more TRF2 limiting non-telomeric binding and vice-versa called the telomere-sequestration-partition (TSP) model (Vinayagamurthy et al., 2020); independent of the

telomere-positioning-effect (TPE) known to alter expression of sub-telomeric genes (up to 10 Mb; (Robin et al., 2014). Analysis of transcriptomes from 31 cancer types revealed a large number of 'telomere-sensitive' genes distributed far from telomeres throughout the genome (Barthel et al., 2017a), consistent with the TSP model. Interestingly, among the top 500 genes that altered with telomere elongation the predominant category was immune response; on further analysis of this we noted 'macrophage inhibitory factor'-genes to be most enriched among the telomere-length-sensitive genes (Supplementary Figure 1A).

Here, with these in mind, we investigated how telomere length might influence TAM in TNBC. Results show about a third of the TNBC tumors we studied had relatively long telomeres (>6 kb in 32 out of 94 cases) and lower TAM compared to tumors with shorter telomeres (<3.5 kb in 38 cases). This is supported by experiments using TNBC-patient-derived organoids, mouse-xenografts and cancer cells. Mechanistically, we show that non-telomeric binding of TRF2 directly activates the Interleukin-1-receptor IL1R1 in a telomere-sensitive way in cancer cells. Resulting activation of IL-1 signaling, through NFKappaB (p65)-phosphorylation, was causal for TAM abundance within the TME. Together these implicate telomere-dependent immunosuppression in TNBC.

Results

Tumors with longer telomeres have reduced immune-suppressive macrophage

We initially analyzed telomere length of 94 TNBC tumor tissue samples (Supplementary Table 1) using a reported qRT-PCR based assay (Cawthon, 2002; O'Callaghan et al., 2008). For reference previously characterized telomere length of HT1080 cells (~4.5 kb) was used (Cristofari and Lingner, 2006; Kahl et al., 2020; Mukherjee et al., 2018). Median telomere length of the 94 TNBC tumors was ~4 kb (0.73-fold of HT1080 cells); tumors with telomeres <50% of the median were designated as TNBC with short telomeres (TNBC-ST) and once with >50% of the median length (as TNBC with long telomeres (TNBC-LT) for this study (Supplementary Figure 1B).

Nine TNBC-ST and nine TNBC-LT tumors were selected and telomere lengths confirmed using flow-cytometry (FACS) with labeled telomeric PNA probes as reported earlier (Baerlocher et al., 2002; Mukherjee et al., 2018). As expected, the mean telomere length of TNBC-LT was significantly higher than TNBC-ST tumors (Figure 1A); the RNA template of telomerase (*TERC*),

but not the catalytic human telomerase subunit (*hTERT*), was significantly higher in TNBC-LT (Supplementary Figure 1C). We screened the 18 TNBC (ST and LT) tumor samples for M2-type tumor-infiltrating macrophages (TAMs) by analyzing the relative proportions of cells expressing well-established markers CD11b (monocyte-derived cells) and CD206 (M2-specific TAMs) using FACS as reported earlier ((Cassetta et al., 2016; Cho et al., 2018; Jaynes et al., 2020). TNBC with relatively long telomeres had lower TAM (TNBC-LT: mean 1.78%, range: 0.18 – 5.41%; TNBC-ST: mean 7.34%, range: 3.76-16.80%; Figure 1B). Consistent with this key TAM marker *CD206* expression was relatively reduced in TNBC-LT compared to TNBC-ST tumors (Supplementary Figure 1D).

Tumor organoids were made from five TNBC-ST and five TNBC-LT clinical tissue; designated as triple-negative-breast-organoid TNBO-ST and TNBO-LT for short or long telomeres respectively. First, following organoid formation the telomere length in each case was quantified by FACS confirming relatively long telomeres in TNBO-LT than TNBO-ST (Figure 1C); both *hTERT* and *TERC* was higher in organoids with longer telomeres (Supplementary Figure 1E). To test TAM infiltration vis-à-vis telomere length in the organoids we derived M2-type macrophages from THP1 cells (Methods; confirmed by CD206 (specific marker for M2-type macrophage; Supplementary Figure 1F) that were labeled with a red-tracker dye (Methods) before co-incubating with each of the five TNBO-ST or five TNBO-LT. Infiltration of M2 macrophage within organoids following 12 hours of incubation was quantified by FACS. TNBO-ST had on average 8.56% infiltration (range: 6.54-10.9%) whereas in case of TNBO-LT this was 3.14% (range: 0.99-4.88%). Together this demonstrates that infiltration of TAM was significantly reduced in case of tumors with relatively long telomeres (Figure 1D).

Further we sought to study tumor xenografts in NOD-SCID mice for TAM infiltration (based on earlier reports that used NOD-SCID mice to study xenograft TAM (Chittezhath et al., 2014a; Li et al., 2020)) using cancer cells with either long or short telomeres. We resorted to previously reported and well-characterized cancer cells with short/long telomeres in cell-isogenic backgrounds: fibrosarcoma HT1080 and its corresponding long-telomere HT1080-LT cells (made by induced expression of *hTERT* and *TERC* RNA) with ~2 to 2.5-fold increase in mean telomere length ((Cristofari and Lingner, 2006); Supplementary Figure 1G, Supplementary Figure 1H).

Xenograft tumors were grown and extracted from five mice for each case HT1080 or HT1080-LT cells and telomere length assessed independently. HT1080-LT had significantly higher

proportion of cells with relatively long telomeres compared to HT1080 derived xenograft tumors (Figure 1E); both *hTERT* and *TERC* were higher in the HT1080-LT tumors (Supplementary Figure 1I). CD11b+CD206+ cells were analyzed to quantify TAM infiltration in the tumor xenografts. For HT1080 we observed 5.21% TAM infiltration whereas this decreased to 1.67% in case of xenografts from HT1080-LT cells (Figure 1F). Consistent with this, expression of TAM-specific markers *CD163* and *CD206* were relatively low in LT xenografts (Supplementary Figure 1J); F4/80^{+} cells representing the total macrophage lineage in mice (Cassetta et al., 2016) did not change significantly in long vs short-telomere xenografts, Supplementary Figure 1K). Together these showed the TAM infiltration was significantly reduced in long vis-à-vis short telomeres, consistent with our observations from clinical tissue and organoids.

Telomere-dependent interleukin-1 signaling impacts immune-suppressive TAM in tumors

To understand altered TAM in short/long telomeres we checked key cytokines implicated in breast cancer TAM such as IL1 and associated receptors (Chittezhath et al., 2014b; Elliott and Sutterwala, 2016; Vasilyev et al., 2015; Yuan et al., 2014); pro-inflammatory cytokines: *IL2, IL6, IL8* and *TNF* (Kovaleva et al., 2016; Yuan et al., 2014); and, anti-inflammatory cytokines *IL10, IL4 and* IL13 (Kaplanov et al., 2019; Medrek et al., 2012).

Pro-inflammatory cytokines *IL2, IL6, IL8* remained largely unaltered in clinical tissue/organoid/xenografts except *TNF-*α (relatively enhanced in TNBC-LT, reduced in organoids TNBO-LT, and did not alter significantly in the xenografts (Supplementary Figure 1L)). Although anti-inflammatory cytokines *IL10, IL4* and IL13 were not consistent across clinical tissue/organoids/xenografts, we noted at least one of the three cytokines was reduced in long compared to short telomere cases, supporting relatively low anti-inflammatory M2-type macrophages in long-telomere cancers (Supplementary Figure 1L).

IL1B and *IL1R1* levels, on the other hand, were significantly low in case of cancers with relatively long telomeres. Notably, this was consistent across clinical tissue, organoids and xenografts (Supplementary Figure 1L). Consistent with this IL1R1 levels, quantified by FACS from each of the five HT1080/HT1080-LT xenograft tumors independently, was lower in LT xenografts (Supplementary Figure 1M); *IL1A* was relatively high in TNBC-LT than ST, but did not change in organoids/xenografts (Supplementary Figure 1L).

To test altered IL1 signaling in long vis-à-vis short telomere TNBC we used organoids. Secreted IL1B (measured using ELISA) in the supernatant media was significantly low in TNBO-LT compared to TNBO-ST (Figure 1G). This was consistent with relatively reduced IL1R1 levels in TNBO-LT than TNBO-ST (Supplementary Figure 1L) supporting reports showing that IL1B secretion was dependent on IL1R1 levels in the tumor cells (Lappano et al., 2020) .

The IL1R1 receptor antagonist IL1RA was used to directly asses the role of IL1R1/IL1B on macrophage infiltration in the TNBC organoids. Labeled M2-type macrophages (described above) when co-incubated with organoids in presence of the IL1RA (Methods) resulted in >50% reduction in macrophage infiltration (independently in both TNBO-ST/LT (Figure 1H)). Accordingly, analysis of IL1 signaling and TAM-specific markers using publicly transcriptomes from 817 TNBC patients (G et al., 2015) showed positive correlation: cancers with low/high expression of both *IL1R1* and *IL1B* also had low/high expression of TAM-specific markers *CD163* and *CD206* respectively (Supplementary Figure 1N). Together these demonstrate that attenuated IL1 signaling due to relatively low IL1R1 levels result in low M2-type macrophage in TNBC with long vis-à-vis short telomeres.

Non-telomeric TRF2 binding at the IL1 receptor R1 promoter is telomere-dependent

We focused on understanding whether and how telomeres might affect IL1 signaling using the well-characterized short/long-telomere cancer cells: HT1080 or the corresponding long-telomere HT1080-LT cells (Cristofari and Lingner, 2006; Mukherjee et al., 2018). The expression of *IL1R1* and pro-inflammatory cytokines like *IL6* and *IL8* was found to be relatively low in HT0180 cells with longer telomeres (Supplementary Figure 2A).

Of note are three recent findings by us: First, non-telomeric binding of the telomere-repeat-binding-factor (TRF2) was sensitive to the telomere length of cancer cells. Second, this resulted in telomere-sensitive expression of genes that were located remote from telomeres (Mukherjee et al., 2018). And, third, TRF2 ChIP-seq (chromatin immunoprecipitation-sequencing) in HT1080 cells revealed bound TRF2 in promoters throughout the genome (Mukherjee et al., 2019a). Extending our previous findings, in the current study we found that TRF2 ChIP-seq reads were enriched ~200 bp upstream of TSS (transcription start site) on the *IL1R1* promoter (Supplementary Figure 2B). TRF2 ChIP followed by qPCR spanning +200 to -1000 bp of the *IL1R1* promoter confirmed TRF2 binding in vivo in HT1080 xenograft tumors (independently in

five tumors; Figure 2A) and HT1080 cells (Figure 2A). Telomeric occupancy of TRF2 was used as a positive control; IL1R1 3'UTR and a region 20 KB upstream of TSS were used as negative controls for ChIP.

Next, we asked if TRF2 binding at the *IL1R1* promoter was dependent on the telomere length. TRF2-ChIP using cells obtained from xenograft tumors in mouse with either HT1080-LT or HT1080 cells (three in each case) revealed TRF2 occupancy on the *IL1R1* promoter was significantly reduced in the proximal promoter (-200 to -400 bp) in HT1080-LT relative to HT1080 xenografts (Figure 2A); +/-controls used as described above (Figure 2B, Supplementary Figure 2C). ChIP using HT1080 and HT1080-LT cells supported this: cells with relatively long telomeres had reduced TRF2 occupancy at the *IL1R1* promoter (Figure 2B, Supplementary Figure 2D).

IL1R1 was significantly reduced in HT1080-LT relative to HT1080 cells (western blot, FACS and IF; Figure 2C-E). Consistent with this, both expression and secretion of IL1B was relatively low in HT1080-LT compared to HT1080 cells (Figure 2F).

To further test telomere length-dependent TRF2 occupancy at the *IL1R1* promoter in a isogenic controlled background, we used *hTERT*-inducible HT1080 cells (Methods) to gradually increase telomere length by ~50% over 12 days (induction saturates beyond 12 days (Figure 2G, Supplementary Figure 2E-F). TRF2 occupancy at the *IL1R1* promoter gradually reduced over 12 days following *hTERT* induction with corresponding increase in telomere length (Figure 2H); telomeric occupancy of TRF2 shown positive control (Supplementary Figure 2G). Further in these cells *IL1R1* expression gradually decreased with telomere elongation over 12 days (Figure 2I) consistent with our observation in HT1080/HT1080-LT cells (Figure 2A-C). *IL1R1* promoter TRF2 occupancy remained unaltered following day-1 of induction indicating this to be independent of hTERT expression.

For orthogonal confirmation, an alternative telomere elongation model was made from triple-negative MDAMB-231 breast cancer cells using G-rich-telomere-repeat (GTR) oligonucleotides based on earlier reports (Methods; (Mukherjee et al., 2018; Wright et al., 1996)). This resulted in MDAMB-231 cells with ~1.8-2-fold increase in telomere length (Supplementary Figure 2H) henceforth called MDAMB-231-LT (long telomere) cells. TRF2 occupancy at the *IL1R1* promoter (Figure 2J, Supplementary Figure 2I); *IL1R1* expression (Figure 2K); and, secreted IL1B was significantly reduced (Supplementary Figure 2J) in cells with relatively long telomeres.

TRF2 transcriptionally activates IL1R1 through direct promoter binding

We sought to directly test the role of TRF2 in *IL1R1* regulation. TRF2 induction (by Flag-TRF2 or doxycycline (dox) treatment of dox-inducible-TRF2 cells) showed distinct increase in *IL1R1* mRNA and protein expression (quantified by FACS); while TRF2 silencing reduced *IL1R1* in HT1080 cells (Figure 3A-E, Supplementary Figure 3A-B). Further, HT1080 cells co-stained with the surface marker CD44 showed that the elevated levels of the IL1R1 receptor in TRF2-high cells migrated, as expected, to the cell surface (Figure 3D).

IL1R1 promoter activity was induced/repressed on TRF2 expression/silencing respectively (luciferase reporter with -1500 bp TSS of *IL1R1* was used (Methods); Figure 3F-G). Flag-TRF2 full length, or without the B domain (delB), or M-domain (delM) necessary for DNA binding (Baker et al., 2009; Bilaud et al., 1997; Mukherjee et al., 2019a; Pedroso et al., 2009; Purohit et al., 2018) showed occupancy of the TRF2 DNA binding mutants was compromised at the *IL1R1* promoter (Figure 3H and Supplementary Figure 3C); consistent with this *IL1R1* promoter activity was markedly reduced in case of the TRF2 delB or delM mutants relative to full-length TRF2 (Figure 3I). Therefore, we can conclude that TRF2 directly binds to the promoter of *IL1R1* and activates *IL1R1* transcription.

TRF2-mediated activation of *IL1R1* was further tested in MDAMB-231 breast cancer (Supplementary Figure 3E-G) and normal MRC5 fibroblasts and HEK293T cells: in all the cell types TRF2 occupancy on the *IL1R1* promoter (Supplementary Figure 3H) as well as TRF2-mediated upregulation of *IL1R1* was clearly evident (Supplementary Figure 3I).

G-quadruplex secondary DNA structure necessary for TRF2 binding to the IL1R1 promoter

We recently reported TRF2 association with promoter G-quadruplex (G4) structures throughout the genome, including the *hTERT* promoter where *hTERT* regulation was directly dependent on TRF2-G4 interaction (Mukherjee et al., 2019a; Shalu Sharma et al., 2021). Therefore, on noting two potential G4 motifs within the TRF2-binding region of the *IL1R1* promoter (Supplementary Figure 3J) we further investigated this. Circular dichroism (CD) experiments confirmed the promoter G4s adopted parallel motifs (+peak ~260 nm, -peak ~240 nm; Figure 3J); and, when

two guanine nucleotides in the G4-stem regions necessary for G4 stability were modified (G>T) the G4-specific CD signatures were substantially reduced (Figure 3J) supporting the formation of stable G4s in solution. ChIP using the BG4 antibody (reported for binding to intracellular G4s (Biffi et al., 2013; Hänsel-Hertsch et al., 2016) showed BG4 enrichment was maximum ~200 bp upstream of TSS on the *IL1R1* promoter (Figure 3K). We next made the G>T substitutions that destabilized the G4s within the luciferase reporter (Supplementary Figure 3K) and found that the TRF2-dependent *IL1R1* promoter activity was compromised in case of both G>T modifications (Figure 3L). Further, based on above we reasoned TRF2-G4 dependent transcription of *IL1R1* would be sensitive to the well-established intracellular G4-binding ligand 360A (Granotier et al., 2005). TRF2-mediated induction of IL1R1 promoter activity, expression and protein levels were significantly reduced in presence of 360A (Figure 3M-O and Supplementary Figure 3L).

To test this further we artificially inserted a *IL1R1* luciferase reporter cassette (comprising -1500 bp upstream of the TSS) at the CCR5 safe-harbor locus in HEK293T cells using CRISPR (Methods). TRF2 binding at the inserted promoter and TRF2-dependent induction of promoter activity from the artificially inserted *IL1R1* promoter-reporter was clearly observed (Figure 3P-Q). To test the dependence of TRF2 binding and TRF2-mediated regulation on promoter G4 we engineered the G>T base substitutions that destabilize the G4s within the inserted promoter cassette. Both, TRF2-dependent *IL1R1* promoter activity (Figure 3Q) and TRF2 occupancy at the inserted promoter was reduced in case of the substitutions; whereas, as expected, telomeric TRF2 occupancy remained unchanged (Figure 3R). Together, these support the role of promoter G4 in regulation of *IL1R1* by TRF2.

TRF2 enhances enrichment of H3K27ac and the histone acetyl transferase p300 on the *IL1R1* promoter

To mechanistically understand TRF2-mediated transcription we screened activation (H3K4me3 and H3K27ac) and repressive (H3K27me3, H3K9me3) histone marks at the *IL1R1* promoter on induction of TRF2 (using TRF2-inducible HT1080 cells; Methods). Interestingly the H3K27ac mark was notably enhanced (Supplementary Figure 4A). Therefore, we checked the H3K27ac mark on the *IL1R1* promoter in TRF2 upregulated or silenced conditions in HT1080 and MDAMB-231 cells. In case of both the cell types H3K27ac mark on the *IL1R1* promoter increased or was reduced on TRF2 expression or silencing, respectively (Figure 4A).

Since our findings suggested the role of TRF2 in activation of *IL1R1* through enhanced histone H3K27 acetylation at the *IL1R1* promoter we looked for a potential histone acetyl transferase (HAT). Preliminary ENCODE analysis showed that the canonical HATs p300/CBP (Roth et al., 2003) were enriched on the *IL1R1* promoter in multiple cell lines (Supplementary Figure 4B). We found enriched p300 occupancy within the 200-400 bp upstream promoter of *IL1R1* in TRF2-up conditions, which was markedly reduced when TRF2 was down regulated, in both HT1080 and MDAMB-231 cells (Figure 4B). Furthermore, occupancy of CBP and acetylated-p300/CBP (activated HAT state) was enriched at the *IL1R1* promoter in TRF2 induced conditions in HT1080 cells (Figure 4C-D). Together these showed the role of TRF2 directly or indirectly in recruitment and acetylation of p300/CBP, resulting in enriched H3K27 acetylation at the *IL1R1* promoter.

Moreover, TRF2 and p300 were reported to physically associate at the telomeres (YR and IK, 2013). Here we performed TRF2-pulldown (co-IP) and found that p300-TRF2 association (Figure 4E) and TRF2-mediated stabilization of p300 in HT1080 cells was evident (Supplementary Figure 4C-D); TRF1 was used as positive control for the co-IP experiment. Cycloheximide-mediated translational block in HT1080 cells showed that p300 levels in TRF2 induced cells was higher and this was independent of the protein degradation machinery (Supplementary Figure 4 D).

p300, CBP, ac-p300/CBP and H3K27ac was relatively reduced on the *IL1R1* promoter in HT1080-LT compared to HT1080 cells with shorter telomeres (Figure 4 F) consistent with lower TRF2 occupancy at the *IL1R1* promoter in LT cells shown earlier (Figure 2E-F). Interestingly, while p300 occupancy was reduced at the *IL1R1* promoter we noted relatively more p300 levels in HT1080-LT cells (Supplementary Figure 4 E-F). This further supported the role of TRF2 in recruitment of p300 to the *IL1R1* promoter.

To investigate any direct role of TRF2 in p300 recruitment we screened Flag-TRF2 mutants (K176R, K179R and K190R deficient in TRF2 interaction with cofactors, and K293R required for TRF2 acetylation (Diala et al., 2013; Huda et al., 2009; Mitchell and Zhu, 2014; Mitchell et al., 2009; YR and IK, 2013) for altered induction of *IL1R1* (Supplementary Figure 4G-I). Induction of TRF2-K293R showed notably compromised activation of *IL1R1* (Figure 4G) and significantly reduced p300 and ac-p300/CBP recruitment on the *IL1R1* promoter in HT1080 cells (Figure 4H). However, binding of the TRF2-K293R at the *IL1R1* promoter remained similar to wild-type TRF2 suggesting that the impaired activity was due to reduced p300 recruitment in presence of

TRF2-K293R(Figure 4H). This was further ascertained by vitro histone-acetyl-transfer assays using purified p300, histone H3 and acetyl-coA (substrate for the acetyl group) with or without recombinant TRF2. Transfer of the acetyl group to histone H3 was enhanced in presence of TRF2 relative to p300 only (Figure 4I). Together, these support direct role of TRF2 in recruitment and HAT activity of p300 resulting in H3K27 acetylation at the *IL1R1* promoter.

Cancer cells with higher TRF2 are sensitive to IL1 mediated p65 (NFKappaB) activation

Primarily ligands IL1A/B via receptors IL1R1/R2 induce IL1 signaling through NFKappaB (p65/RELA)-Ser536 phosphorylation. This, in turn, induces expression of *IL1B* - the ligand that activates IL1 signaling - along with other inflammatory genes including *IL6, IL8, TNFα* (Figure 5A; (A et al., 2010; K and K, 1994; Liu et al., 2017). In addition, p65-Ser536 phosphorylation can be induced through the TNFα receptor in a IL1-independent pathway (Akiyama et al., 2003) (Figure 5A).

To test TRF2 function in IL1 signaling, we first checked for p65-Ser536 phosphorylation up to 12 hrs following stimulation with IL1A/B in presence/absence of TRF2 in HT1080. TRF2-induced cells had relatively enhanced p65-Ser536 phosphorylation that sustained over a longer duration compared to uninduced cells, whereas p65 levels remained relatively unaltered (Figure 5B); this was further supported by similar increase in phosphorylated I-KappaB, which is necessary for p65-Ser536 phosphorylation (Teo et al., 2010a). Similarly, in MDAMB231 cells also we found TRF2 induction resulted in enhanced and sustained p65-Ser536 phosphorylation relative to uninduced cells (Figure 5C).

We reasoned that in cells with longer telomeres IL1 signaling would be affected due to low TRF2 binding at *IL1R1* promoter, and resultant reduced potential of TRF2-mediated activation of *IL1R1*. In case of HT1080-LT cells p65-Ser536 phosphorylation, following IL1B-mediated stimulation, showed a notably delayed response (detectable with 30 min, versus 3 hr, in HT10180 and HT1080-LT, respectively; Figure 5D). This was consistent with reduced expression of p65 targets *IL6, IL8, TNFα* and *IL1B* (Supplementary Figure 2A), and lower secretion of IL1B in HT1080-LT cells relative to HT1080 cells (Figure 2F).

Next, we checked for p65 activation by IL1A, IL1B or TNFα on TRF2 downregulation. While TRF2 silencing affected IL1A or IL1B-mediated p65 activation as observed from p65-Ser536

phosphorylation, TNFα-mediated activation remained relatively unaffected (Supplementary Figure 5A). Consistent with this in cells with TRF2 silencing the p65 targets *IL6, IL8* and *TNFα* were relatively reduced in response to IL1A or IL1B stimulation, but not TNFα, supporting the role of TRF2 in IL1-depenent signaling specifically (Figure 5E).

To test specificity, we further investigated the role of the receptor IL1R1 in TRF2-mediated activation of p65. Reasoning that the receptor antagonist IL1RA would impede signaling through IL1R1, but not the TNF receptor, TRF2-high HT1080 cells were stimulated with either IL1A or IL1B in presence/absence of IL1RA. IL1A or IL1B-mediated activation of *IL6, IL8* and *TNF* in TRF2-high condition was rescued in presence of IL1RA, but not in case of TNFα treatment (Figure 5F). Furthermore, on administering different doses (5, 10 or 20 ng/ml) of IL1RA, expression of *IL6, IL8,* and *TNFα* were repressed in a dose-dependent way (Supplementary Figure 5B). As expected from induced IL1 signaling, secreted IL1B was enhanced in HT1080 with relatively high TRF2 (Supplementary Figure 5C). Together, these demonstrate the direct role of TRF2 in upregulation of *IL1R1* and induction of IL1 signaling, resulting in increased secretion of IL1B.

TRF2 mediated IL1R1 activation is important for TAM infiltration in cancer cells

Enhanced IL1 signaling was reported to induce infiltration of M2-type macrophage in breast and other cancers (Chittezhath et al., 2014b; Oner et al., 2020). Here, because of TRF2-mediated induction of IL1 signaling we asked if TRF2 affected TAM infiltration in tumor cells. HT1080 cells with doxycycline-inducible-TRF2 were used to make tumor xenografts in NOD-SCID mice. Intra-tumor TRF2 was stimulated by oral administration of doxycycline when tumors were ~100 mm^3 in size on average (Methods). After three weeks tumors were retrieved, TRF2 induction and consequently elevated IL1R1 in each of the five doxycycline-treated (TRF2-induced) xenograft tumors was confirmed by FACS (Figure 6A-B) and mRNA expression (Supplementary Figure 6A), relative to the five uninduced tumors.

TAM ($CD11b^{high}CD206^{high}$) was enhanced from ~5% to ~10% in TRF2-induced xenografts (Figure 6C). Accordingly, expression of TAM markers (CD163 and CD206; Supplementary Figure 6B) and p65 targets *IL1B* and *TNFα* were enhanced in TRF2-induced tumors relative to the uninduced condition supporting activated IL1 signaling; however, IL6 decreased and IL8 levels remained unchanged (Figure 6D). Pro-inflammatory markers that were checked showed

lower *IL6* but higher *IL1B* and *TNF* in TRF2 induced tumors while the anti-inflammatory marker *IL13* was found to be higher (Figure 6D).

We further reasoned that the increase in M2-type macrophage would result in higher invasion potential of cells based on earlier work (Hu et al., 2015; M et al., 2016). An in-vitro co-culture assay to test this showed HT1080 cells with relatively high TRF2 had enhanced invasion potential in presence of M2-type macrophages (derived from THP1 cells) compared to uninduced cells (Supplementary Figure 6C). Together these support the role of TRF2 in enhanced presence of immune-suppressive TAM, through induced IL1 signaling, and are consistent with more aggressive proliferation reported in TRF2-high tumors (El Maï et al., 2014; Muñoz et al., 2006).

Discussion

Results herein show telomere length of tumor cells impact M2-type immune suppressive macrophage infiltration in breast cancer. Relatively long telomeres resulted in compromised IL1 signaling due to reduced expression of *IL1R1*. Mechanistically, non-telomeric TRF2 directly activates *IL1R1* through promoter binding; in case of tumors with relatively long telomeres TRF2 binding at the *IL1R1* promoter was markedly reduced, and therefore resulted in low IL1R1 and attenuated IL1 signaling. Because of compromised IL1 signaling in tumors with longer telomeres downstream canonical activation of p65 through Ser536 phosphorylation was negatively affected giving reduced induction and secretion of IL1-beta (Figure 6E). This impacted TAM presence negatively in tumors with relatively long telomeres consistent with earlier work suggesting the role of IL1-induction in TAM infiltration (Briukhovetska et al., 2021; Gelfo et al., 2020; Guo et al., 2016). We tested these observations, and the underlying mechanisms, in different contexts comprising clinical tissue from TNBC, xenograft tumors in mouse, and ex-vivo in TNBC-patient-derived organoids and cancer cells. Together, these consistently showed how short/long telomeres affect anti-tumor immune suppression.

Cancer cells tend to have predominantly short but maintained telomeres relative to corresponding normal cells (Harley, 1991; Maser and DePinho, 2002): Consistent with this most TNBC tissues we examined had lower telomere length than paired adjacent normal tissue (Supplementary Table 1) (Barthel et al., 2017a; Weischer et al., 2013). On comparing across TNBC we found about a third of the cases had relatively short telomeres (Artandi and DePinho,

2009; Aviv et al., 2017); ~30% of the cases had relatively long telomeres (>6 kb; Supplementary Figure 1B).

We found that DNA secondary structure G4s present on the *IL1R1* promoter are necessary for TRF2 binding. Perturbation of the G4s genetically by destabilizing base substitutions, or on using small molecules that bind to G4 inside cells resulted in reduced promoter TRF2 binding and *IL1R1* expression. This is in agreement with our results showing G4-dependent non-telomeric TRF2 binding throughout the genome, and how TRF2 recruitment to specific promoters leads to epigenetic histone modifications (Mukherjee et al., 2018, 2019b, 2019a). Further, we recently reported G4s at the human telomerase (*hTERT*) promoter are critical for binding of non-telomeric TRF2, which induced suppressive histone modifications through TRF2-dependent engagement of the repressor complex REST, and repressed *hTERT* (Mukherjee et al., 2018, 2019b, 2019a; Shalu Sharma et al., 2021). We note here in the case of *IL1R1*, interestingly, TRF2 functions as an activator through p300-dependent H3K27 acetylation. Together these not only underscore the role of TRF2 as a G4-dependent transcription factor but also show TRF2-depedent gene activation/repression based on recruitment of distinct cofactors, implicating possible context-specific function of post-translationally modified non-telomeric TRF2, as has been reported in case of telomeric TRF2 (Huda et al., 2009; Mitchell and Zhu, 2014; Mitchell et al., 2009; Rizzo et al., 2017; YR and IK, 2013).

p300/CBP have been keenly studied in cancer epigenetics and specifically breast cancers (Iyer et al., 2004; Ramadan et al., 2021; Ring et al., 2020). Recent findings also show acetylated H3K27 enrichment at the telomeres through p300-dependent HAT activity (Cubiles et al., 2018); however role of TRF2 in p300 engagement or H3K27 acetylation at the telomeres was not investigated. Notably, here we found TRF2-dependent p300 recruitment, and HAT activity resulting in H3K27 acetylation at the *IL1R1* promoter. Together, these support the role of non-telomeric TRF2 as an activating transcription factor through p300 implicating a broader role of TRF2-p300-dependent histone modifications in cancer. Further these suggest the possibility of similar functions of telomeric TRF2 in H3K27 acetylation at the telomeres (Cubiles et al., 2018).

TRF2 has been linked with cancer progression and immune response to cancer including blocking Natural Killer (NK) cells and promoting infiltration of Myeloid Derived immuno-Suppressive Cells (MDSC) (Biroccio et al., 2013; Cherfils-Vicini et al., 2019) (Martínez and Blasco, 2011; Muñoz et al., 2006). Recently, another study showed correlation between TRF2 levels and MDSC in melanoma cells (Ilié et al., 2021) However, the function of non-telomeric

TRF2 in either IL signaling, or in a telomere-sensitive role in immune suppression, has not been reported. It is of interest to note that other than TRF2, non-telomeric function of another shelterin protein RAP1 was reported, where RAP1 was found to directly interact with the NFKappaB complex (Ghosh and Tergaonkar, 2010; Teo et al., 2010b).

Cancers with longer telomeres had consistently lower *IL1-beta* and *IL1R1* expression across different models supporting compromised IL1 signaling. However, we noted that the expression of pro-inflammatory cytokines though overall more in case of long telomeres had model-specific outcomes (Figure 6F). In TNBC-LT and xenograft LT-tumors *IL2* and *IL6* were relatively more than ST; in TNBO-LT *IL6*, *IL8* and *TNF*; while LT cancer cells in ex-vivo culture *IL2* and *TNF* were higher. Higher TAM infiltration is typically associated with low pro-inflammatory cytokines (Chittezhath et al., 2014a; H et al., 2018; Oner et al., 2020), therefore, conversely, higher expression of pro-inflammatory cytokines in LT tumors is largely consistent with reduced TAM. Interestingly, it is possible that the TME (as in case of TNBC clinical tissue/xenografts) resulted in higher expression of pro-inflammatory cytokines in case of LT tumors compared to ex-vivo cells. Anti-inflammatory cytokines were lower in most LT cancers supporting reduced TAM, consistent with high anti-inflammatory cytokines in TAM infiltration (Hu et al., 2015). Further, RNA-seq in HT1080 and HT1080-LT cells (Methods) showed inflammatory genes, including IL1 signaling-related ones, were largely downregulated in LT cells consistent with our observations (Supplementary Figure 7).

Results from TNBC organoids here show that blocking IL1R1 using IL1RA specifically in macrophages was sufficient for restricting M2 infiltration (Figure 1H) suggesting that the IL1 signaling within the tumor cell is important. However, particularly because macrophages are known to be rich source of IL1B (Carmi et al., 2009; Duque and Descoteaux, 2014; Mantovani et al., 2018), and given the model-specific changes noted by us, further experiments will be required to understand how telomeres influence paracrine/juxtacrine signaling mechanisms through immune cells.

Although we observed a range of telomere lengths across cancers from different patients (Supplementary Figure 1B), as also observed by other groups (Londoño-Vallejo, 2004; Pellatt et al., 2013; Shen et al., 2007; Wentzensen et al., 2011; Willeit et al., 2010), it is broadly understood that most cancer tissues have short telomeres. On a wider perspective based on our results, and other reports suggesting immunomodulation in cancers with relatively short telomeres (Barthel et al., 2017b; Hirashima et al., 2013b), it is tempting to speculate the

possibility that short-telomere cancers might be 'selectively' better equipped to evade host immune cells.

IL1 signaling in relation to inflammation in cancer has been extensively studied and consequently IL1B blockers and the receptor antagonist IL1RA are of clinical interest (F Balkwill, 2001)(B Homey, 2002; Kaplanov et al., 2019; Lappano et al., 2020)(Chittezhath et al., 2014a). Further, the effect of altered cancer cell-IL1 signaling on M2-type TAM infiltration was reported in multiple cancer types (Chanmee et al., 2014; Hu et al., 2015). TAM infiltration has been consistently linked to tumor aggressiveness (Oner et al., 2020) and recent work on targeting (Lee et al., 2019; TL and I, 2011) and modifying TAMs from M2-like states to a more anti-tumorigenic M1-like states (Jaynes et al., 2020) have shown promise as strategies for intervention in cancer. Our findings bring forth a heretofore not reported angle of IL1 regulation that is telomere-sensitive. These implicate new molecular links between telomeres and anti-tumor immune suppression that might be significant in better understanding patient-specific response to cancer immunotherapy.

Acknowledgement

We acknowledge Manish Rai (confocal imaging), Debojyoti Chakraborty Lab (DeltaVision Microscopy), Vivek Rao (THP1 cells) and Mohit Agarwal (ELISA experiments) from CSIR-IGIB. Fellowships from CSIR (AKM, AS, SSR, SS, ASG, SVM, SB and DS); DBT-Wellcome Trust India Alliance (AKM, AS, MC, MV and AP); and DST (DK) are acknowledged. This work was supported by the DBT/Wellcome Trust India Alliance Fellowship [grant number IA/S/18/2/504021] awarded to SC, and research funding from the Council of Scientific and Industrial Research (CSIR) and Department of Biotechnology (DBT).

References:

A, W., P, W., and M, K. (2010). Interleukin-1 (IL-1) pathway. Sci. Signal. *3*.

Akiyama, M., Hideshima, T., Hayashi, T., Tai, Y.-T., Mitsiades, C.S., Mitsiades, N., Chauhan, D., Richardson, P., Munshi, N.C., and Anderson, K.C. (2003). Nuclear factor-kappaB p65 mediates tumor necrosis factor alpha-induced nuclear translocation of telomerase reverse transcriptase protein. Cancer Res. *63*, 18–21.

Artandi, S.E., and DePinho, R. a. (2009). Telomeres and telomerase in cancer. Carcinogenesis *31*, 9–18.

Aviv, A., Anderson, J.J., and Shay, J.W. (2017). Mutations, Cancer and the Telomere Length Paradox. Trends in Cancer *3*, 253–258.

B Homey, A.M.A.Z. (2002). Chemokines: agents for the immunotherapy of cancer? Nat. Rev. Immunol. *2*, 175–184.

Baerlocher, G.M., Mak, J., Tien, T., and Lansdorp, P.M. (2002). Telomere length measurement by fluorescence in situ hybridization and flow cytometry: tips and pitfalls. Cytometry *47*, 89–99.

Baker, A.M., Fu, Q., Hayward, W., Lindsay, S.M., and Fletcher, T.M. (2009). The Myb/SANT domain of the telomere-binding protein TRF2 alters chromatin structure. Nucleic Acids Res. *37*, 5019–5031.

Barthel, F.P., Wei, W., Tang, M., Martinez-Ledesma, E., Hu, X., Amin, S.B., Akdemir, K.C., Seth, S., Song, X., Wang, Q., et al. (2017a). Systematic analysis of telomere length and somatic alterations in 31 cancer types. Nat. Genet. 2017 493 *49*, 349–357.

Barthel, F.P., Wei, W., Tang, M., Martinez-Ledesma, E., Hu, X., Amin, S.B., Akdemir, K.C., Seth, S., Song, X., Wang, Q., et al. (2017b). Systematic analysis of telomere length and somatic alterations in 31 cancer types. Nat. Genet. *49*, 349–357.

Biffi, G., Tannahill, D., McCafferty, J., and Balasubramanian, S. (2013). Quantitative visualization of DNA G-quadruplex structures in human cells. Nat. Chem. *5*, 182–186.

Bilaud, T., Brun, C., Ancelin, K., Koering, C.E., Laroche, T., and Gilson, E. (1997). Telomeric localization of TRF2, a novel human telobox protein. Nat. Genet. *17*, 236–239.

Biroccio, A., Cherfils-Vicini, J., Augereau, A., Pinte, S., Bauwens, S., Ye, J., Simonet, T.,

Horard, B., Jamet, K., Cervera, L., et al. (2013). TRF2 inhibits a cell-extrinsic pathway through which natural killer cells eliminate cancer cells. Nat. Cell Biol. *15*, 818–828.

Briukhovetska, D., Dörr, J., Endres, S., Libby, P., Dinarello, C.A., and Kobold, S. (2021). Interleukins in cancer: from biology to therapy. Nat. Rev. Cancer 2021 218 *21*, 481–499.

Burkholder, B., Huang, R.Y., Burgess, R., Luo, S., Jones, V.S., Zhang, W., Lv, Z.Q., Gao, C.Y., Wang, B.L., Zhang, Y.M., et al. (2014). Tumor-induced perturbations of cytokines and immune cell networks. Biochim. Biophys. Acta - Rev. Cancer *1845*, 182–201.

Carmi, Y., Voronov, E., Dotan, S., Lahat, N., Rahat, M.A., Fogel, M., Huszar, M., White, M.R., Dinarello, C.A., and Apte, R.N. (2009). The Role of Macrophage-Derived IL-1 in Induction and Maintenance of Angiogenesis. J. Immunol. *183*, 4705–4714.

Cassetta, L., Noy, R., Swierczak, A., Sugano, G., Smith, H., Wiechmann, L., and Pollard, J.W. (2016). Isolation of Mouse and Human Tumor-Associated Macrophages. Adv. Exp. Med. Biol. *899*, 211.

Cawthon, R.M. (2002). Telomere measurement by quantitative PCR. Nucleic Acids Res. *30*, e47.

Chanmee, T., Ontong, P., Konno, K., and Itano, N. (2014). Tumor-Associated Macrophages as Major Players in the Tumor Microenvironment. Cancers 2014, Vol. 6, Pages 1670-1690 *6*, 1670–1690.

Cherfils-Vicini, J., Iltis, C., Cervera, L., Pisano, S., Croce, O., Sadouni, N., Győrffy, B., Collet, R., Renault, V.M., Rey-Millet, M., et al. (2019). Cancer cells induce immune escape via glycocalyx changes controlled by the telomeric protein TRF2. EMBO J. *38*, e100012.

Chew, V., Toh, H.C., and Abastado, J.P. (2012). Immune microenvironment in tumor progression: Characteristics and challenges for therapy. J. Oncol. *2012*.

Chittezhath, M., Dhillon, M.K., Lim, J.Y., Laoui, D., Shalova, I.N., Teo, Y.L., Chen, J., Kamaraj, R., Raman, L., Lum, J., et al. (2014a). Molecular Profiling Reveals a Tumor-Promoting Phenotype of Monocytes and Macrophages in Human Cancer Progression. Immunity *41*, 815–829.

Chittezhath, M., Dhillon, M.K., Lim, J.Y., Laoui, D., Shalova, I.N., Teo, Y.L., Chen, J., Kamaraj, R., Raman, L., Lum, J., et al. (2014b). Molecular Profiling Reveals a Tumor-Promoting

Phenotype of Monocytes and Macrophages in Human Cancer Progression. Immunity *41*, 815–829.

Cho, H., Seo, Y., Loke, K.M., Kim, S.W., Oh, S.M., Kim, J.H., Soh, J., Kim, H.S., Lee, H., Kim, J., et al. (2018). Cancer-stimulated CAFs enhance monocyte differentiation and protumoral TAM activation via IL6 and GM-CSF secretion. Clin. Cancer Res. *24*, 5407–5421.

Cristofari, G., and Lingner, J. (2006). Telomere length homeostasis requires that telomerase levels are limiting. EMBO J. *25*, 565–574.

Cubiles, M.D., Barroso, S., Vaquero-Sedas, M.I., Enguix, A., Aguilera, A., and Vega-Palas, M.A. (2018). Epigenetic features of human telomeres. Nucleic Acids Res. *46*, 2347–2355.

Diala, I., Wagner, N., Magdinier, F., Shkreli, M., Sirakov, M., Bauwens, S., Schluth-Bolard, C., Simonet, T., Renault, V.M., Ye, J., et al. (2013). Telomere protection and TRF2 expression are enhanced by the canonical Wnt signalling pathway. EMBO Rep. *14*, 356–363.

Duque, G.A., and Descoteaux, A. (2014). Macrophage Cytokines: Involvement in Immunity and Infectious Diseases. Front. Immunol. *5*.

El Maï, M., Wagner, K.-D., Michiels, J.-F., Ambrosetti, D., Borderie, A., Destree, S., Renault, V., Djerbi, N., Giraud-Panis, M.-J., Gilson, E., et al. (2014). The Telomeric Protein TRF2 Regulates Angiogenesis by Binding and Activating the PDGFRβ Promoter. Cell Rep. *9*, 1047–1060.

Elliott, E.I., and Sutterwala, F.S. (2016). Monocytes Take Their Own Path to IL-1β. Immunity *44*, 713–715.

F Balkwill, A.M. (2001). Inflammation and cancer: back to Virchow? Lancet *357*, 539–545.

Fares, C.M., Van Allen, E.M., Drake, C.G., Allison, J.P., and Hu-Lieskovan, S. (2019). Mechanisms of Resistance to Immune Checkpoint Blockade: Why Does Checkpoint Inhibitor Immunotherapy Not Work for All Patients? Am. Soc. Clin. Oncol. Educ. B. 147–164.

G, C., ML, G., AH, B., MD, W., SK, R., A, P., H, Z., M, M., C, Y., C, K., et al. (2015). Comprehensive Molecular Portraits of Invasive Lobular Breast Cancer. Cell *163*, 506–519.

Gelfo, V., Romaniello, D., Mazzeschi, M., Sgarzi, M., Grilli, G., Morselli, A., Manzan, B., Rihawi, K., and Lauriola, M. (2020). Roles of IL-1 in Cancer: From Tumor Progression to Resistance to Targeted Therapies. Int. J. Mol. Sci. *21*, 1–14.

Ghosh, A.S., and Tergaonkar, V. (2010). Telomeres and inflammation: Rap1 joins the ends? Cell Cycle *9*, 3834–3835.

Goronzy, J.J., Fujii, H., and Weyand, C.M. (2006). Telomeres, immune aging and autoimmunity. Exp. Gerontol. *41*, 246–251.

Granotier, C., Pennarun, G.G., Riou, L., Hoffschir, F.F., Gauthier, L.R., De Cian, A., Gomez, D., Mandine, E., Riou, J.-F.F., Mergny, J.-L.L., et al. (2005). Preferential binding of a G-quadruplex ligand to human chromosome ends. Nucleic Acids Res. *33*, 4182–4190.

Guo, B., Fu, S., Zhang, J., Liu, B., and Li, Z. (2016). Targeting inflammasome/IL-1 pathways for cancer immunotherapy. Sci. Reports 2016 61 *6*, 1–12.

H, G., C, H., and Z, W. (2018). Roles of the immune system in cancer: from tumor initiation to metastatic progression. Genes Dev. *32*, 1267–1284.

Hanahan, D., and Weinberg, R. a. (2000). The hallmarks of cancer. Cell *100*, 57–70.

Hanahan, D., and Weinberg, R.A. (2011). Hallmarks of cancer: the next generation. Cell *144*, 646–674.

Hänsel-Hertsch, R., Beraldi, D., Lensing, S. V, Marsico, G., Zyner, K., Parry, A., Di Antonio, M., Pike, J., Kimura, H., Narita, M., et al. (2016). G-quadruplex structures mark human regulatory chromatin. Nat. Genet. *48*, 1267–1272.

Harley, C.B. (1991). Telomere loss: mitotic clock or genetic time bomb? Mutat. Res. *256*, 271–282.

Hirashima, K., Migita, T., Sato, S., Muramatsu, Y., Ishikawa, Y., and Seimiya, H. (2013a). Telomere Length Influences Cancer Cell Differentiation In Vivo . Mol. Cell. Biol. *33*, 2988–2995.

Hirashima, K., Migita, T., Sato, S., Muramatsu, Y., Ishikawa, Y., and Seimiya, H. (2013b). Telomere Length Influences Cancer Cell Differentiation In Vivo. Mol. Cell. Biol. *33*, 2988–2995.

Hodes, R.J., Hathcock, K.S., and Weng, N.P. (2002). Telomeres in T and B cells. Nat. Rev. Immunol. *2*, 699–706.

Hu, W., Li, X., Zhang, C., Yang, Y., Jiang, J., and Wu, C. (2015). Tumor-associated macrophages in cancers. Clin. Transl. Oncol. 2015 183 *18*, 251–258.

Huda, N., Tanaka, H., Mendonca, M.S., and Gilley, D. (2009). DNA Damage-Induced Phosphorylation of TRF2 Is Required for the Fast Pathway of DNA Double-Strand Break Repair. Mol. Cell. Biol. *29*, 3597.

Hung, N.A., Eiholzer, R.A., Kirs, S., Zhou, J., Ward-Hartstonge, K., Wiles, A.K., Frampton, C.M., Taha, A., Royds, J.A., and Slatter, T.L. (2016). Telomere profiles and tumor-associated macrophages with different immune signatures affect prognosis in glioblastoma. Mod. Pathol. 2016 293 *29*, 212–226.

Ilié, M., Lantéri, E., Chamorey, E., Thamphya, B., Hamila, M., Montaudié, H., Picard-Gauci, A., Gardrat, S., Passeron, T., Lassalle, S., et al. (2021). Association of TRF2 expression and myeloid-derived suppressor cells infiltration with clinical outcome of patients with cutaneous melanoma. Undefined *10*.

Iyer, N.G., Özdag, H., and Caldas, C. (2004). p300/CBP and cancer. Oncogene 2004 2324 *23*, 4225–4231.

Jaynes, J.M., Sable, R., Ronzetti, M., Bautista, W., Knotts, Z., Abisoye-Ogunniyan, A., Li, D., Calvo, R., Dashnyam, M., Singh, A., et al. (2020). Mannose receptor (CD206) activation in tumor-associated macrophages enhances adaptive and innate antitumor immune responses. Sci. Transl. Med. *12*, 6337.

Jeong, H., Hwang, I., Kang, S.H., Shin, H.C., and Kwon, S.Y. (2019). Tumor-Associated Macrophages as Potential Prognostic Biomarkers of Invasive Breast Cancer. J. Breast Cancer *22*, 38–51.

K, K., and K, M. (1994). The IL-1 receptor signaling pathway. J. Leukoc. Biol. *56*, 542–547.

Kahl, V.F.S., Allen, J.A.M., Nelson, C.B., Sobinoff, A.P., Lee, M., Kilo, T., Vasireddy, R.S., and Pickett, H.A. (2020). Telomere Length Measurement by Molecular Combing. Front. Cell Dev. Biol. *0*, 493.

Kaplanov, I., Carmi, Y., Kornetsky, R., Shemesh, A., Shurin, G. V., Shurin, M.R., Dinarello, C.A., Voronov, E., and Apte, R.N. (2019). Blocking IL-1β reverses the immunosuppression in mouse breast cancer and synergizes with anti–PD-1 for tumor abrogation. Proc. Natl. Acad. Sci. *116*, 1361–1369.

Kovaleva, O. V., Samoilova, D. V., Shitova, M.S., and Gratchev, A. (2016). Tumor Associated

Macrophages in Kidney Cancer. Anal. Cell. Pathol. *2016*.

Lappano, R., Talia, M., Cirillo, F., Rigiracciolo, D.C., Scordamaglia, D., Guzzi, R., Miglietta, A.M., Francesco, E.M. De, Belfiore, A., Sims, A.H., et al. (2020). The IL1β-IL1R signaling is involved in the stimulatory effects triggered by hypoxia in breast cancer cells and cancer-associated fibroblasts (CAFs). J. Exp. Clin. Cancer Res. 2020 391 *39*, 1–22.

Lee, C., Jeong, H., Bae, Y., Shin, K., Kang, S., Kim, H., Oh, J., and Bae, H. (2019). Targeting of M2-like tumor-associated macrophages with a melittin-based pro-apoptotic peptide. J. Immunother. Cancer 2019 71 *7*, 1–14.

Li, C., Xue, V.W., Wang, Q.-M., Lian, G.-Y., Huang, X.-R., Lee, T.-L., To, K.-F., Tang, P.M.-K., and Lan, H.-Y. (2020). The Mincle/Syk/NF-κB Signaling Circuit Is Essential for Maintaining the Protumoral Activities of Tumor-Associated Macrophages. Cancer Immunol. Res. *8*, 1004–1017.

Liu, T., Zhang, L., Joo, D., and Sun, S.-C. (2017). NF-κB signaling in inflammation. Signal Transduct. Target. Ther. 2017 21 *2*, 1–9.

Londoño-Vallejo, J.A. (2004). Telomere length heterogeneity and chromosome instability. Cancer Lett. *212*, 135–144.

Lopez-Doriga, A., Valle, L., Alonso, M.H., Aussó, S., Closa, A., Sanjuan, X., Barquero, D., Rodríguez-Moranta, F., Sanz-Pamplona, R., and Moreno, V. (2018). Telomere length alterations in microsatellite stable colorectal cancer and association with the immune response. Biochim. Biophys. Acta - Mol. Basis Dis. *1864*, 2992–3000.

M, J., J, H., SJ, N., JE, L., and S, K. (2016). Elevated IL-1β expression induces invasiveness of triple negative breast cancer cells and is suppressed by zerumbone. Chem. Biol. Interact. *258*, 126–133.

Mantovani, A., and Locati, M. (2013). Tumor-associated macrophages as a paradigm of macrophage plasticity, diversity, and polarization lessons and open questions. Arterioscler. Thromb. Vasc. Biol. *33*, 1478–1483.

Mantovani, A., Barajon, I., and Garlanda, C. (2018). IL-1 and IL-1 Regulatory Pathways in Cancer Progression and Therapy. Immunol. Rev. *281*, 57.

Martínez, P., and Blasco, M. a (2011). Telomeric and extra-telomeric roles for telomerase and the telomere-binding proteins. Nat. Rev. Cancer *11*, 161–176.

Maser, R.S., and DePinho, R. a (2002). Connecting chromosomes, crisis, and cancer. Science *297*, 565–569.

Medrek, C., Pontén, F., Jirström, K., and Leandersson, K. (2012). The presence of tumor associated macrophages in tumor stroma as a prognostic marker for breast cancer patients. BMC Cancer 2012 121 *12*, 1–9.

Mitchell, T.R.H., and Zhu, X.-D. (2014). Methylated TRF2 associates with the nuclear matrix and serves as a potential biomarker for cellular senescence. Aging (Albany NY) *6*, 248.

Mitchell, T.R.H., Glenfield, K., Jeyanthan, K., and Zhu, X.-D. (2009). Arginine Methylation Regulates Telomere Length and Stability. Mol. Cell. Biol. *29*, 4918–4934.

Mukherjee, A.K., Sharma, S., Sengupta, S., Saha, D., Kumar, P., Hussain, T., Srivastava, V., Roy, S.D., Shay, J.W., and Chowdhury, S. (2018). Telomere length-dependent transcription and epigenetic modifications in promoters remote from telomere ends. PLOS Genet. *14*, e1007782.

Mukherjee, A.K., Sharma, S., Bagri, S., Kutum, R., Kumar, P., Hussain, A., Singh, P., Saha, D., Kar, A., Dash, D., et al. (2019a). Telomere repeat-binding factor 2 binds extensively to extra-telomeric G-quadruplexes and regulates the epigenetic status of several gene promoters. J. Biol. Chem. *294*, 17709–17722.

Mukherjee, A.K., Sharma, S., and Chowdhury, S. (2019b). Non-duplex G-Quadruplex Structures Emerge as Mediators of Epigenetic Modifications. Trends Genet. *35*, 129–144.

Muñoz, P., Blanco, R., and Blasco, M.A. (2006). Role of the TRF2 telomeric protein in cancer and ageing. Cell Cycle *5*, 718–721.

O'Callaghan, N.J., Dhillon, V.S., Thomas, P., and Fenech, M. (2008). A quantitative real-time PCR method for absolute telomere length. Biotechniques *44*, 807–809.

Oner, G., Altintas, S., Canturk, Z., Tjalma, W., Verhoeven, Y., Berckelaer, C. Van, Berneman, Z., Peeters, M., Pauwels, P., and Dam, P.A. van (2020). Triple-negative breast cancer—Role of immunology: A systemic review. Breast J. *26*, 995–999.

Pawelec, G., Goldeck, D., and Derhovanessian, E. (2014). Inflammation, ageing and chronic disease. Curr. Opin. Immunol. *29*, 23–28.

Pedroso, I.M., Hayward, W., and Fletcher, T.M. (2009). The effect of the TRF2 N-terminal and

TRFH regions on telomeric G-quadruplex structures. Nucleic Acids Res. *37*, 1541–1554.

Pellatt, A.J., Wolff, R.K., Torres-Mejia, G., John, E.M., Herrick, J.S., Lundgreen, A., Baumgartner, K.B., Giuliano, A.R., Hines, L.M., Fejerman, L., et al. (2013). Telomere length, telomere-related genes, and breast cancer risk: The breast cancer health disparities study. Genes, Chromosom. Cancer *52*, 595–609.

Purohit, G., Mukherjee, A.K., Sharma, S., and Chowdhury, S. (2018). Extratelomeric Binding of the Telomere Binding Protein TRF2 at the PCGF3 Promoter Is G-Quadruplex Motif-Dependent. Biochemistry *57*, 2317–2324.

Ramadan, W.S., Talaat, I.M., Hachim, M.Y., Lischka, A., Gemoll, T., and El-Awady, R. (2021). The impact of CBP expression in estrogen receptor-positive breast cancer. Clin. Epigenetics *13*.

Ring, A., Kaur, P., and Lang, J.E. (2020). EP300 knockdown reduces cancer stem cell phenotype, tumor growth and metastasis in triple negative breast cancer. BMC Cancer *20*.

Rizzo, A., Iachettini, S., Salvati, E., Zizza, P., Maresca, C., D'Angelo, C., Benarroch-Popivker, D., Capolupo, A., Del Gaudio, F., Cosconati, S., et al. (2017). SIRT6 interacts with TRF2 and promotes its degradation in response to DNA damage. Nucleic Acids Res. *45*, 1820–1834.

Robin, J.D., Ludlow, A.T., Batten, K., Magdinier, F., Stadler, G., Wagner, K.R., Shay, J.W., and Wright, W.E. (2014). Telomere position effect: regulation of gene expression with progressive telomere shortening over long distances. Genes Dev. *28*, 2464–2476.

Roth, S.Y., Denu, J.M., and Allis, C.D. (2003). Histone Acetyltransferases. Http://Dx.Doi.Org/10.1146/Annurev.Biochem.70.1.81 *70*, 81–120.

Sansoni, P., Vescovini, R., Fagnoni, F., Biasini, C., Zanni, F., Zanlari, L., Telera, A., Lucchini, G., Passeri, G., Monti, D., et al. (2008). The immune system in extreme longevity. Exp. Gerontol. *43*, 61–65.

SD, J., M, C., TH, T., AA, M.Z., KC, A., and ES, C. (2020). Evaluating the Polarization of Tumor-Associated Macrophages Into M1 and M2 Phenotypes in Human Cancer Tissue: Technicalities and Challenges in Routine Clinical Practice. Front. Oncol. *9*.

Shalu Sharma, A., Kishore Mukherjee, A., Shekhar Roy, S., Nesse, G., Prakash Pandey, D., Sharma, S., Bagri, S., Lier, S., Verma, M., Sengupta, A., et al. (2021). Human telomerase is directly regulated by non-telomeric TRF2-G-quadruplex interaction. CellReports *35*, 109154.

Shen, J., Terry, M.B., Gurvich, I., Liao, Y., Senie, R.T., and Santella, R.M. (2007). Short Telomere Length and Breast Cancer Risk: A Study in Sister Sets. Cancer Res. *67*, 5538–5544.

Shun, C.T., Tsai, M.-F., and Chen, C.-H. (2005). Tumor-Associated Macrophages: The Double-Edged Sword in Cancer Progression. Artic. J. Clin. Oncol.

Teo, H., Ghosh, S., Luesch, H., Ghosh, A., Wong, E.T., Malik, N., Orth, A., De Jesus, P., Perry, A.S., Oliver, J.D., et al. (2010a). Telomere-independent Rap1 is an IKK adaptor and regulates NF-κB-dependent gene expression. Nat. Cell Biol. *12*, 758–767.

Teo, H., Ghosh, S., Luesch, H., Ghosh, A., Wong, E.T., Malik, N., Orth, A., de Jesus, P., Perry, A.S., Oliver, J.D., et al. (2010b). Telomere-independent Rap1 is an IKK adaptor and regulates NF-kappaB-dependent gene expression. Nat. Cell Biol. *12*, 758–767.

TL, R., and I, H. (2011). Tumour macrophages as potential targets of bisphosphonates. J. Transl. Med. *9*.

Vasilyev, F.F., Silkov, A.N., and Sennikov, S. V. (2015). Relationship between interleukin-1 type 1 and 2 receptor gene polymorphisms and the expression level of membrane-bound receptors. Cell. Mol. Immunol. *12*, 222–230.

Vinayagamurthy, S., Ganguly, A., and Chowdhury, S. (2020). Extra-telomeric impact of telomeres: Emerging molecular connections in pluripotency or stemness. J. Biol. Chem. *295*, 10245–10254.

Wang, M., Zhao, J., Zhang, L., Wei, F., Lian, Y., Wu, Y., Gong, Z., Zhang, S., Zhou, J., Cao, K., et al. (2017). Role of tumor microenvironment in tumorigenesis. J. Cancer *8*, 761–773.

Weischer, M., Nordestgaard, B.G., Cawthon, R.M., Freiberg, J.J., Tybjaerg-Hansen, a., and Bojesen, S.E. (2013). Short Telomere Length, Cancer Survival, and Cancer Risk in 47102 Individuals. JNCI J. Natl. Cancer Inst. *105*, 459–468.

Weng, N. ping (2012). Telomeres and immune competency. Curr. Opin. Immunol. *24*, 470–475.

Wentzensen, I.M., Mirabello, L., Pfeiffer, R.M., and Savage, S.A. (2011). The Association of Telomere Length and Cancer: a Meta-analysis. Cancer Epidemiol. Prev. Biomarkers *20*, 1238–1250.

Willeit, P., Willeit, J., Mayr, A., Weger, S., and Oberhollenzer, F. (2010). Telomere length and

risk of incident cancer and cancer mortality. JAMA *304*.

Wright, W.E., Brasiskyte, D., Piatyszek, M. a, and Shay, J.W. (1996). Experimental elongation of telomeres extends the lifespan of immortal x normal cell hybrids. EMBO J. *15*, 1734–1741.

YR, H., and IK, C. (2013). p300-mediated acetylation of TRF2 is required for maintaining functional telomeres. Nucleic Acids Res. *41*, 2267–2283.

Yuan, Z.-Y., Luo, R.-Z., Peng, R.-J., Wang, S.-S., and Xue, C. (2014). High infiltration of tumor-associated macrophages in triple-negative breast cancer is associated with a higher risk of distant metastasis. Onco. Targets. Ther. *7*, 1475.

Supplementary Material and Methods:

Cell lines, media and culture conditions

HT1080 fibrosarcoma cell line was purchased from ATCC. HT1080-LT cells (Cristofari and Lingner, 2006) were a kind gift from Dr. J. Ligner. HT1080 and MRC5 (ATCC) cells and corresponding telomere elongated cells were maintained in Modified Eagle's medium (MEM) supplemented with 10% Fetal Bovine Serum (FBS). MDAMB231 and HEK293T (NCCS, Pune) cells were maintained in DMEM-HG (Dulbecco's Modified Eagle's medium - High Glucose) with a supplement of 10% FBS. All THP1 cell line (gift from Dr Vivek Rao laboratory, IGIB, Delhi) and derivatives were maintained in RPMI with 10% FBS and 1X Anti-Anti (anti-biotic and anti-mycotic from Thermofisher).

All cultures were grown in incubators maintained at 37ºC with 5% CO_2.

Patient tissue

Previously collected tumor tissues from the biorepository of Rajiv Gandhi Cancer Institute (RGCI&RC) and Research Center (Delhi) were used following approvals by the Institutional Human Ethics Committee (IGIB) and the Institutional Scientific Committee and the Institutional Review Board (IRB, RGCI&RC). Informed consent, consistent with the guidelines of the IRB, was obtained from all patients. Detailed clinical characteristics of patients are provided in Supplementary Table 1.

Organoid generation and culture:

TNBC tissue was used to make tumor organoids using the following protocol-

1. The fresh tissue was stored in 5 ml of Media 1 (Advanced DMEM F12 + 1X Glutamax + 10mM HEPES + 1X AA).

2. 1-3 mm^3 tissue piece was cut, washed and minced in 10ml (Media 1).

3. The minced tissue was digested overnight on shaker in Media 1 with 1-2mg/ml of collagenase.

4. After overnight incubation the digested tissue was sequentially sheared using 1 ml pipette.

5. After each shearing step, the suspension was strained using 100µm filter to retain tissue pieces. Thus entering in subsequent shearing step with approximately 10 ml Advanced DMEM F12.

6. To this was added 2% FCS and centrifuged at 400 rcf.

7. The pellet was resuspended in 10mg/ml cold cultrex growth factor reduced BME Type 2 and 40µl drops of BME suspension was allowed to solidify on pre-warmed 24 well culture plates at 37°C 5% CO_2 for 30 min.

8. Upon complete gelation 400 µl of BC organoid medium was added to each well and plates transferred to 37°C 5% CO_2.

Medium component	Supplier	Catalogue number	Final concentration
R-Spondin 3	R&D	3500-RS/CF	250 $ng \cdot ml^{-1}$
Neuregulin 1	Peprotech	100-03	5 nM
FGF 7	Peprotech	100-19	5 $ng \cdot ml^{-1}$
FGF 10	Peprotech	100-26	20 $ng \cdot ml^{-1}$
EGF	Peprotech	AF-100-15	5 $ng \cdot ml^{-1}$ [a]
Noggin	Peprotech	120-10C	100 $ng \cdot ml^{-1}$
A83-01	Tocris	2939	500 nM
Y-27632	Abmole	Y-27632	5 mM
SB202190	Sigma	S7067	500 nM [b]
B27 supplement	Gibco	17504-44	1x
N-Acetylcysteine	Sigma	A9165-5g	1.25 mM
Nicotinamide	Sigma	N0636	5 mM
GlutaMax 100x	Invitrogen	12634-034	1x
Hepes	Invitrogen	15630-056	10 mM
Penicillin/Streptomycin	Invitrogen	15140-122	100 $U \cdot ml^{-1}$ / 100 $mg \cdot ml^{-1}$
Primocin	Invivogen	Ant-pm-1	50 $mg \cdot ml^{-1}$
Advanced DMEM/F12	Invitrogen	12634-034	1x

9. The media was changed every fourth day.

10. The culture was grown for 10 days before passaging.

II. Passaging Organoid Cultures

1. Cultrex growth factor reduced BME Type 2 geltrex was thawed overnight on ice at 4 °C.

2. Media was removed from the organoid wells and washed twice with PBS-EDTA.

3. Foreach well of 24 well plate 300 µl of TrypLE was added and incubated at 37°C 5% CO_2 for 5 min.

4. 600 µl of washing media (DMEM F12) was added and organoids were dissociated vigorously by pipetting.

5.. Organoid solution was transferred to 15 ml falcon with 5 ml washing media and centrifuged at 1000rpm for 5 min to pellet organoids.

6. Supernatant was carefully aspirated leaving behind 200ul media and 500ul of fresh media, mixed well gently and transferred to 1.5ml tube for centrifugation at 650*g for 5min at 4 °C .

7. Supernatant was gently aspirated and resuspended in cold cultrex and 40ul drop/well was seed in a pre-warmed 24 well plate.

8. Incubated for 30 min and add 400 µl of BC organoid medium.

M2 macrophage generation from THP1 cells:

THP1 cells (0.5 million cells in 1ml) were seeded in a 35 mm dish and treated with PMA (10 ng/ml) for 24 hrs in RPMI complete media (+ 10% FBS). PMA was removed and cells were cultured for 48 hrs in RPMI to get semi-adherent M0 cells. Following this, cells were treated with IL4 (10 ng/ml) and IL13 (20 ng/ml) for 24 hrs in RPMI complete media. Cells were checked for expected morphological changes and trypsinzed for use as M2 macrophages.

M2 macrophage infiltration assay in TNBC tumor organoids:

M2 macrophages were labelled with Cell Tracker red dye (Thermoscientific) for 30 mins and the excess dye was washed off. 10000 labelled M2 macrophages in 20 ul 1X PBS were introduced in a 96 well with TNBC organoids in a dome with Supplement enriched media (200 µl). 12 hrs later, the media was washed off with 3 1X PBS washes and the organoid dome was extracted with 100 µl Tryple E and resuspended with 100 ul chilled 1X PBS. This cocktail was kept on ice for 5 mins and centrifuged at 1000g for 10 mins. The supernatant was discarded and the process was repeated once more.

The cells were resuspended in 500 ul chilled 1X PBS and subjected to Flow-cytometric analysis for scoring percentage of labelled (red) M2 macrophages.

Vector constructs

The pCMV6-myc-DDK(FLAG)-TRF2 vector (TRF2 WT) was procured from Origene (RC223601). The mutants delB and delM constructs used in the study have been previously reported(Hussain et al., 2017) and made through mutagenesis of the TRF2 WT construct. TRF2 shRNA was procured from Origene (TL308880). Side-directed Mutagenesis was performed on the TRF2 WT plasmid to generate the PTM mutants.

Transfections

TRF2 wildtype (myc/DDK tag) or mutant mammalian expression vector pCMV6 was transfected into HT1080 /MDAMB231 cells that were 60 % confluent using Lipofectamine 2000 transfection reagent (following the manufacturers' protocol). 2-4µg of plasmid was used for transfection in a 35 mm well for each case.

In case of TRF2 shRNA (Origene)/TERC shRNA (SantaCruz), 4µg of plasmid was used for transfection in a 35 mm well for each case and Fugene HD transfection reagent was used as per manufacturer's protocol. Cells were then maintained in 1µg/ml of puromycin for stable shRNA maintenance.

TRF2 silencing by siRNA:

HT1080 cells were transfected with TRF2 siRNA oligonucleotides (synthesized from Eurogenetics Pvt. Limited)(Shalu Sharma et al., 2021) using lipofectamine 2000 (Invitrogen) transfection reagent according to manufacturer's instructions. Silencing was checked after 48 hr of transfection. Pooled SCR siRNA was used as control.

Luciferase assay:

IL1R1 promoter (upto 1500 bp upstream of transcription start site) was cloned in PGL3 basic vector upstream of firefly luciferase construct. G4 motif disrupting mutations were introduced in the promoter construct by site directed mutagenesis.

Plasmid (pGL4.73) containing a CMV promoter driving Renilla luciferase was co-transfected as transfection control for normalization. After 48h, cells were harvested and luciferase activities of cell lysate were recorded by using a dual-luciferase reporter assay system (Promega).

CCR5-IL1R1 promoter insert cells:

IL1R1 promoter and downstream firefly luciferase (and G4 mutant variant) was inserted in HEK293T cells by using strategy previously standardized and reported for TERT promoter-gaussia insertion in the same locus(Shalu Sharma et al., 2021).

HT1080 TRF2 and TERT inducible cells:

TRF2 cDNA sequence was inserted into pENTR11 vector and the cassette was transferred into lentiviral plasmid pCW57.1 by gateway cloning. Following this viral particles were generated from HEK293T cells and the viral soup was used for transduction. Cells with insert were selected with 1µg/ml of puromycin and tested for TRF2 induction using varying doxycycline concentrations.

Similarly TERT cDNA was amplified from a mammalian expression vector and inserted into pENTR11 vector. Subsequently, the same strategy was used to generate and test TERT inducible HT1080 cells.

Xenograft tumor generation in NOD-SCID mice:

The xenograft tumor generation experiments in NOD-SCID mice were performed by Vivo Biotech Private Limited (Telangana, India) following necessary regulatory approval from Animal Ethics Committee. 2.5 million cells (HT1080, HT1080-LT or HT1080-TRF2 inducible) were subcutaneously injected in healthy male mice (4-6 weeks old) and tumor growth was allowed. In case of TRF2 inducible HT1080 cells, tumors were allowed to grow to 100 mm^3 before oral dosage of doxycycline (or placebo control) was started at 2 mg/kg of body weight of mice. Mice were sacrificed to obtain tumors when tumors reached an average volume of 600 mm^3(± 100).

Processing of tumor/xenograft tissue

Approximately 10 milligram of tumor tissue was weighed and washed thrice with ice-cold 1X PBS- 1 ml (filtered). About 300 microlitres of PBS was left to submerge the tissue after the final wash. Using a sanitized razor blade, the tumor was cut into small pieces (the efficiency of the digestion is dependent on how well the tumor is minced; large pieces will not digest properly and may need extra digestion time). The tumor soup was transferred into a 15 ml tube using a P1000 pipette (cut the top of the tip in order to be able to take all the tissue) and the volume was adjusted to 4 ml of 1X pre-chilled PBS. 80 µl of Liberase TL stock solution (Roche)was mixed using a vortex and incubate for 45 min at 37 °C under continuous rotation. The sample was checked visually; the cell suspension should look smooth (if the cell suspension still contains tissue fragments digest for an additional 15 min). To end the enzymatic digestion ,10 ml PBS 1 % w/v BSA was added. The cells were filtered using a 100 µm cell strainer in a 50 ml tube and the volume adjusted to 20 ml with 1X PBS (pre-chilled). Cells were centrifuged for 7 min at 500 g and 4 °C. The supernatant was discarded and the cells were re-suspended in 1 ml Serum-free media. Subsequently, cells were counted and volume made up to get a cell density of 1 million cells/ ml. Following this, cell suspension was used for ChIP, DNA/RNA isolation and flow-cytometry.

Antibodies

Primary antibodies:

TRF2 rabbit polyclonal (Novus NB110-57130)- ChIP, IP, WB

TRF2 mouse monoclonal (Millipore 4A794)- Flow cytometry

TRF1 mouse monoclonal (Novus NB110-68281)-WB

IL1R1 rabbit polyclonal (abcam ab106278)- IF, Flow-Cytometry, WB

DDK/FLAG mouse monoclonal (Sigma-F1804)- ChIP, WB

BG4 recombinant antibody (Sigma Aldrich MABE917)- ChIP

P300 (CST D2X6N) rabbit monoclonal- ChIP, IF, WB

Ac-p300/CBP (CST 4771) rabbit monoclonal-ChIP,WB

CBP (CST 7389) rabbit monoclonal- ChIP,WB

P65(NFKB) (CST 8242) rabbit monoclonal- WB

Ser536 P p65 NFKB (CST 3033) rabbit monoclonal- WB

IKB (CST 4814) mouse monoclonal- WB

p-IKB (CST 2589) rabbit monoclonal- WB

Histone H3 rabbit polyclonal (Abcam ab1791)-ChIP

H3K27ac rabbit polyclonal (Abcam ab4729)-ChIP

H3K4me3 rabbit polyclonal (Abcam ab8580)- ChIP

H3K27me3 rabbit monoclonal (Abcam ab192985)- ChIP

H3K9me3 rabbit polyclonal (Abcam ab8898)- ChIP

Beta-actin mouse monoclonal (Santacruz C4)-WB

GAPDH mouse monoclonal (Santacruz 6C5)-WB

CD11b Monoclonal Antibody (ICRF44), eBioscience™- Flow cytometry

F4/80 Monoclonal Antibody (BM8), eBioscience™- Flow cytometry

CD206 Monoclonal Antibody (MR5D3) Invitrogen- Flow cytometry

Anti-Rabbit IgG/Anti-mouse IgG (Millipore) was used for isotype control.

Secondary antibodies:

anti-Rabbit-HRP(CST), anti-Mouse-HRP(CST),mouse-ALP (sigma),rabbit-ALP(sigma) anti-rabbit Alexa Fluor® 488, anti-mouse Alexa Fluor® 594 (Molecular Probes, Life Technologies).

ChIP (Chromatin Immunoprecipitation)

ChIP assays were performed as as previously reported by Mukherjee *et al.*,2018,2019(Mukherjee et al., 2018, 2019a). Briefly, 3-5 million cells were fixed with ~1% formaldehyde for 10 min and lysed. Chromatin was sheared to an average size of ~300-400 bp using the instrument Biorupter (from Diagenode). 10% of the sonicated fraction was processed as input using phenol–chloroform and ethanol precipitation. ChIP was performed for endogenous/ectopically expressed protein using 1:100 dilution (v/v) of the respective ChIP grade antibody incubated overnight at 4°C. Immune complexes were collected using Salmon sperm DNA-saturated Magnetic Dyna-beads (-50 µg per sample) and washed extensively. Immunoprecipitated DNA and Input fractions were isolated using Phenol-chloroform-isoamylalcohol for phase separation and subsequent precipitation. ChIP DNA was quantified by Qubit HS ds DNA kit from Thermofisher. Quantified ChIP DNA samples were validated for target sites by qRT-PCR.

Flow-cytometry:

The procedure for Flow-cytometry was adapted from basic flow cytometry guidelines from CST and has been previously reported in Sharma *et al*,2021(Shalu Sharma et al., 2021). The cell suspension was fixed with 4% formaldehyde and permeabilized with 0.1% triton X (in 1XPBS) for nuclear proteins. Incubation of primary antibody (1:500 v/v in 1% BSA in 1X PBS) for 1 µg/ml antibody concentration for 2 hours at RT or at 4 degrees Celsius overnight, was followed by PBS wash (3 times) and fluorescently labelled secondary antibody (1:1000 v/v) for 2hours at RT. Following this, cells were washed with 1X PBS (3 times) and re-suspended in 1XPBS for flow-cytometric analysis.

For single channel analysis, histogram prolife (log scale) was generated in ungated sample-SSC-FSC plots. For quadrant gating for double positive cells (two channels), biex- scale plots were used.

Relative Telomeres length (RTL) by Flow-cytometry:

The RTL value is calculated as the ratio between the telomere signal of each sample and the control cell with correction for the DNA index of G0/1 cells. This correction is done to normalize the telomere signal to the DNA content of the cells. The propidium iodide staining of DNA included in the Telomere PNA Kit/FITC procedure is under saturated and should not be used for

DNA content determination. The process has been previously standardized and reported (Mukherjee et al., 2018)

Immunofluorescence microscopy:

Adherent cells were seeded on coverslips and allowed to reach a confluency of ~ 70%. Cells were fixed using freshly prepared 4% Paraformaldehyde by incubating for 10 min at RT. Cells were permeabilized with 0.25% Triton™ X-100 (10 min at RT) and treated with blocking solution (5% BSA in PBS) for 2 hrs at RT. All the previously stated were followed by three consecutive washes with ice cold PBS for 5 mins. Post-blocking, cells treated with relevant antibodies (1:500 for TRF2, 1:500 for IL1R1 and 1:1000 for CD44/p300) and incubated overnight at 4ºC in a humid chamber. Post-incubation, cells were washed alternately with PBS and PBST three times and probed with secondary Ab (rabbit Alexa Fluor® 488(1:1000) / mouse Alexa Fluor® 594 (1:1000)) for 2 hrs at RT. Cells were washed with PBS /PBST three times and mounted using Prolong® Gold anti-fade reagent containing DAPI. Images were taken on Leica TCS-SP8 confocal microscope/ Cytiva delta vision microscope. Lasers of emission wavelength 405nm, 488nm and 532 nm were used imaging for DAPI, Alexa Fluor® 488 secondary Ab and Alexa Fluor® 594 Ab respectively. Laser intensity was kept 20% for DAPI and 40-60% for Alexa Fluor® secondary antibodies. ImageJ (FIJI) software was used to calculate signal intensity (a.u.).

Immunoprecipitation:

Immunoprecipitation of proteins was performed using modified version of suggested IP protocol from CST. Cells were lysed using cell lysis buffer ((1X) 20 mM Tris (pH 7.5), 150 mM NaCl, 1 mM EDTA, 1 mM,EGTA, 1% Triton X-100, 2X mPIC) and treated with relevant primary antibody (1: 100 v/v) overnight at 4 degrees Celsius or mock IgG on rotor. 50 µg of Dyanbeads (blocked with BSA-5% for 60 mins at RT) was added to the lysis soup and kept for 2 hrs in mild agitation. Dynabeads were magnetically separated and washed thrice (with 1X PBS with 0.1% Tween-20). The beads were resuspended with 1X RIPA (50 µl) and 1X lamelli buffer. This was followed by denaturation at 95 degree Celsius for 10 mins and followed by western blot for specific proteins.

Western blotting:

For western blot analysis, protein lysates were prepared by suspending cell pellets in 1X RIPA (with 1x mammalian protease inhibitor cocktail). Protein was separated using 10%/12% SDS-PAGE and transferred to polyvinylidenedifluoride membranes (Immobilon FL, Millipore). After blocking, the membrane was incubated with primary antibodies. Post incubation with primary antibodies (1:1000 v/v), the membrane was washed with 1X PBS and then incubated with appropriate secondary antibodies (1:2000 v/v). Following secondary antibody incubation, the membrane was washed with 1XPBS. The blot was finally developed using HRP substrate/BCP NBT and reagents from Millipore.

Invasion assay with HT1080 cells:

HT1080 cells (50000 cells) were seeded in invasion chamber (BD Biosciences) in 200 µl MEM(serum free). In the bottom chamber, 700 µl of MEM (+10% FBS) was added with and without 500 M2 macrophages. Invasion was checked after 36 hrs using CV staining as per manufacturer's protocol.

Real time PCR

Total RNA was isolated according to manufacturer's instructions using TRIzol® Reagent (Invitrogen, Life Technologies) .A relative transcript expression level for genes was measured by quantitative real-time PCR using a SYBR Green based method. Average fold changes was calculated by the difference in threshold cycles (Ct) between test and control samples. *GAPDH* / 18S gene was used as internal control for normalizing the cDNA concentration of each sample.

For telomere length assessment by qRT PCR, telomere specific primers and single copy number gene 36B4 for normalization was used in PCR reactions with sample DNA using reported protocol(O'Callaghan et al., 2018).

RT PCR primers used have been enlisted in Additional Supplementary table 1.

RNA-seq analysis:

Raw Illumina sequencing reads were checked for quality using FastQC (version 0.11.9) and adapter clipping and trimming using Trimmomatic (version 0.39) was done using default parameters. Trimmed reads were aligned to the human reference genome (GRCh38, GENCODE v36) with STAR aligner (version 2.7.8a). FeatureCounts (subread package version 2.0.1) was utilized to quantify gene expression. Quality checks at each step were performed using the MultiQC tool (version 1.10.1). Differential gene expression analysis was done using the DESseq2 package (version 1.30.0) in R (version 4.0.3). The analysis was done after eliminating the effects of confounding variables such as batch and replicate using the appropriate design formulae. Gene expression was normalized using variant stabilizing transformation (vst) for the purposes of visualization. Genes with BH-adjusted p value < 0.05 and absolute Log2 fold change greater than 1 (at least 100% fold change in either direction) were considered as significantly differentially expressed genes.

IL1B ELISA:

IL1B ELISA was performed using Human IL-1 beta/IL-1F2 DuoSet ELISA kit by R&D Biosystems Cat no-DY201. As per manufacturer's protocol 96 well microplate was coated with100ul per well of freshly prepared Capture Antibody diluted 100 times in PBS without carrier protein. Thereafter the plate was sealed and incubated overnight at room temperature. Following day the capture antibody was aspirated after which each well was washed three times with 1X Wash Buffer (PBST). After the last wash, the remaining wash buffer was removed

carefully and completely by aspiration and blotting it against clean paper towels. The prepped, empty wells were blocked at room temperature for 1hr by adding 300 µL of Reagent Diluent (20% BSA in 1X PBST) to each well. Wash the wells as in the step above. Next we added the samples and standard protein of known increasing concentrations (100ul in volume) diluted in Reagent Diluent. The plates were then covered with an adhesive strip and incubated for 2 hours at room temperature. Post incubation, the wells were washed as above for plate preparation. Following the washes we added 100ul of freshly prepared Detection Antibody diluted 100 times in PBS. The plate was covered and incubated for 2hrs at room temperature. Post incubation the wells were washed thrice as in the previous step. Finally for generating detectable signal we added 100 µL of Streptavidin-HRP to each well, covered the plate and incubated it in dark at room temperature for 20mins. Next the wells were washed thrice as in steps above. After aspirating the wells clean of any buffer we added 100ul of Substrate Solution to each well and incubated the plates again in dark at room temperature for 20minutes. Finally, 50ul of stop solution was added to each well and mixed well by gentle tapping. The signal was measured using a microplate reader set to 450 nm, 570 and 540nm. Perform wavelength correction by subtracting readings at 540 nm or 570 nm from the readings at 450 nm.

HAT assay:

Histone acetyl transferase (HAT) assay was performed as per manufacturers' protocol from Active motif. Mammalian TRF2 and p300 full length were commercially procured from origene and abcam respectively and used for the assay.

Circular Dichroism

Circular Dichroism profiles (220 nm to 300 nm) were obtained for representative G4 motifs identified within IL1R1 promoter and an overlap with TRF2 high confidence ChIP seqpeak. Circular Dichroism showed the formation of G4-motif with the unaltered sequence while mutated G4 sequence gave partial/complete disruption of the G4-motif under similar conditions (buffer used for G- quadruplex formation -10mM Na cacodylate and 100 mM KCl). The circular dichroism (CD) spectra were recorded on a Jasco-89spectropolarimeter equipped with a Peltier temperature controller. Experiments were carried out using a 1mm path-length cuvette over a wavelength range of 200-320 nm. Oligonucleotides were synthesized commercially from Sigma-Aldrich. 2.5uMoligonucleotides were diluted in sodium cacodylate buffer (10 mM sodium cacodylate and 100 mM KCl, pH 7.4) and denatured by heating to 95ºC for 5 min and slowly cooled to 15ºC for several hours. The CD spectra reported here are representations of three averaged scans taken at 20ºC and are baseline corrected for signal contributions due to the buffer.

Gene ontology and cBIO PORTAL ANALYSIS:

Gene ontology analysis was done using gene list (Barthel et al., 2017b) using publicly available resource –The Gene Ontology Resource database (http://geneontology.org/). Fold enrichment, FDR values and p-values were calculated using PANTHER. Ontology plot was made using MS Excel multivariate plot. Immune related gene expression correlation was done using cBioPortal(https://www.cbioportal.org/) in the TCGA Breast Invasive carcinoma dataset.

Statistical Analysis:

For all datasets with N> 5, Mann Whitney U test was performed using interface provided within GRAPHPAD PRISM software. For paired datasets, T Test was performed for significance. Median values and correlations were calculated using MS Excel functions.

Figure 1

A

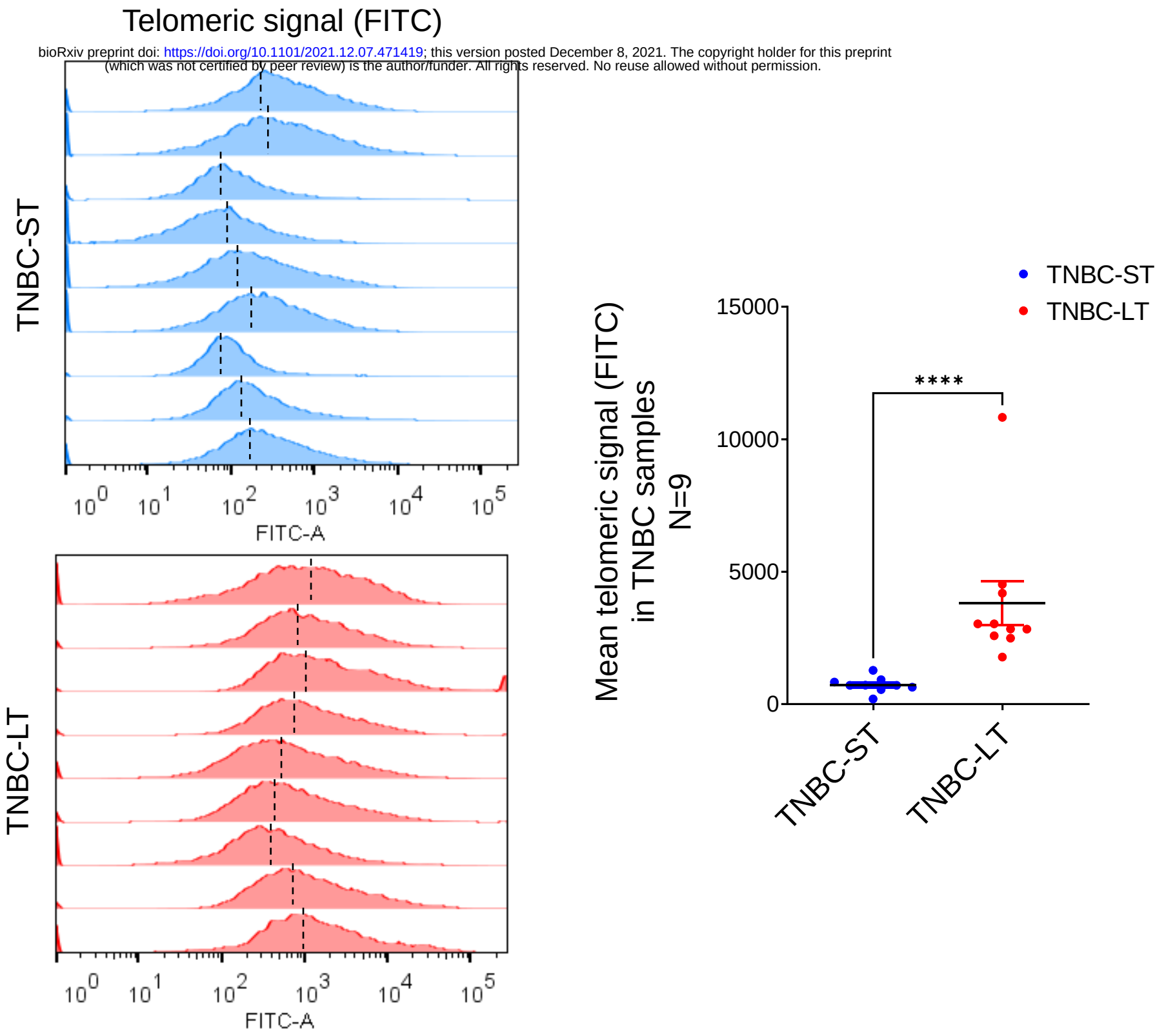

B

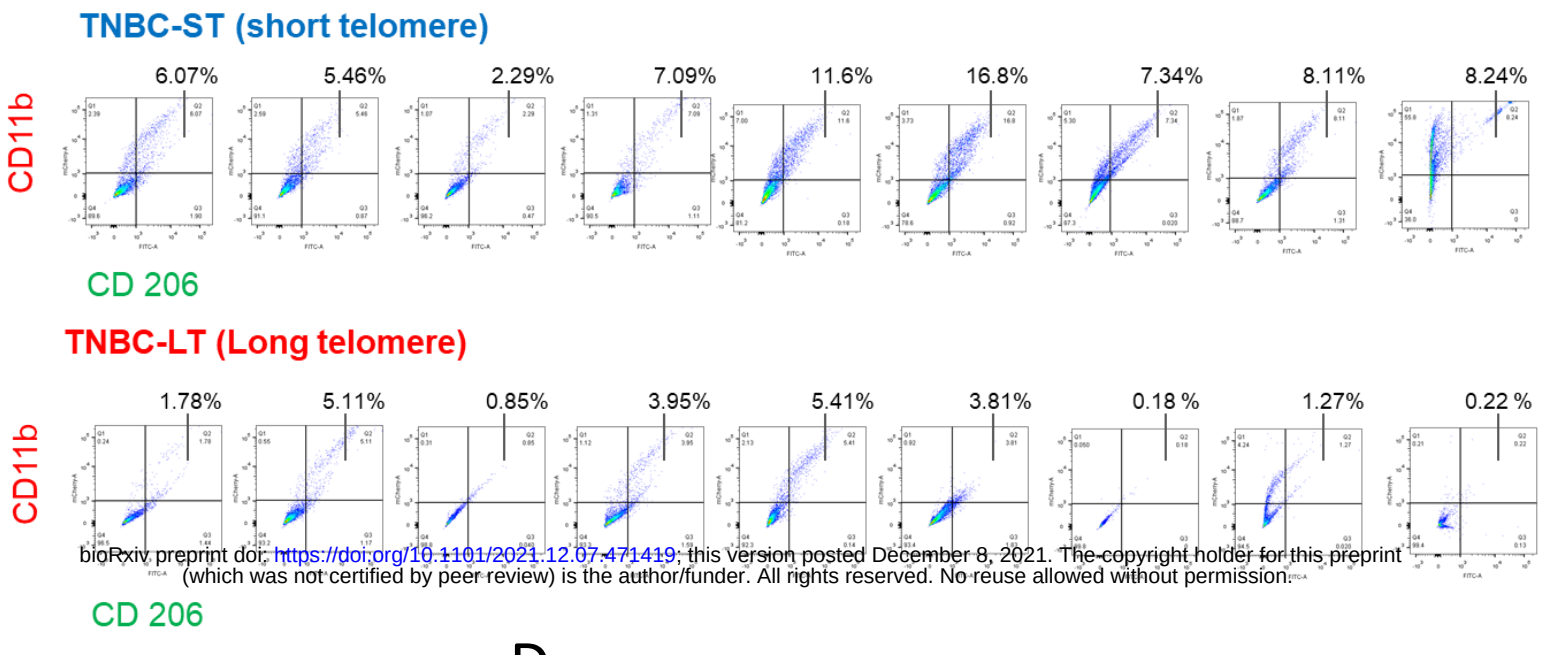

C

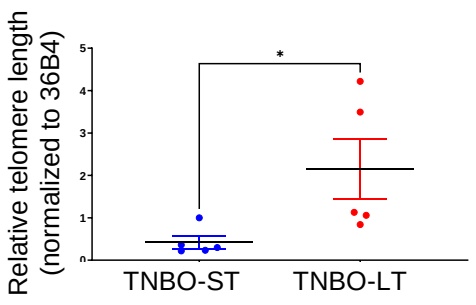

D

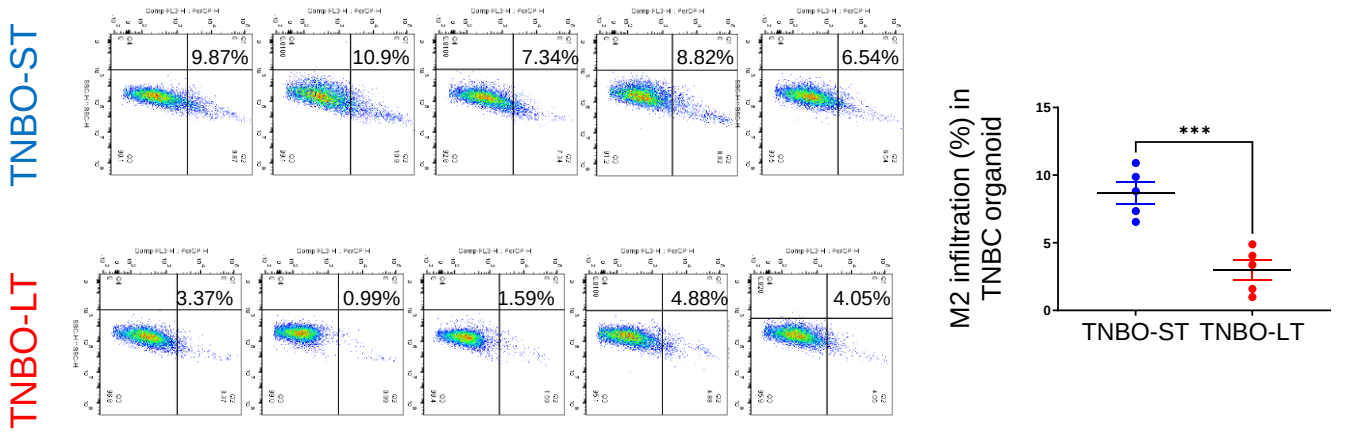

E

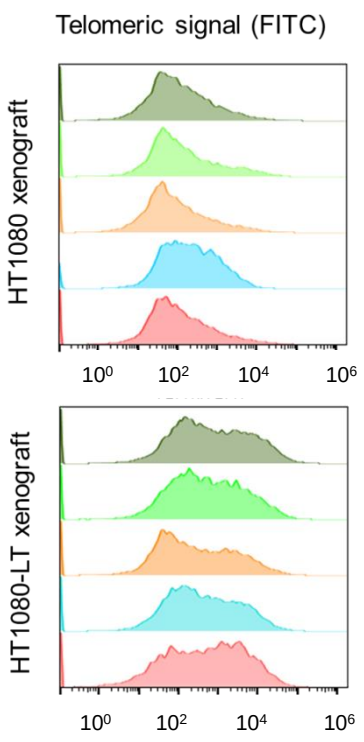

F

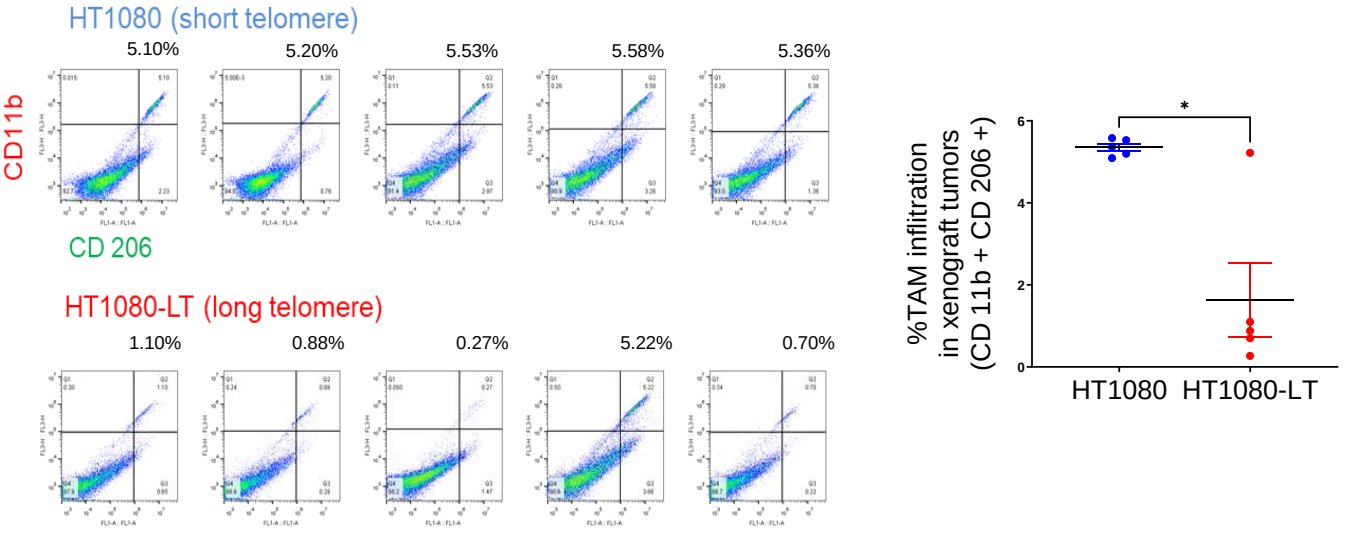

G

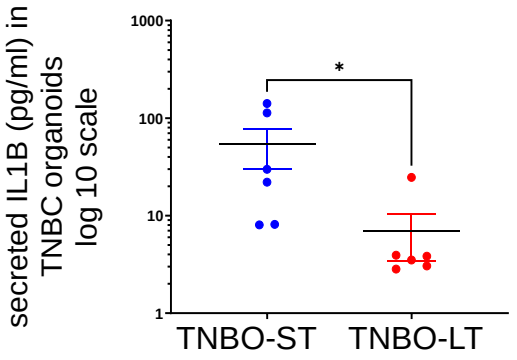

H

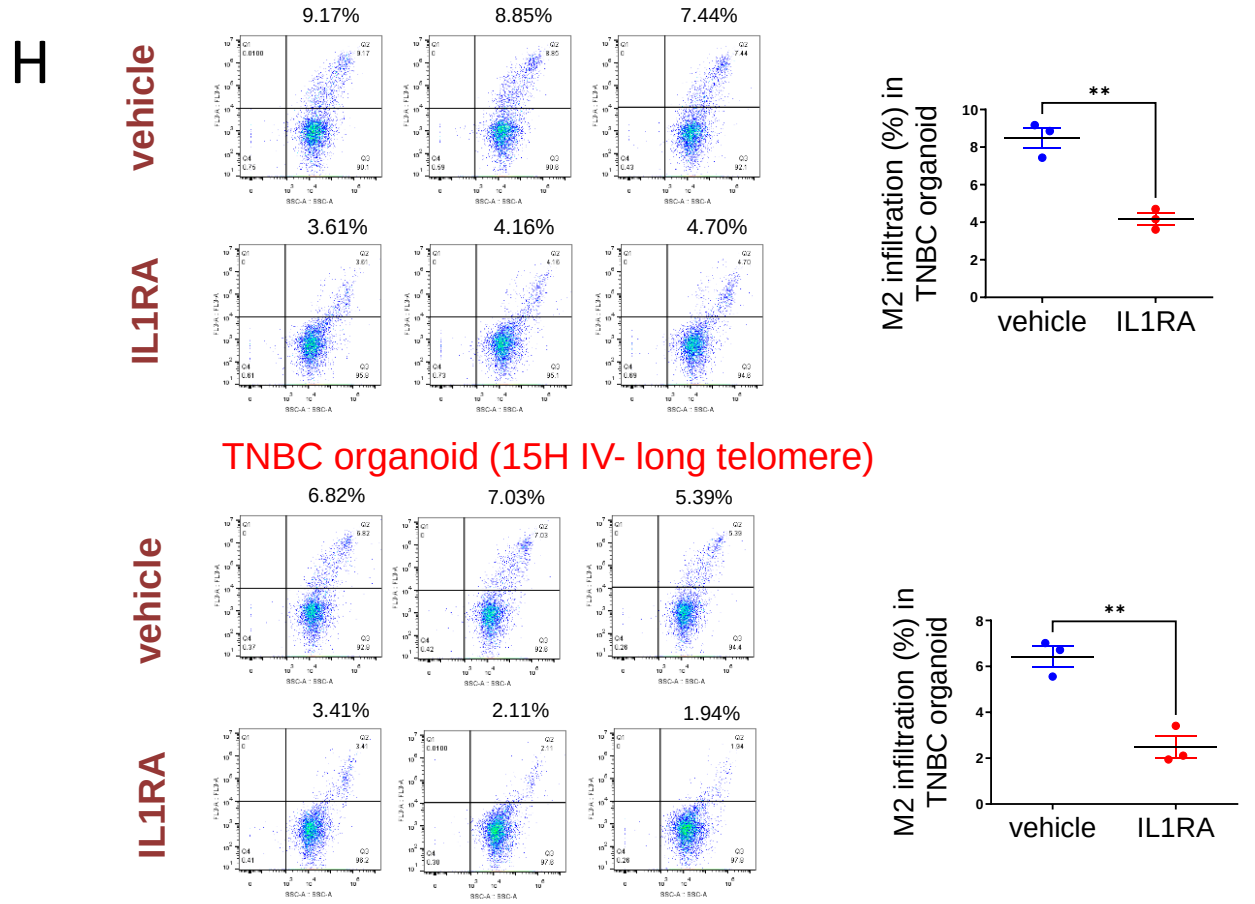

Figure 1 – Cancers with long telomeres have relatively low tumor associated macrophages (TAM) and compromised IL1 signalling

A. Relative telomere length of Triple Negative Breast Cancer (TNBC) samples estimated by Telomeric signal (FITC) using telomere–specific probes in flow cytometry based assays: Mean telomeric signal for nine TNBC-ST (short telomere) and nine TNBC-LT (long telomere) are shown.
B. Percentage of TAM was estimated in TNBC samples using markers CD11b and CD206 (CD11b+ CD206+ cells in top right quadrant). Percentage of TAM in individual TNBC samples shown above top and plotted for TNBC-ST and TNBC-LT.

C. Relative telomere length of Triple negative breast tumor organoids (TNBO) derived from TNBC samples: five TNBO-ST (short telomere) and five TNBO-LT (long telomere) was estimated by qRT-PCR (Methods).
D. Labelled (red) M2 macrophages derived from THP1 cells (Methods) were incubated with TNBO in matrigel domes for 12 hours and infiltration of M2 macrophages in the organoids was estimated as percentage of labelled (red) M2 macrophages . The percentage values for five TNBO-ST and five TNBO-LT samples plotted and also marked in top of each individual flow-cytometry plot where red florescence signal (FL3) is represented along the x-axis in log scale.
E. Relative telomere length of xenograft tumors generated from HT1080 fibrosarcoma cells and their long telomere counterpart cells HT1080-LT (long telomere) cells injected in NOD-SCID mice (N=5 in each case; Methods) was estimated by flow cytometry.
F. Percentage of TAM in xenograft tumors (HT1080 and HT1080-LT) using markers CD11b and CD206. The percentage values for HT1080 and HT1080-LT tumors shown in the adjoining summary graph.
G. Secreted IL1B (pg/ml) form TNBO-ST and TNBO-LT was estimated by ELISA using media supernatant form organoid culture (see methods) .
H. Labelled(red) M2 macrophage assay was performed in presence or absence of IL1RA (20 ng/ml) for a TNBO-ST and a TNBO-LT in three replicates respectively and the percentage values for M2 infiltration was plotted. Red florescence (FL3) plotted along the y-axis in log scale for individual flow cytometry plots and respective percentage M2 infiltration values marked on the top of the plots.

Statistical significance has been calculated using Mann-Whitney's non-parametric test for individual graphs (p values : * ≤ 0.05, ** ≤ 0.01, *** ≤ 0.001, **** ≤ 0.0001)

Figure 2

A

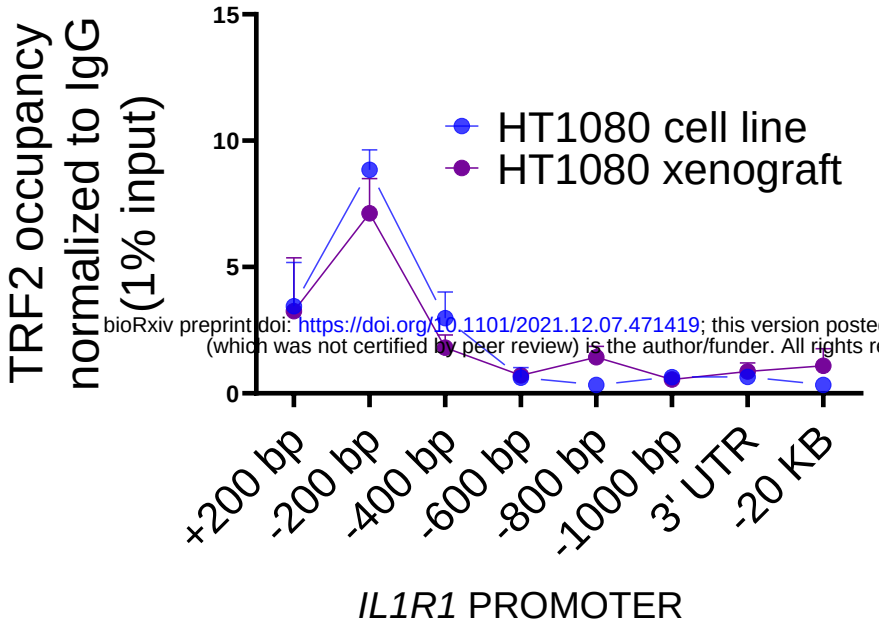

B

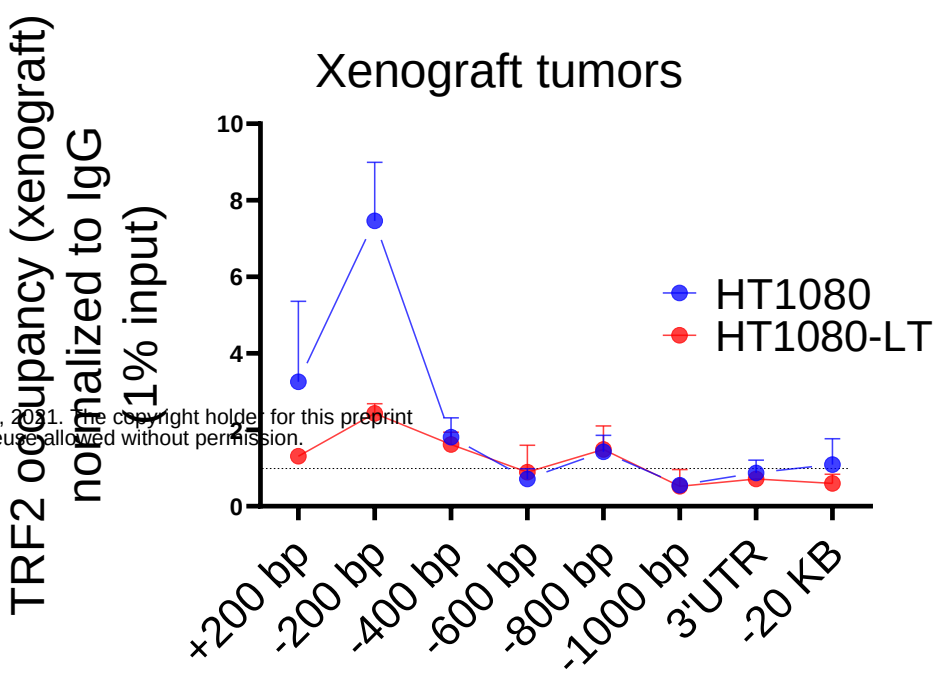

C

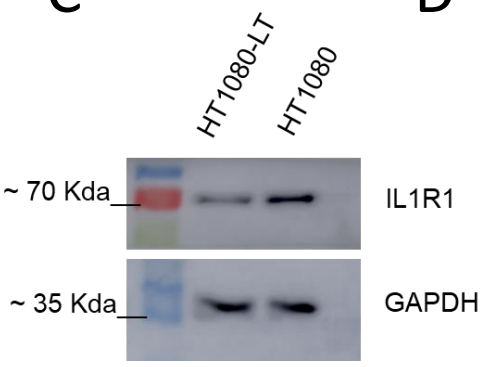

D

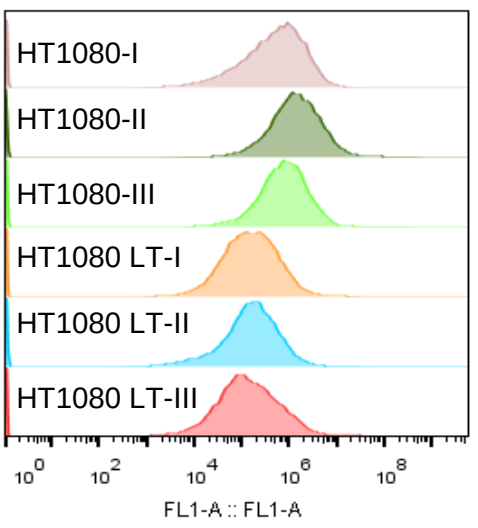

E

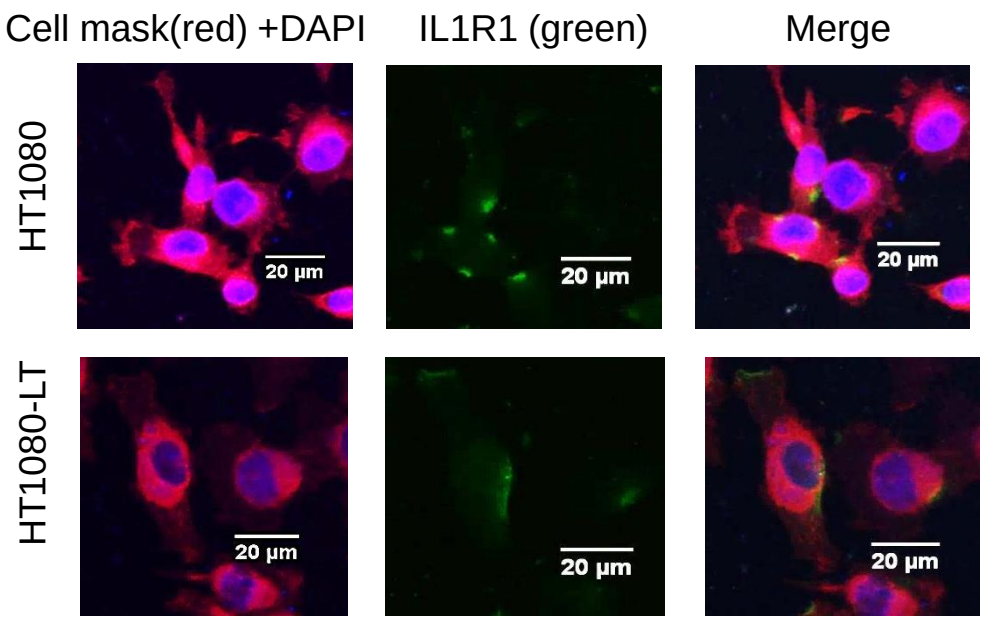

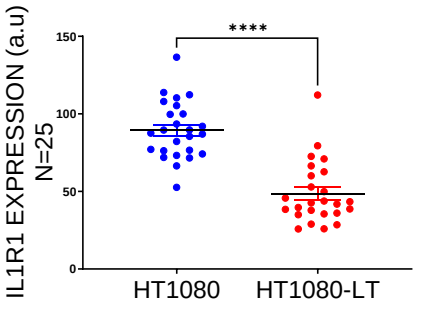

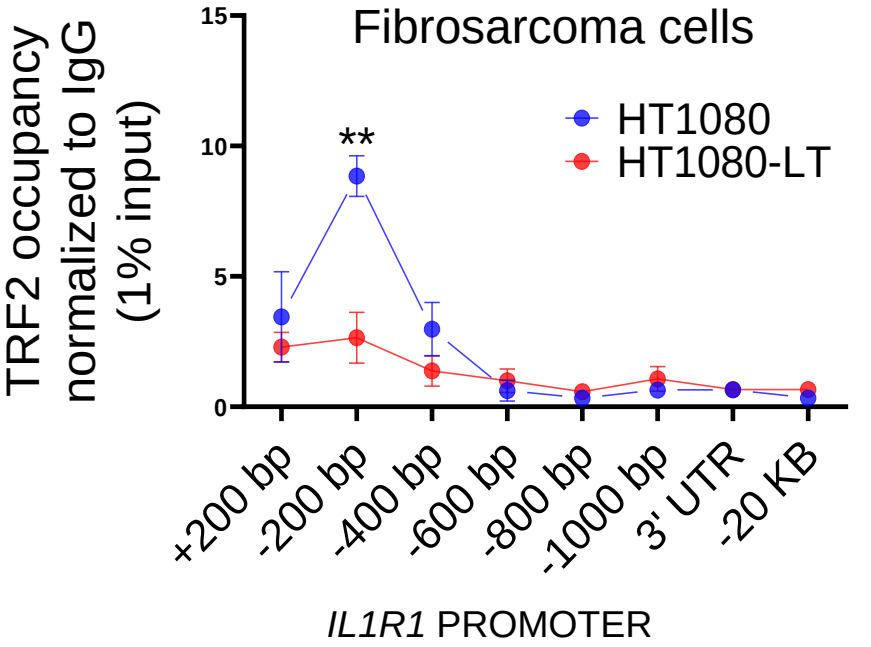

F

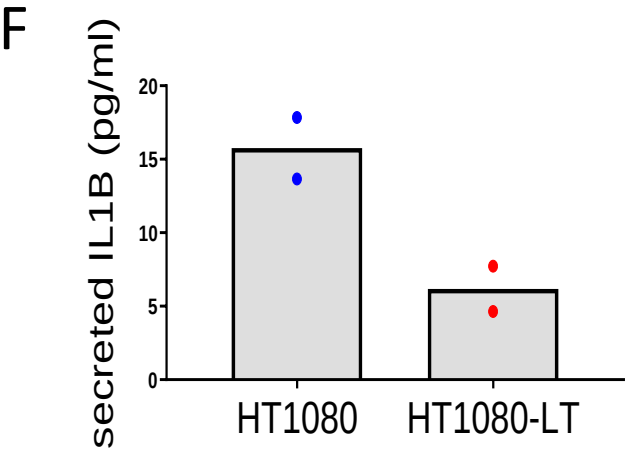

G

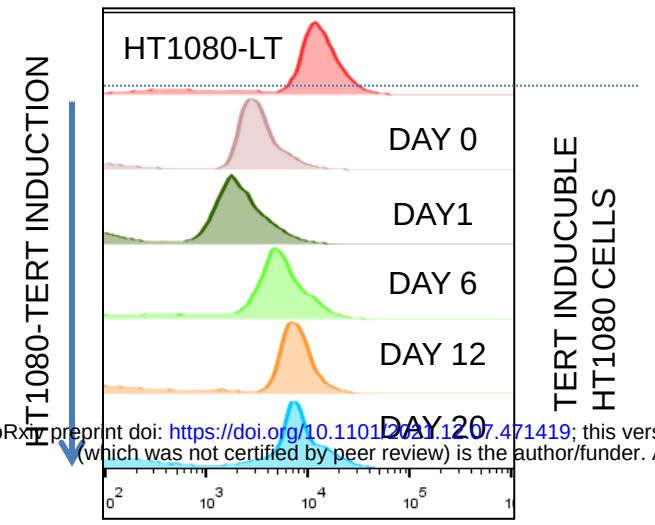

H

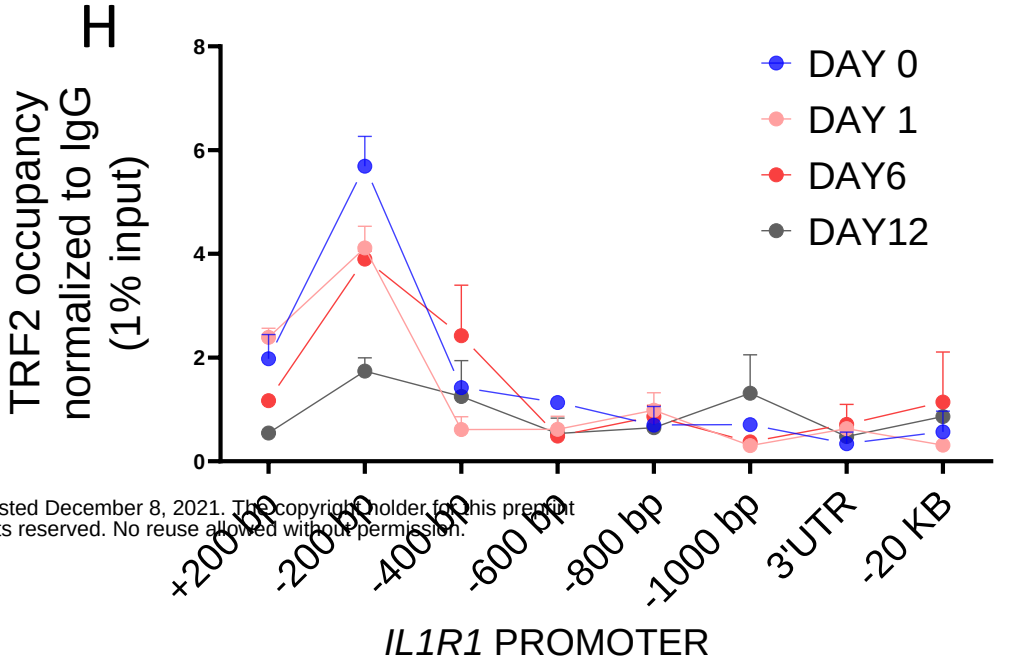

I

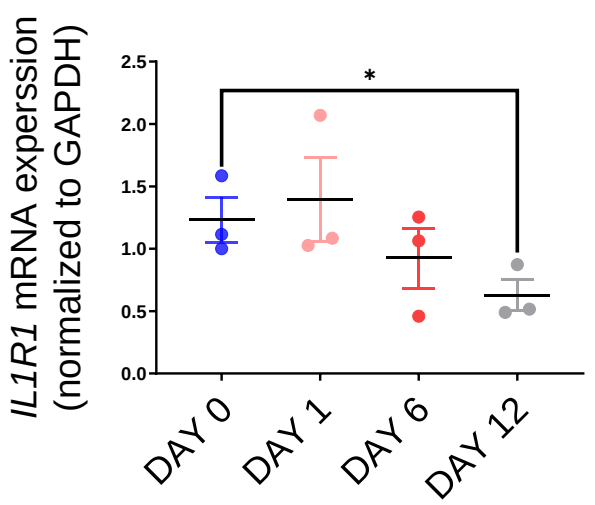

J

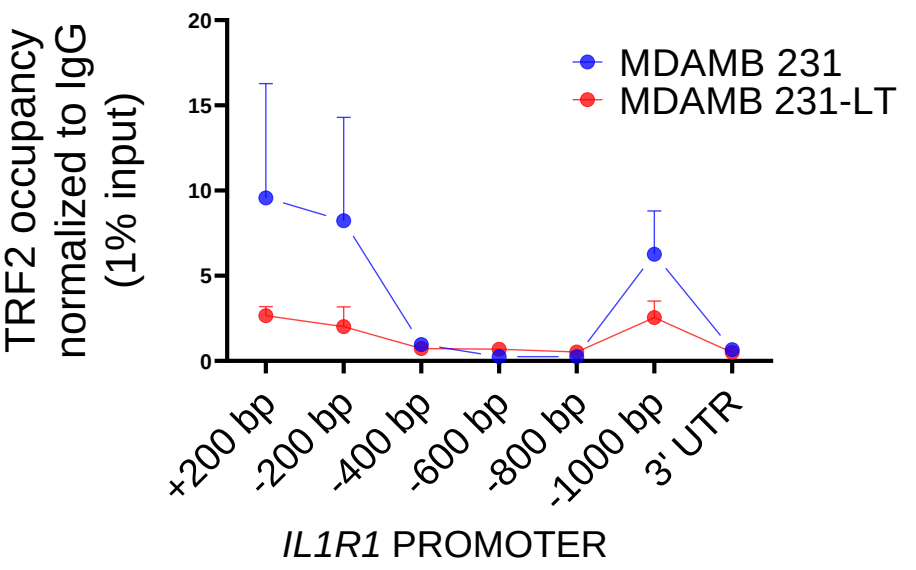

K

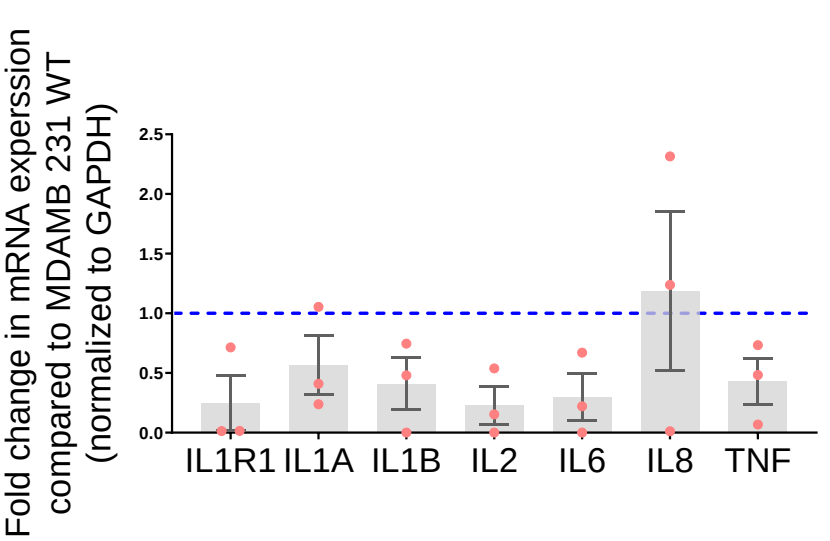

Figure 2 – *IL1R1* expression is sensitive to telomere length and affected by TRF2 binding at the *IL1R1* gene promoter

A. Occupancy of TRF2 at the *IL1R1* promoter was checked in xenograft tumors (N=5) and HT1080 cells by chromatin immunoprecipitation (ChIP) followed by qPCR. Primers spanning +200 bp from TSS (transcription start site) to -1000 bp were used; regions 3'UTR and -20 Kb upstream of TSS used as negative control for TRF2 binding; fold change of occupancy was calculated over mock IgG after normalizing signal to 1% input.
B. Occupancy of TRF2 at the *IL1R1* promoter was lower in xenograft tumors and HT1080-LT compared to HT1080 cells by ChIP followed by qPCR.
C. IL1R1 protein levels in HT1080 and HT1080-LT cells by western blot; GAPDH was used as loading control.
D. IL1R1 protein by immuno-flow cytometry in HT1080 and HT1080-LT cells with three independent replicates for each. IL1R1 expression was plotted along the X-axis in log scale.
E. Expression of IL1R1 on cell surface by immunofluorescence microscopy in in HT1080 and HT1080-LT cells. Cells were stained with cell-mask red for visualization and DAPI for marking the cell nucleus. Average IL1R1 expression from 25 individual cells were plotted in the adjoining graph.
F. Secreted IL1B (pg/ml) in supernatant media from HT1080 and HT1080-LT cells in two independent experiments.
G. Relative telomere length by flow-cytometry based estimation of telomeric signal in HT1080 cells following 0, 1, 6, 12 or 20 days of TERT induction (Methods). HT1080-LT was used as a positive control for enhanced telomere length in the assay.
H. TRF2 occupancy on the *IL1R1* promoter in HT1080 cells following 0, 1, 6 or 12 days of TERT induction (see methods) in ex-vivo culture using primers and normalizations as stated earlier in Figure 2A.
I. *IL1R1* mRNA expression (normalized to *GAPDH*) in HT1080 cells following 0, 1, 6 and 12 days of TERT induction (see methods) in ex-vivo culture.
J. TRF2 occupancy on the *IL1R1* promoter in MDAMB231 cells and MDAMD231-LT (long telomere) cells using primers and normalizations as stated earlier in Figure 2A.
K. Expression for *IL1R1* and other relevant cytokines: *IL1A,IL1B, IL2,IL6,IL8* and *TNF* in MDAMB231 cells and MDAMD231-LT cells. *GAPDH* was used for normalization.

Statistical significance has been calculated using Mann-Whitney's non-parametric test for individual graphs where N≥5. In case of independent repetitions of the same experiment , unpaired T test with Welsh's correction was performed for significance (p values : * ≤ 0.05, ** ≤ 0.01, *** ≤ 0.001, **** ≤ 0.0001). Error bar correspond to standard error of mean from three independent experiments unless N is stated otherwise.

Figure 3

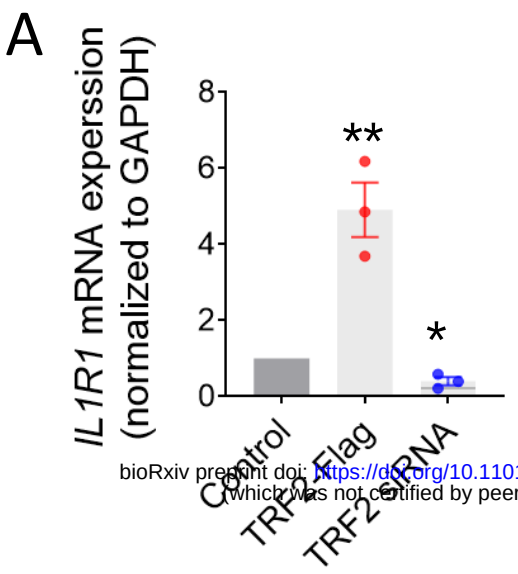

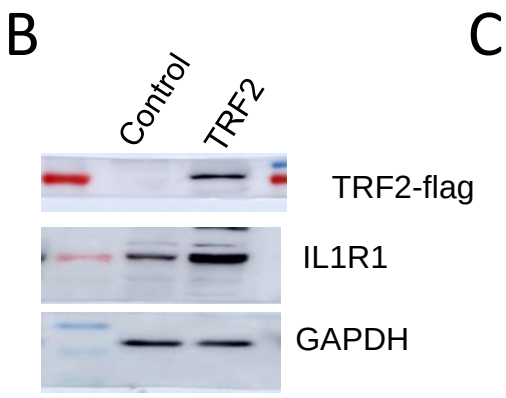

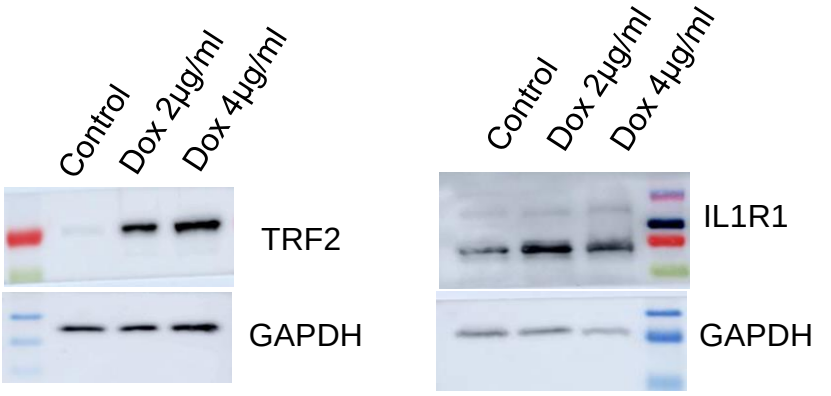

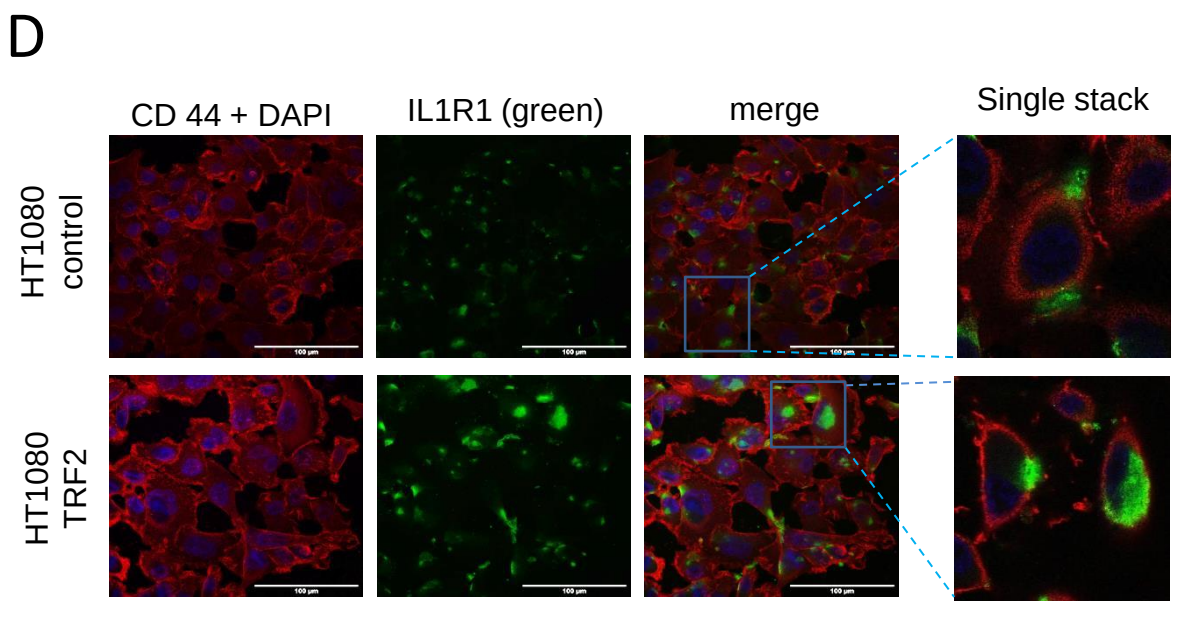

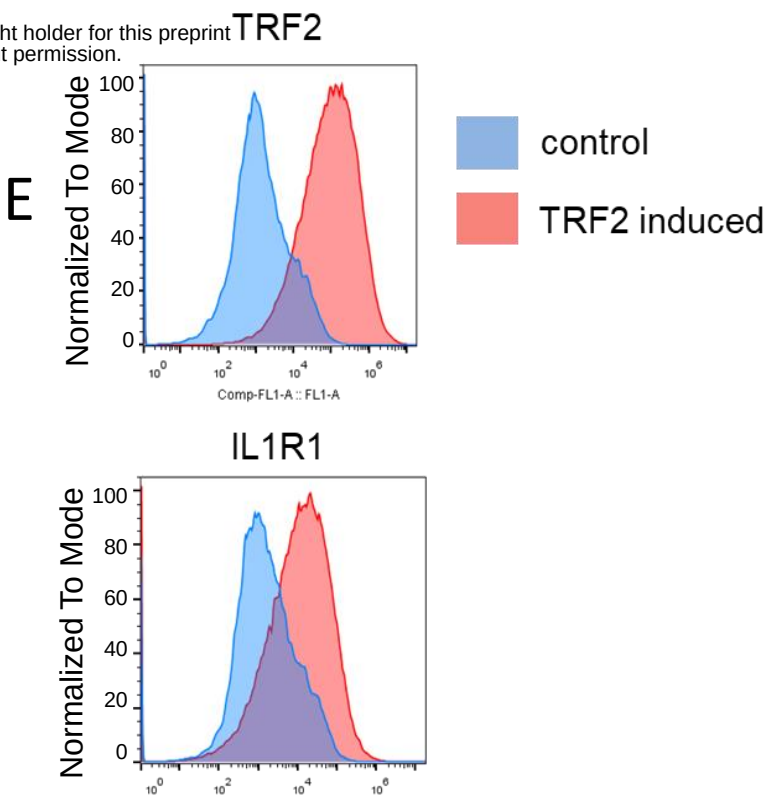

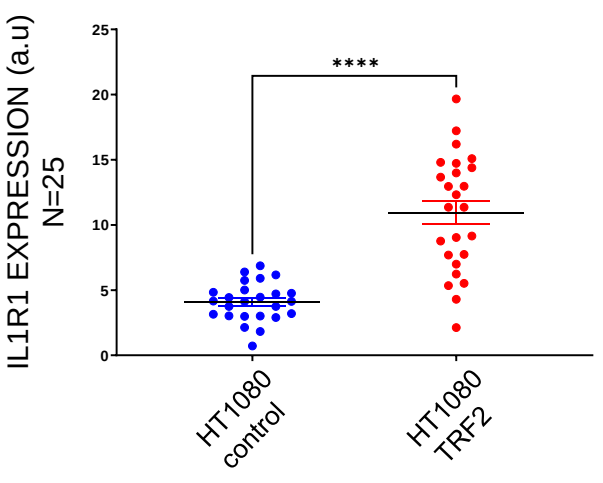

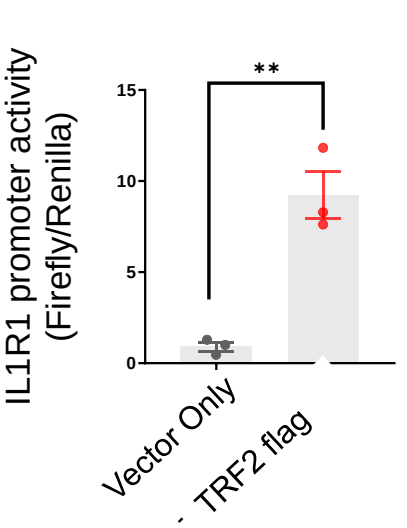

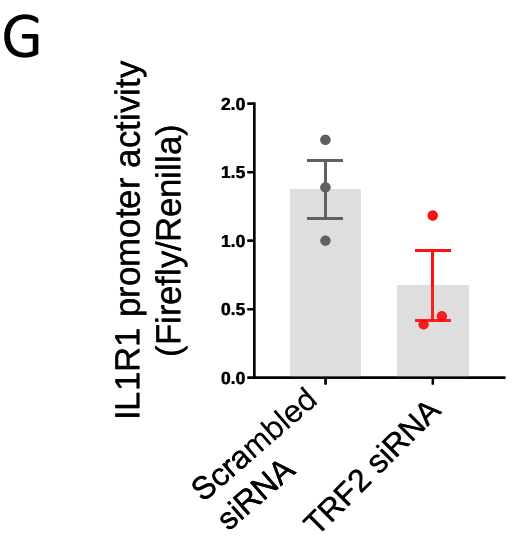

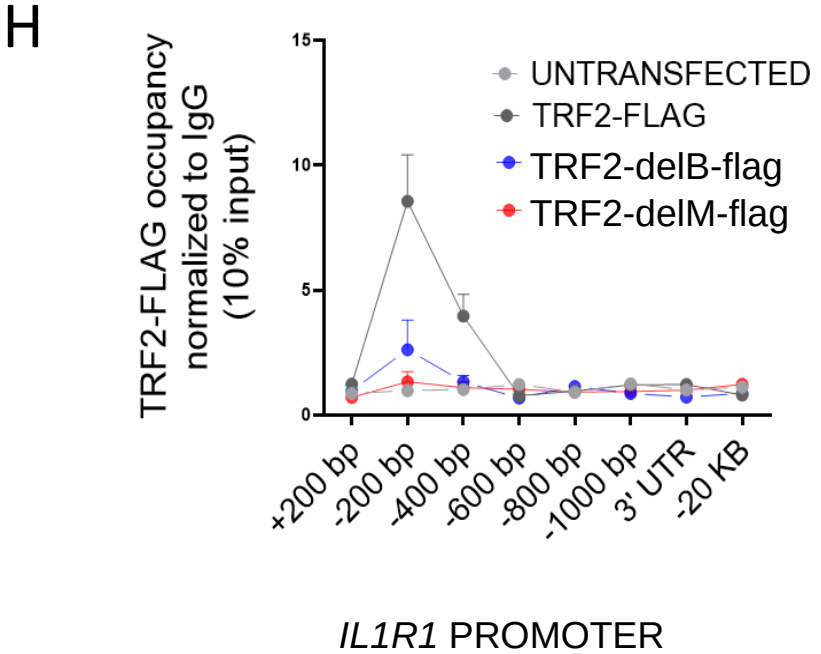

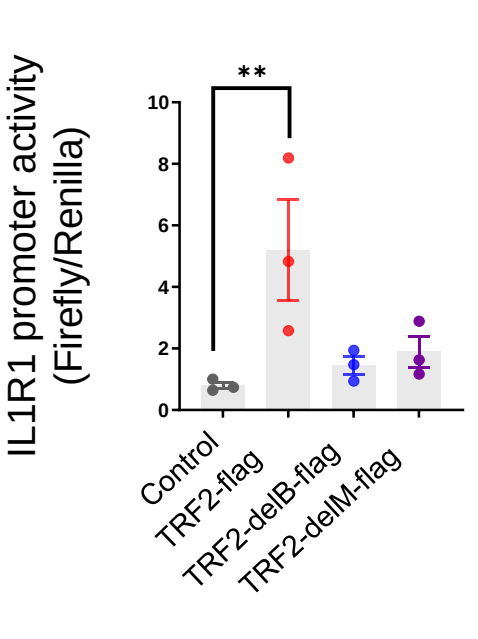

J

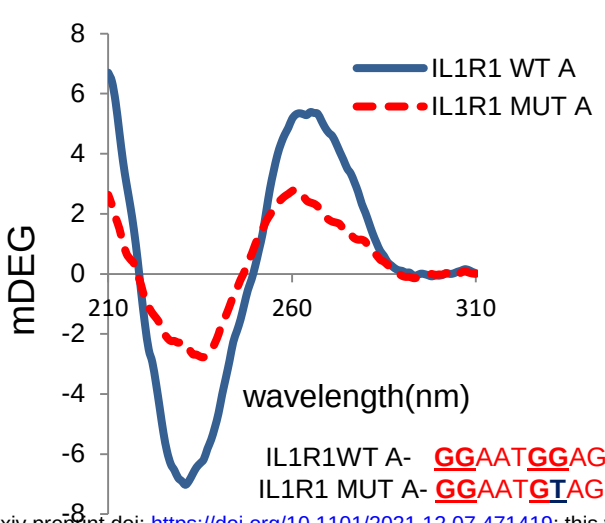

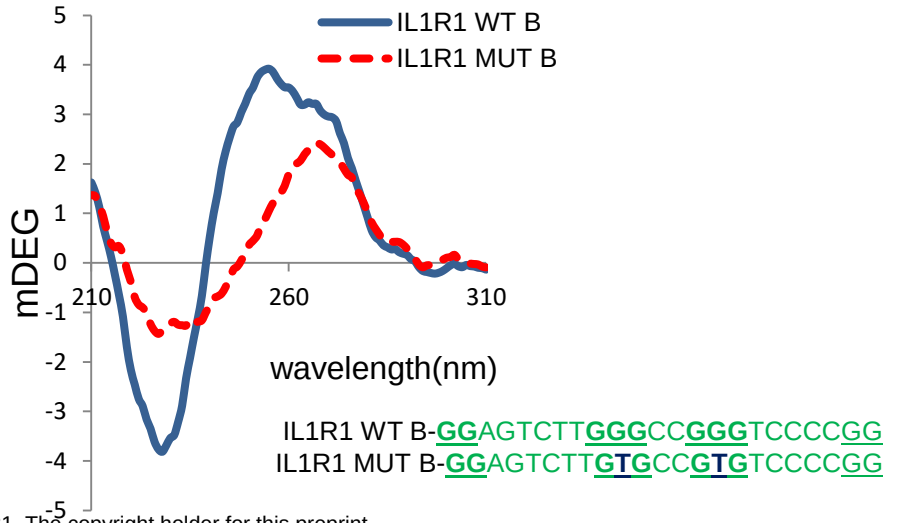

K

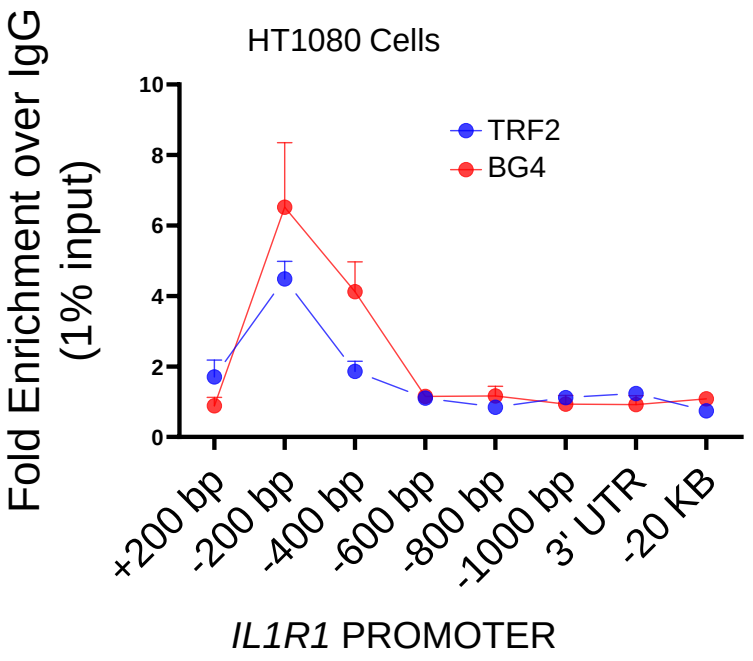

L

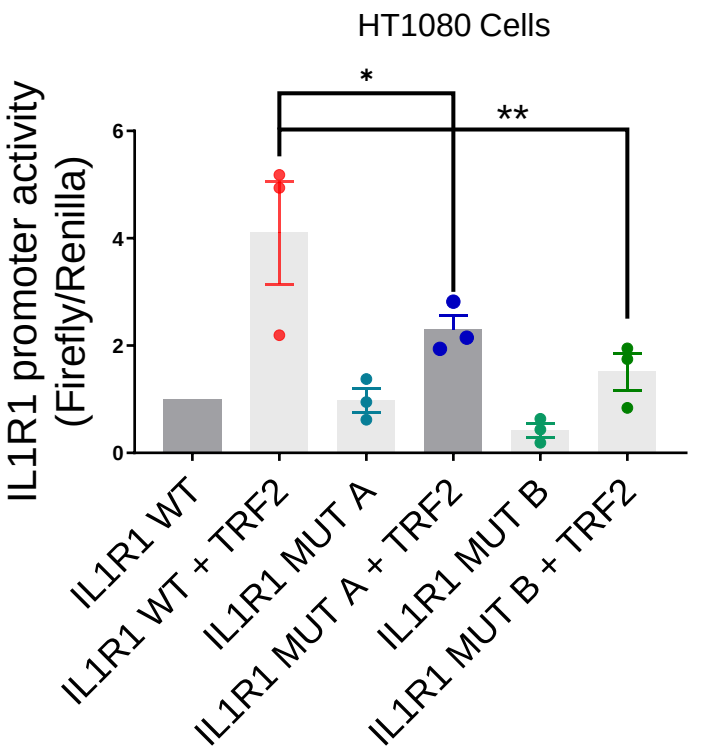

M

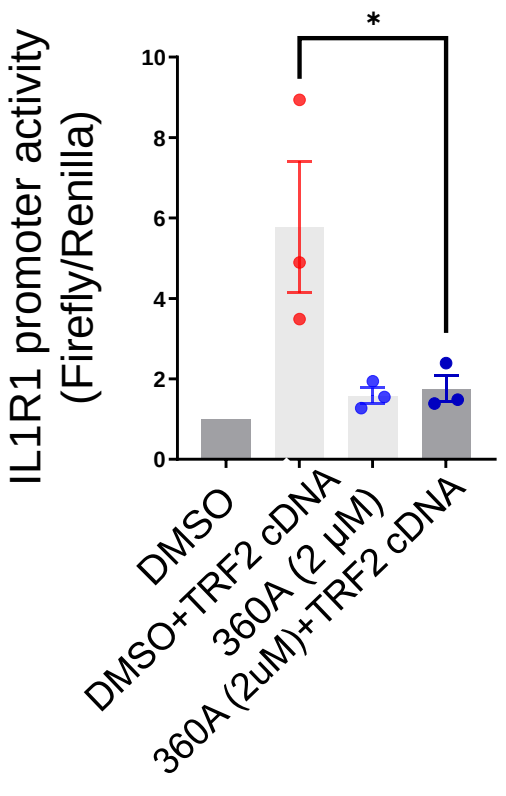

N

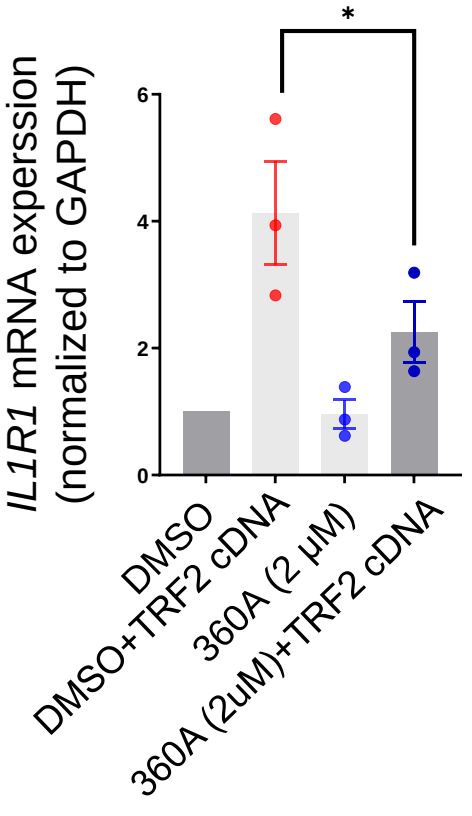

O

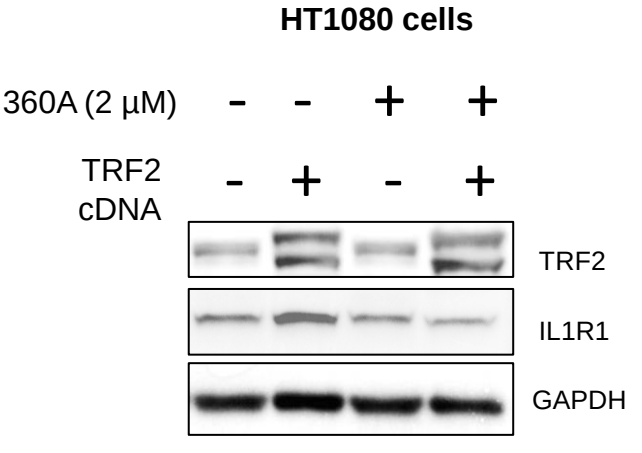

P

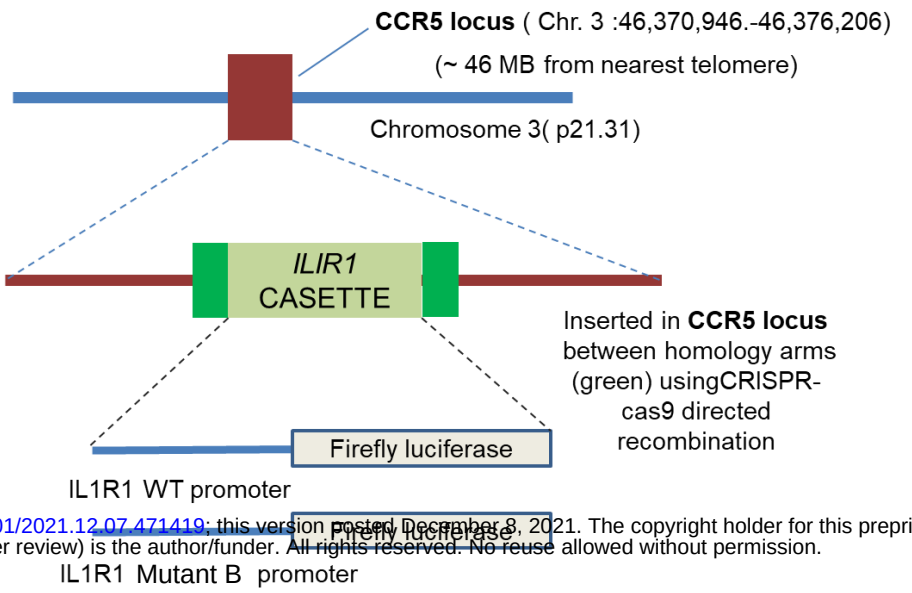

Q

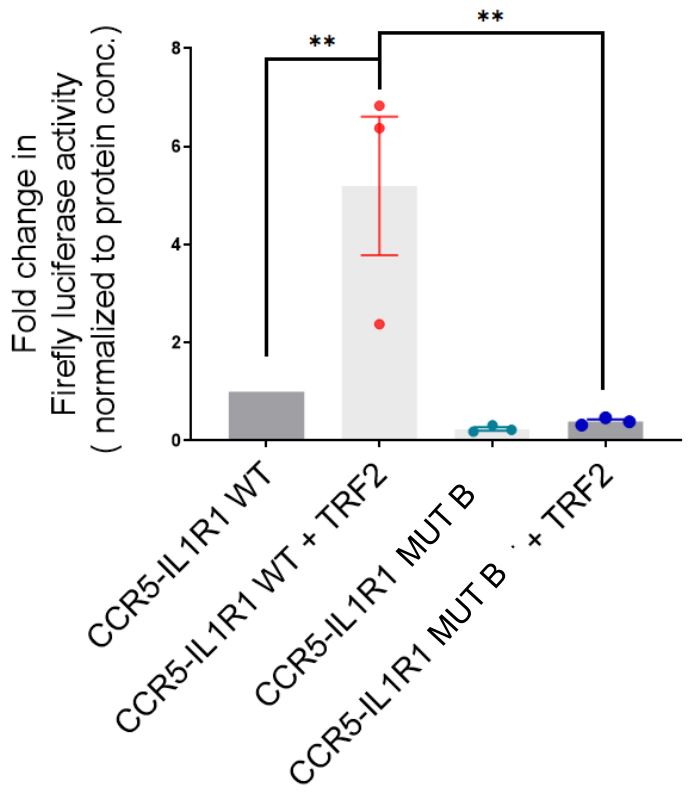

R

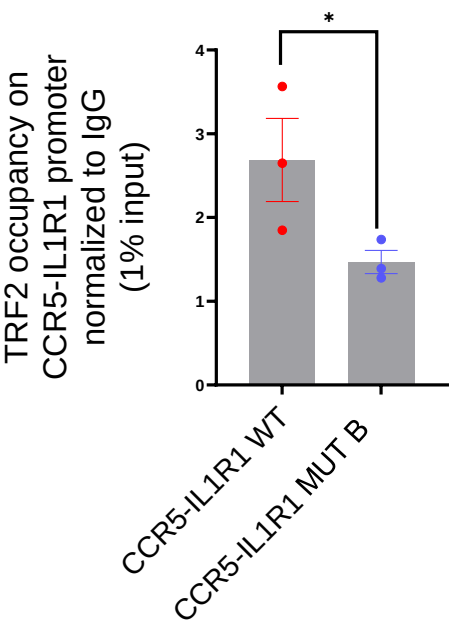

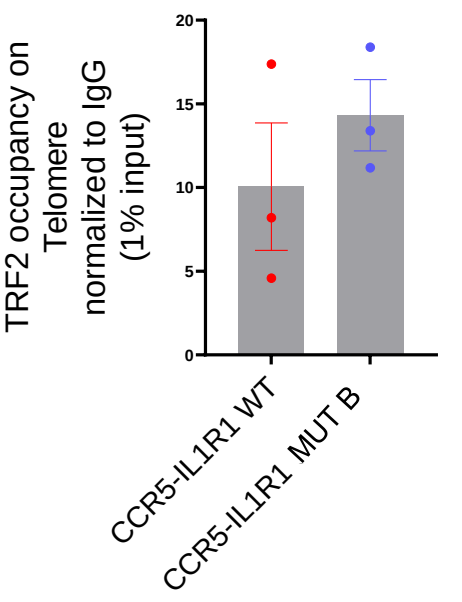

Figure 3 – TRF2 directly activates *IL1R1* by binding to the promoter in a G-quadruplex-dependent fashion

A. *IL1R1* expression was checked by qRT PCR post over-expression of TRF2-flag construct or TRF2 silencing by siRNA (see methods) transiently for 48 hrs. in HT1080 cells.
B. IL1R1 protein expression was checked following over-expression of TRF2-flag construct for 48 hrs in HT1080 cells. GAPDH was used as a loading control in the experiments.
C. TRF2 was induced in stable-TRF2-inducible-HT1080 cells (see methods) by treatment with 2 µg/ml or 4 µg/ml doxycycline in media for 48 hrs. TRF2 induction was checked by western blot and subsequently *IL1R1* expression was checked by western blot. GAPDH was used as a loading control in the experiments.
D. IL1R1 levels on the cell surface was checked in control and TRF2 over-expressing HT1080 cells. CD44 was used as a cell surface marker and nuclei were stained with DAPI; 25 individual cells were scored for IL1R1 expression in control and TRF2 over-expressing cells and plotted in the summary graph.
E. IL1R1 in control and TRF2 induced HT1080 cells by flow-cytometry. TRF2 and IL1R1 was plotted along the x-axis in log scale for 20 thousand cells.
F. IL1R1 promoter activity (see methods) in control (vector only) or transient TRF2-flag-expression for 48 hrs in HT1080 cells.
G. IL1R1 promoter activity (see methods) in control (scrambled) or following TRF2-siRNA transfection for 48 hrs in HT1080 cells.
H. TRF2 WT (flagged tag) or mutants delB and delM were transiently transfected in HT1080 cells and cells harvested after 48hrs were used for ChIP using antibody for flag-tag. Subsequently occupancy was checked on *IL1R1* promoter by qRT PCR using primers as previously stated.
I. IL1R1 promoter activity was checked (see methods) in control (vector only) along with TRF2-flag, delB and delM over-expressed conditions for 48 hrs in HT1080 cells.
J. Circular dichroism profile (220-310 nm wavelength) of oligonucleotides (5 µM) bearing sequence of the G4 motifs (or base substituted mutants) present in the *IL1R1* promoter (within 200 bp upstream of TSS) in solution.
K. IL1R1 promoter occupancy (fold enrichment over mock) was checked by qRT PCR following BG4 ChIP and overlaid with TRF2 occupancy (fold enrichment over IgG) in HT1080 cells.
L. IL1R1 promoter activity was checked in control or on TRF2 over-expression (48 hrs) for the IL1R1 WT luciferase construct or the G4 motif mutants A and B in HT1080 cells.

M-O. IL1R1 promoter activity, mRNA and protein expression in control and TRF2 over-expressed condition (48 hrs post transfection) in presence or absence of the G4 binding ligand 360A (2 µM).

P-R. IL1R1 promoter (with our without the G4 motif mutant B) along with downstream firefly luciferase was inserted at the CCR5 locus by CRISPR-cas9 gene editing in HEK293T cells (see methods). Firefly signal (promoter activity) was checked in IL1R1 WT or the G4 mutant inserts followed by TRF2 ChIP at the inserted promoter; TRF2 ChIP at telomeres was used as positive control.

Statistical significance has been calculated using Mann-Whitney's non-parametric test for individual graphs where N≥5. In case of independent repetitions of the same experiment , unpaired T test with Welsh's correction was performed for significance (p values : * ≤ 0.05, ** ≤ 0.01, *** ≤ 0.001, **** ≤ 0.0001). Error bar correspond to standard error of mean from three independent experiments unless N is stated otherwise.

Figure 4

A

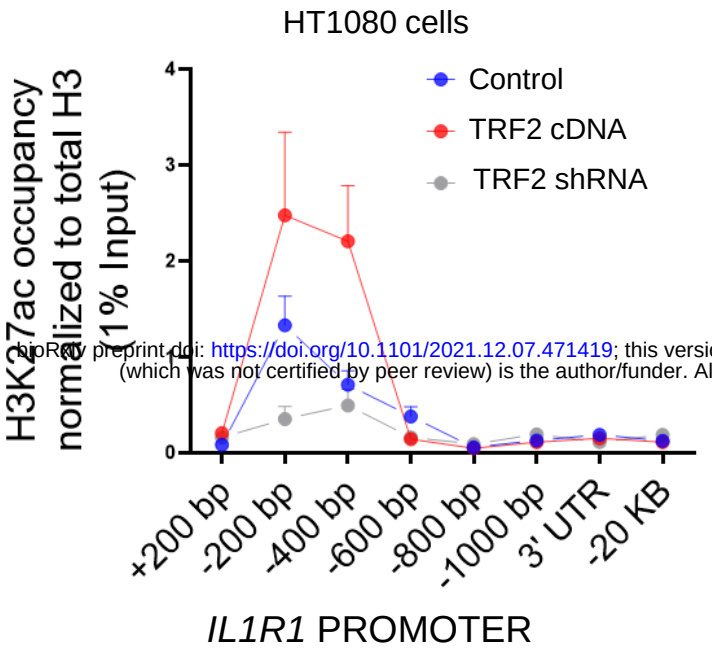

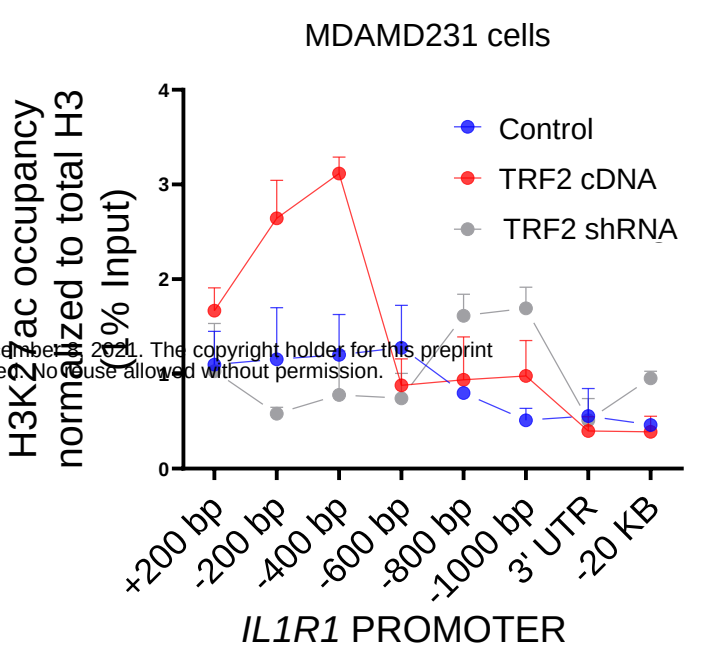

B

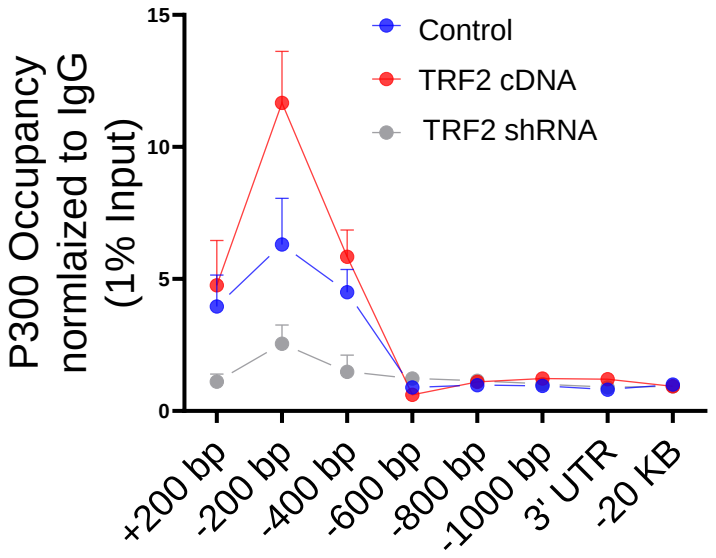

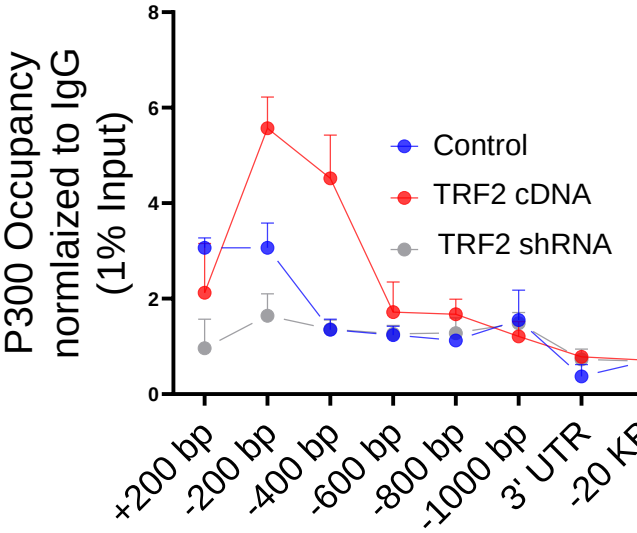

C

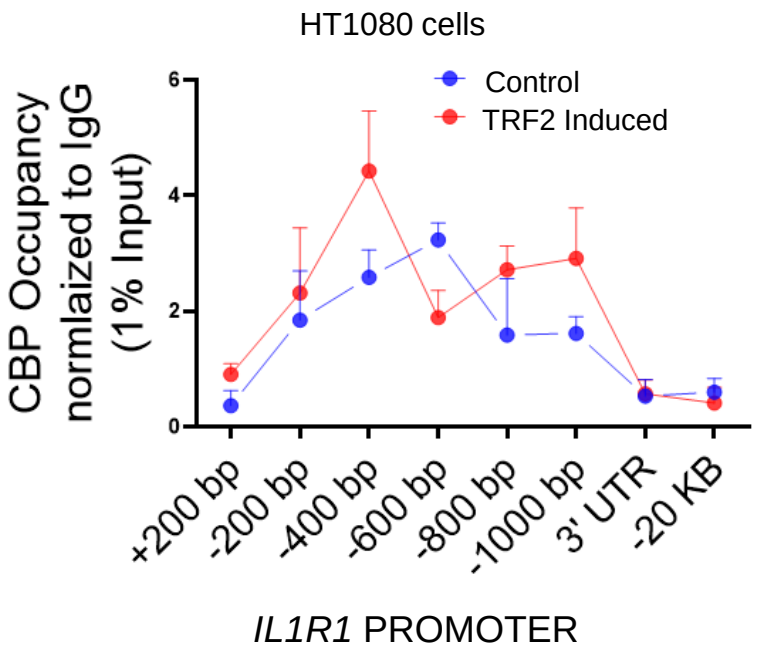

D

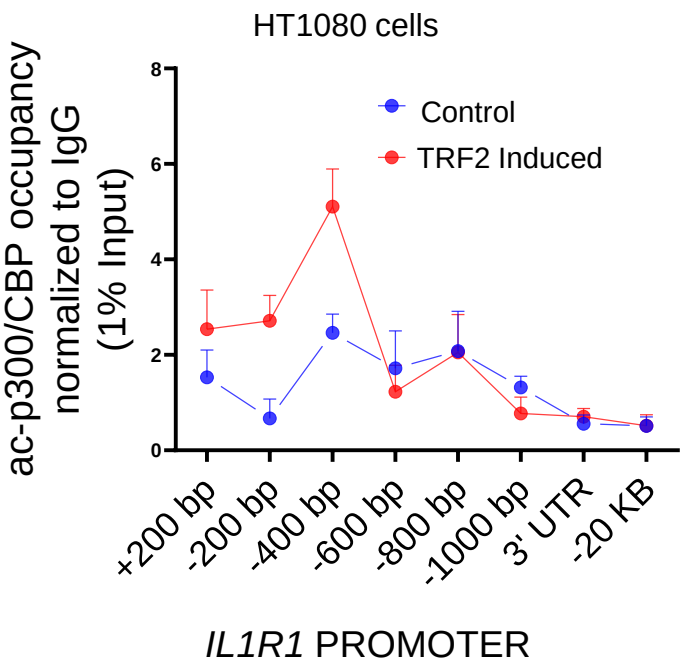

E

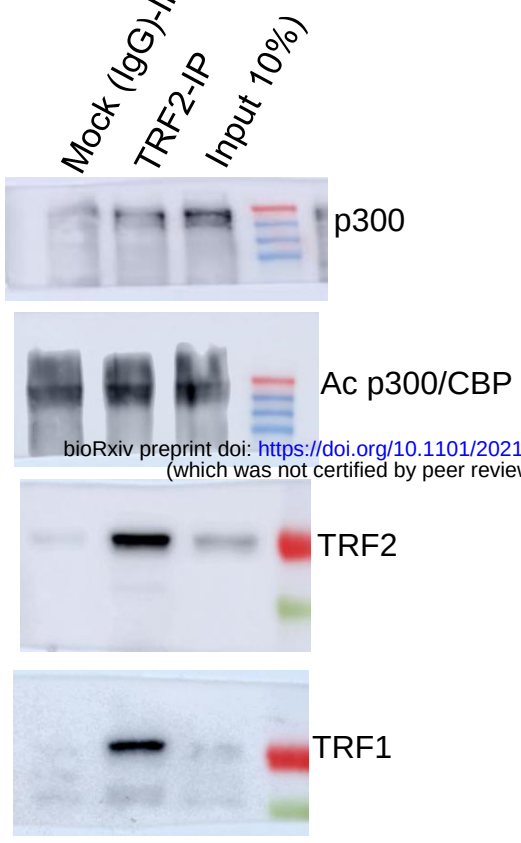

F

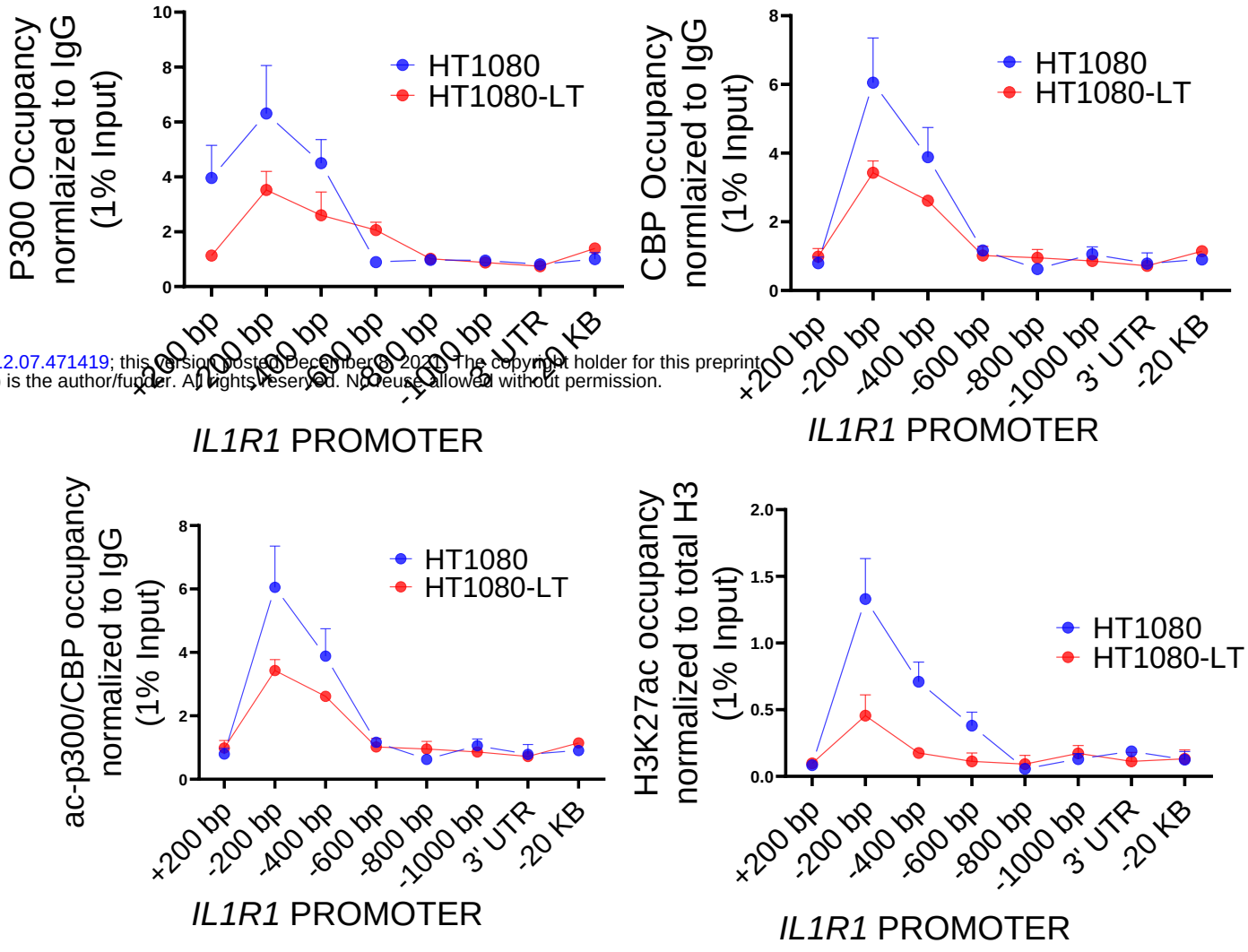

G

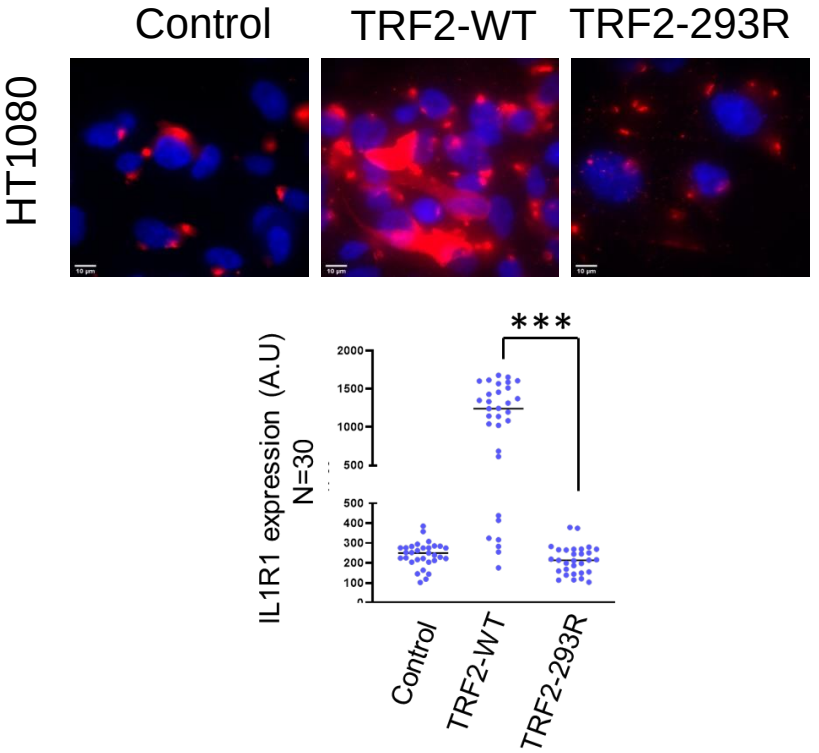

H

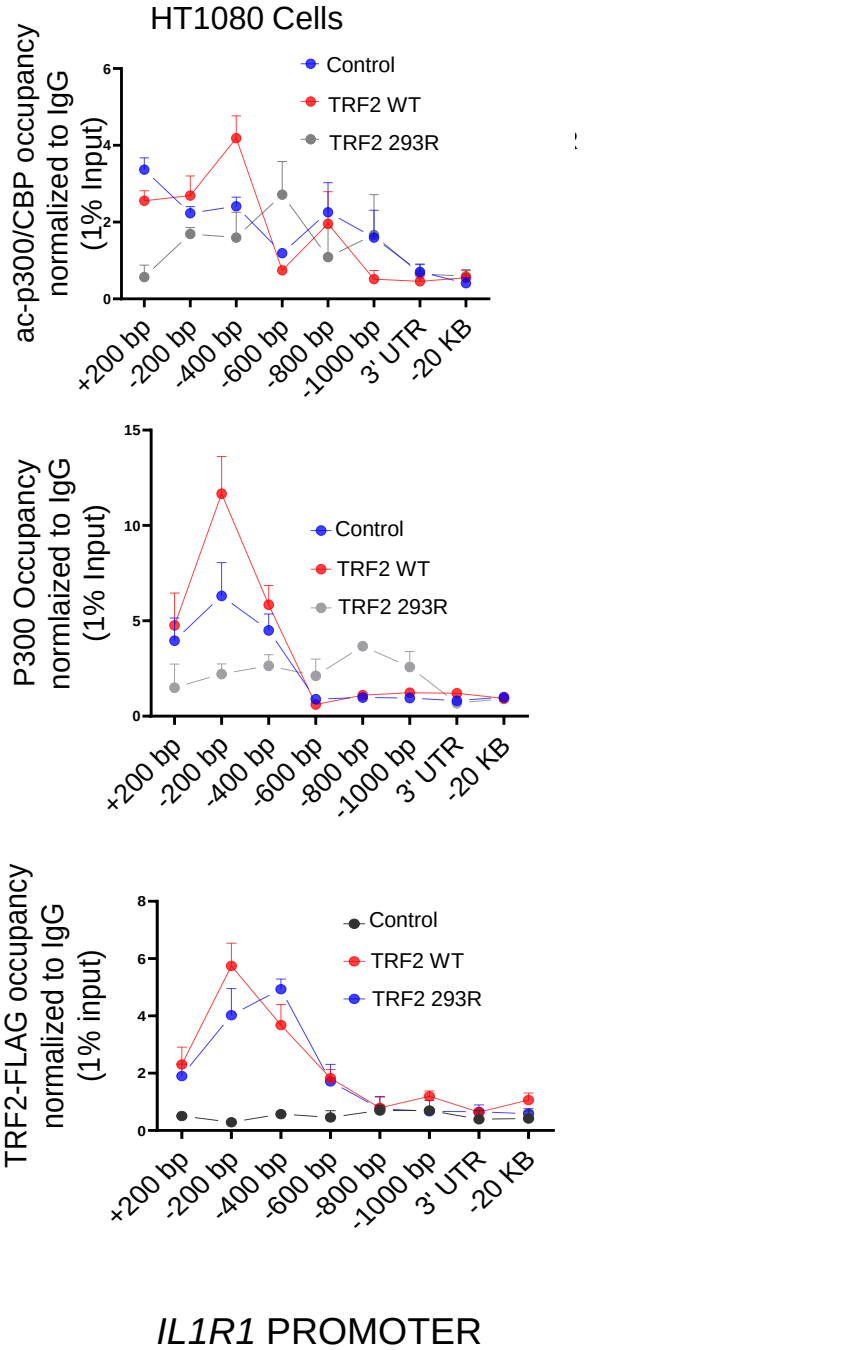

I

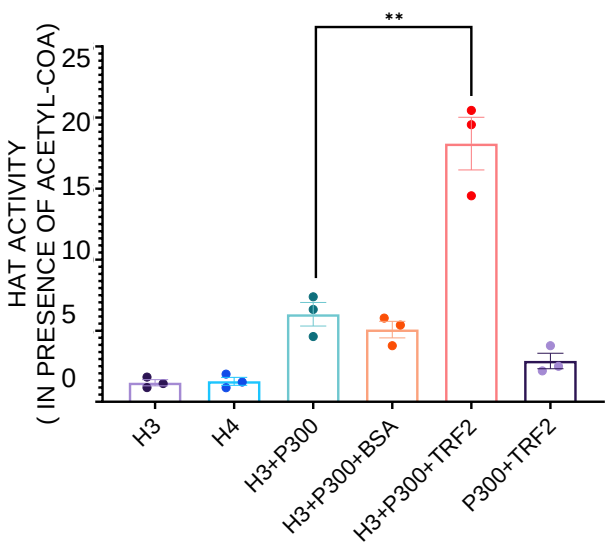

Figure 4 – TRF2 recruits p300 histone acetyl transferase to the *IL1R1* promoter

A. H3K27ac occupancy (normalized to total H3) over 1% input was checked on the *IL1R1* promoter in HT1080 and MDAMB231 cells in TRF2 high (cDNA) or low (shRNA) conditions.
B. p300 occupancy on the *IL1R1* promoter in HT1080 and MDAMB231 cells in TRF2 high (cDNA) and low (shRNA) conditions.
C-D. CBP and ac-p300/CBP occupancy on the *IL1R1* promoter in HT1080 cells in control or TRF2-induced conditions.
E. Immunoprecipitation (IP) in HT1080 cells using TRF2 antibody probed for p300, acp300/CBP, TRF2 or TRF1 (positive control) in input, TRF2 IP fraction or mock IP fraction.

F. Occupancy on the *IL1R1* promoter in HT1080 and HT1080-LT cells for p300, CBP and acp300/CBP. H3K27ac occupancy (normalized to total H3) over 1% input on the *IL1R1* promoter in the respective cell lines.
G. IL1R1 protein by immunofluorescence in HT1080 cells following transient over-expression of TRF2 WT-flag and the mutant TRF2-293R-flag (48 hrs post transfection).
F. acp300/CBP, p300 and flag-tag occupancy on the *IL1R1* promoter in HT1080 cells in control and cells transiently over-expressing TRF2 WT-flag or the mutant TRF2-293R-flag (48 hrs post transfection).
I. Histone acetyl transferase (HAT) assay was performed (see methods) using histone H3/H4 as a substrate for full length p300 in presence or absence of purified mammalian TRF2.

All protein ChIPs, other than histones, were normalized to 1% input and fold-change shown over respective IgGs. Statistical significance has been calculated using Mann-Whitney's non-parametric test for individual graphs where N≥5. In case of independent repetitions of the same experiment , unpaired T test with Welsh's correction was performed for significance (p values : * ≤ 0.05, ** ≤ 0.01, *** ≤ 0.001, **** ≤ 0.0001). Error bar correspond to standard error of mean from three independent experiments unless N is stated otherwise

Figure 5

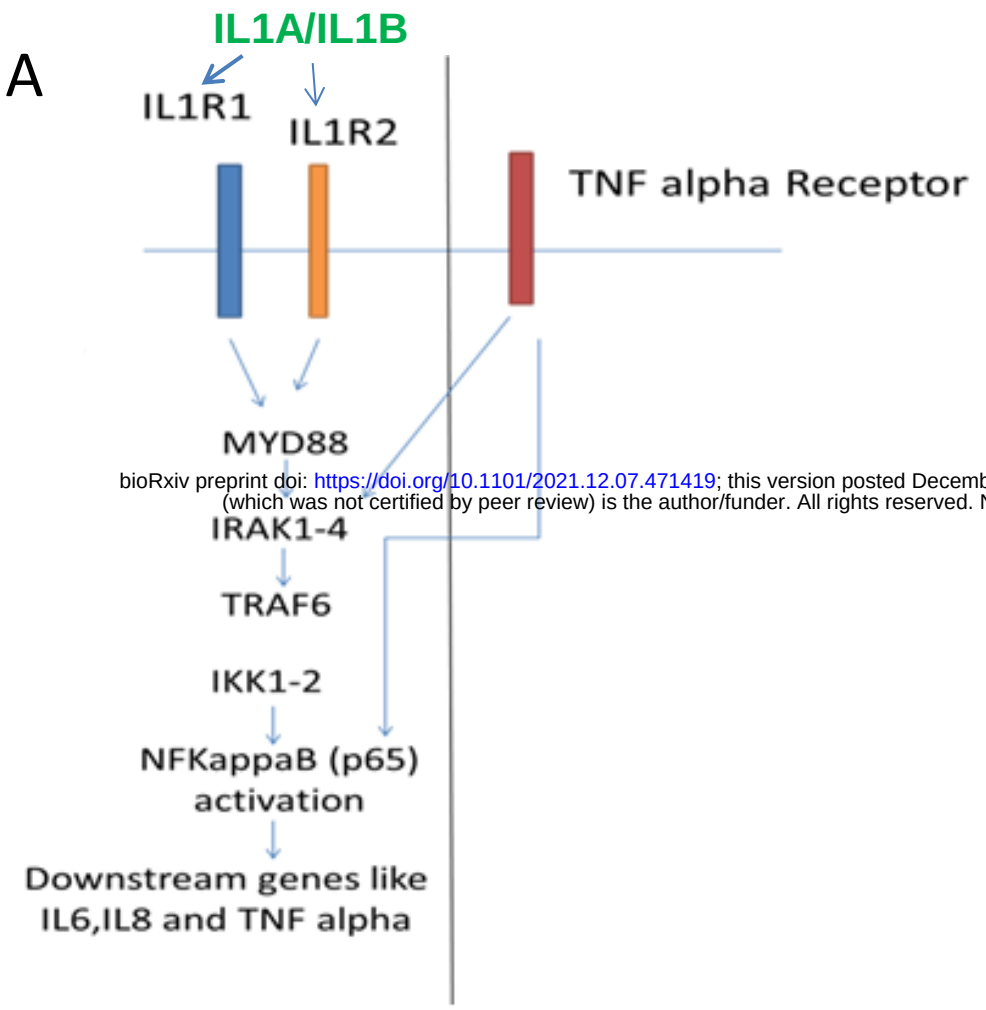

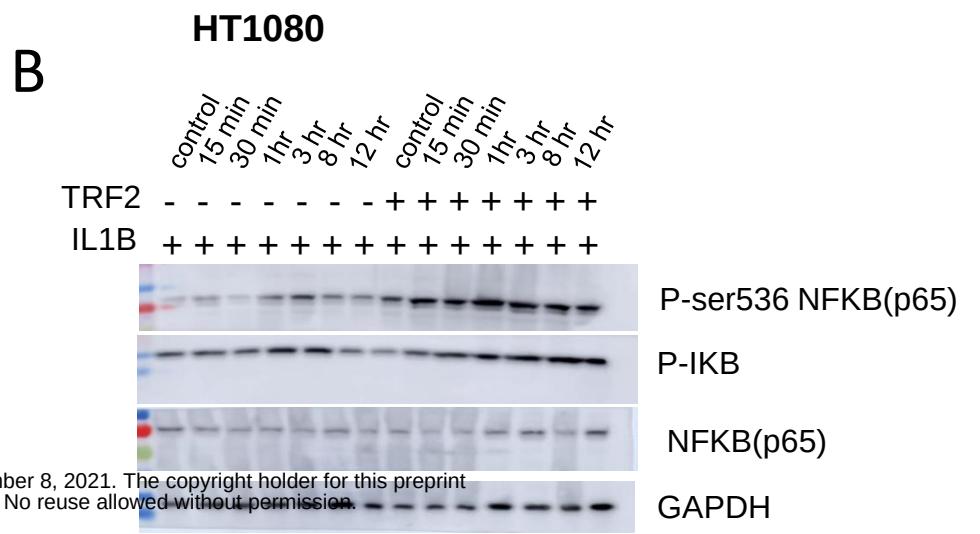

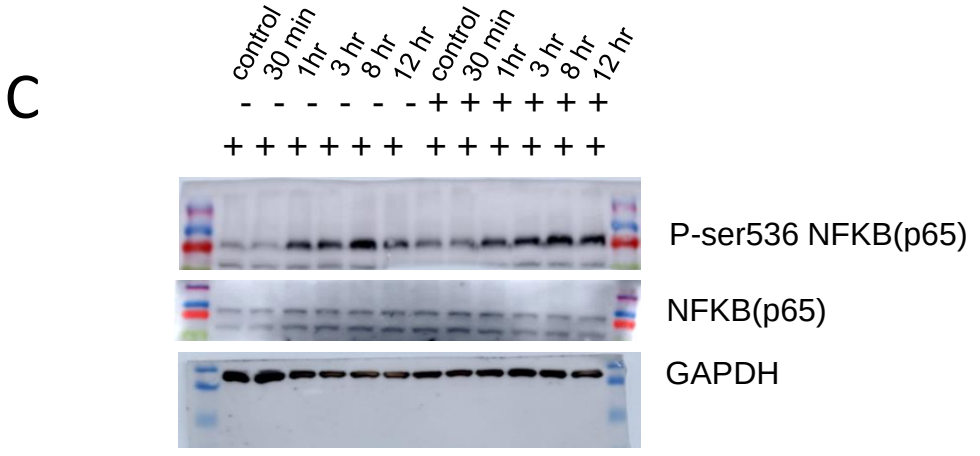

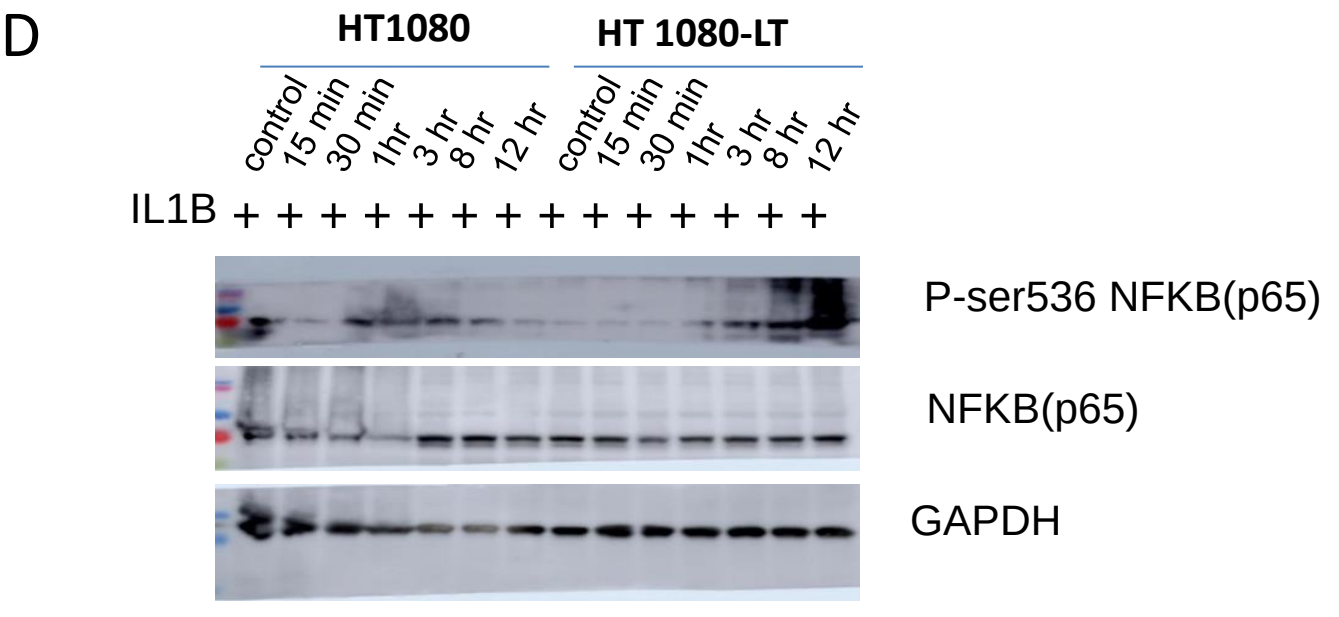

E

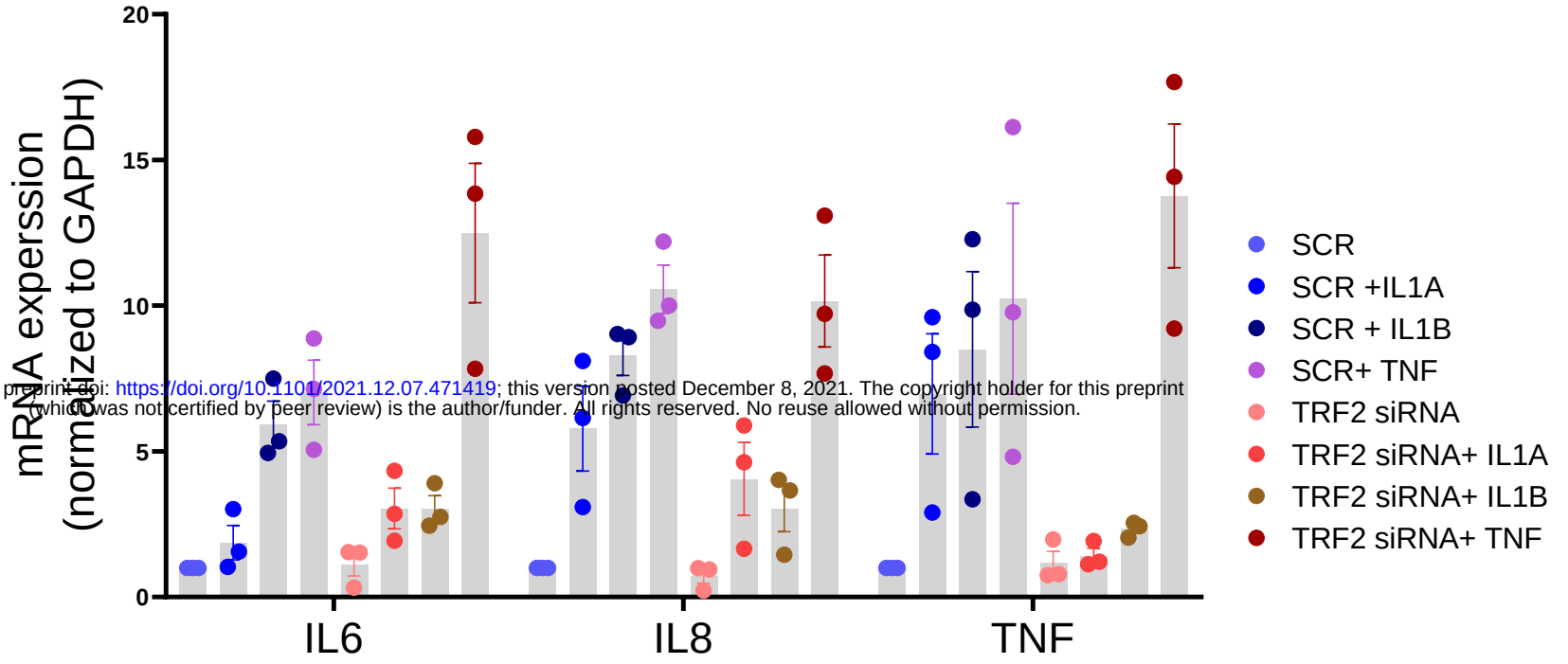

F

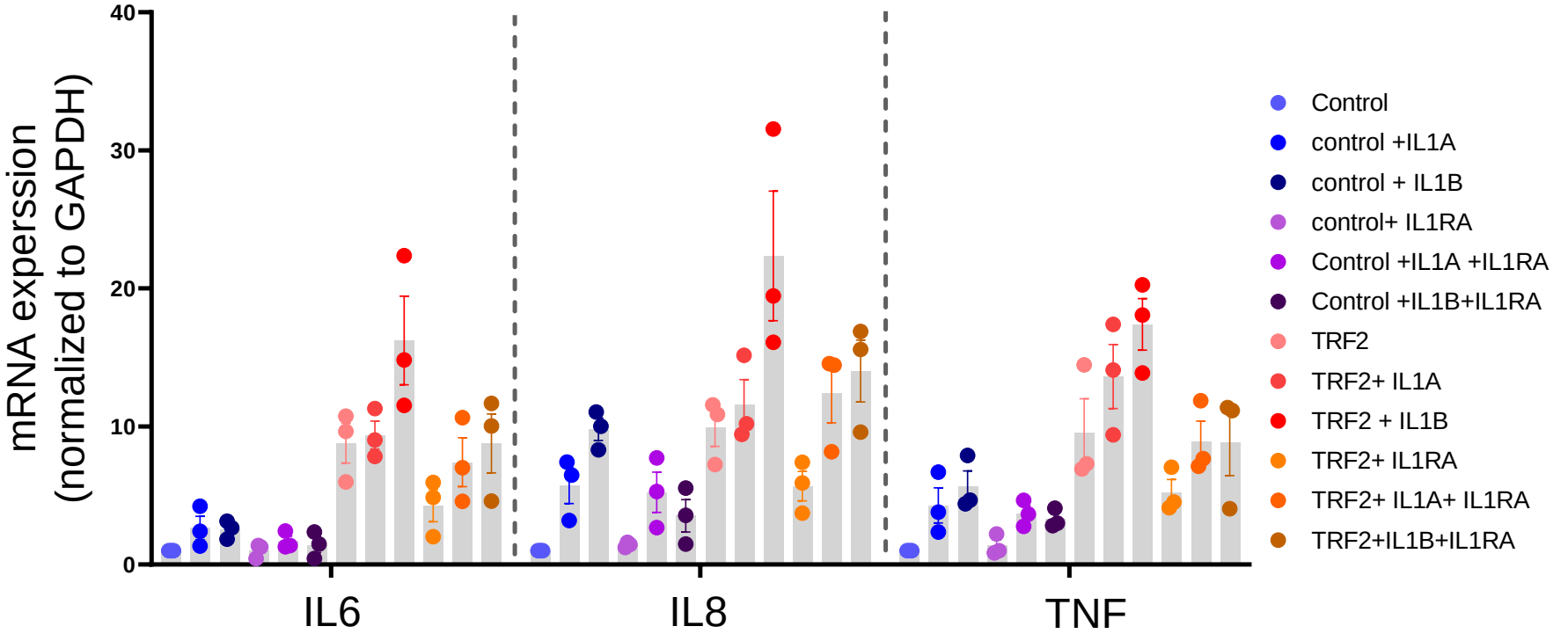

Figure 5 – TRF2 affects NFKappaB signaling through activation of *IL1R1*

A. Scheme showing the IL1 pathway (cognate receptors and ligands) that leads to NFKappaB (p65/RELA) activation via sub-cellular intermediates.

B-D. IL1B treatment (10 ng/ml) in HT1080 and MDAMB231 cells led to higher NFKappaB activation in cells with high TRF2. Activation of NFKappaB signaling was confirmed through Ser536 phosphorylation of NFKappaB (normalized to total NFKappaB) up to 12 hours following IL1B stimulation in HT1080 (B) and MDAMB231 (C) cells; further, phospho-inhibitory-Kappa-B (p-IKB in (B)) and NFkappaB activation in HT1080 versus HT1080-LT cells following IL1B stimulation (D) was consistent with TRF2-dependent activation of *IL1R1*.

E. NFKappaB downstream targets –IL6, IL8 and TNF were checked in HT1080 cells post IL1A, IL1B and TNF A treatment (10 ng/ml respectively) for 24 hrs in control (scrambled siRNA) or TRF2 low (TRF2 siRNA mediated knockdown) conditions respectively.

F. NFKappaB downstream targets –IL6, IL8 and TNF were checked in HT1080 cells post IL1B treatment (10 ng/ml) for 24 hrs in control or TRF2 over-expressed conditions in presence/absence of IL1 receptor antagonist (IL1RA; 20 ng/ml).

In case of independent repetitions of the same experiment , unpaired T test with Welsh's correction was performed for significance (p values : * ≤ 0.05, ** ≤ 0.01, *** ≤ 0.001, **** ≤ 0.0001). Error bar correspond to standard error of mean from three independent experiments unless N is stated otherwise.

Figure 6

A

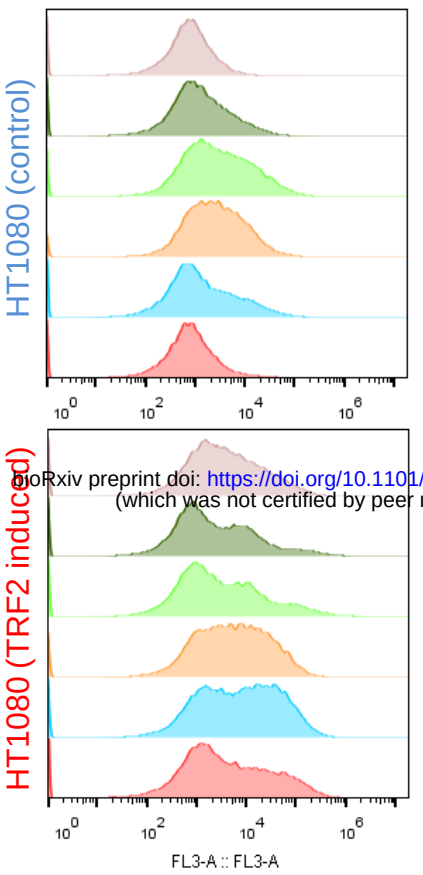

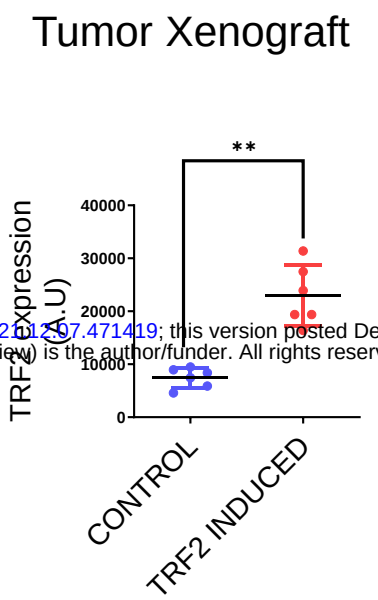

B

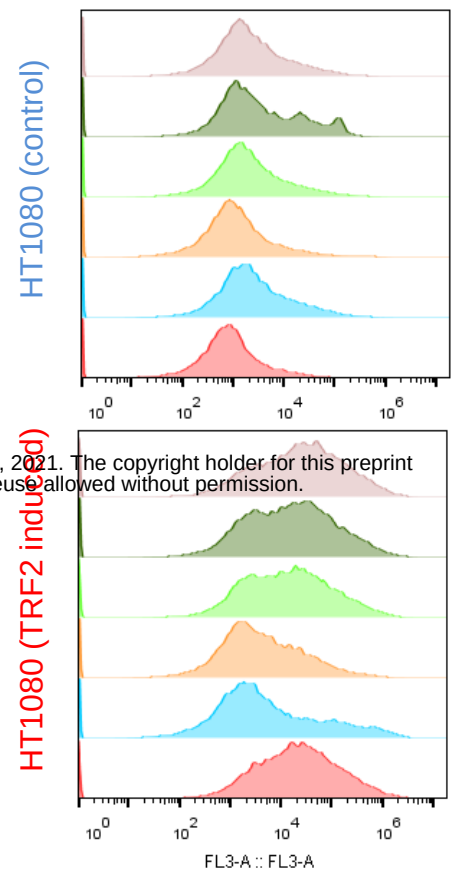

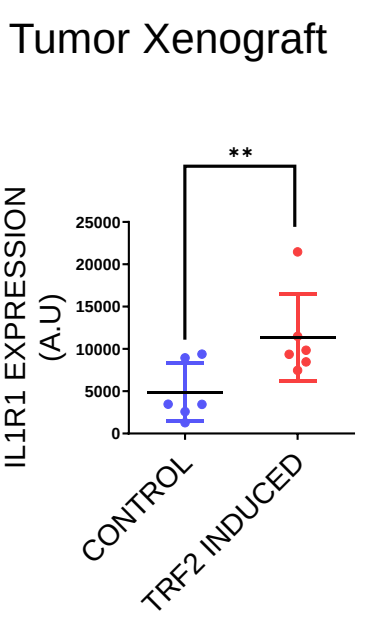

C

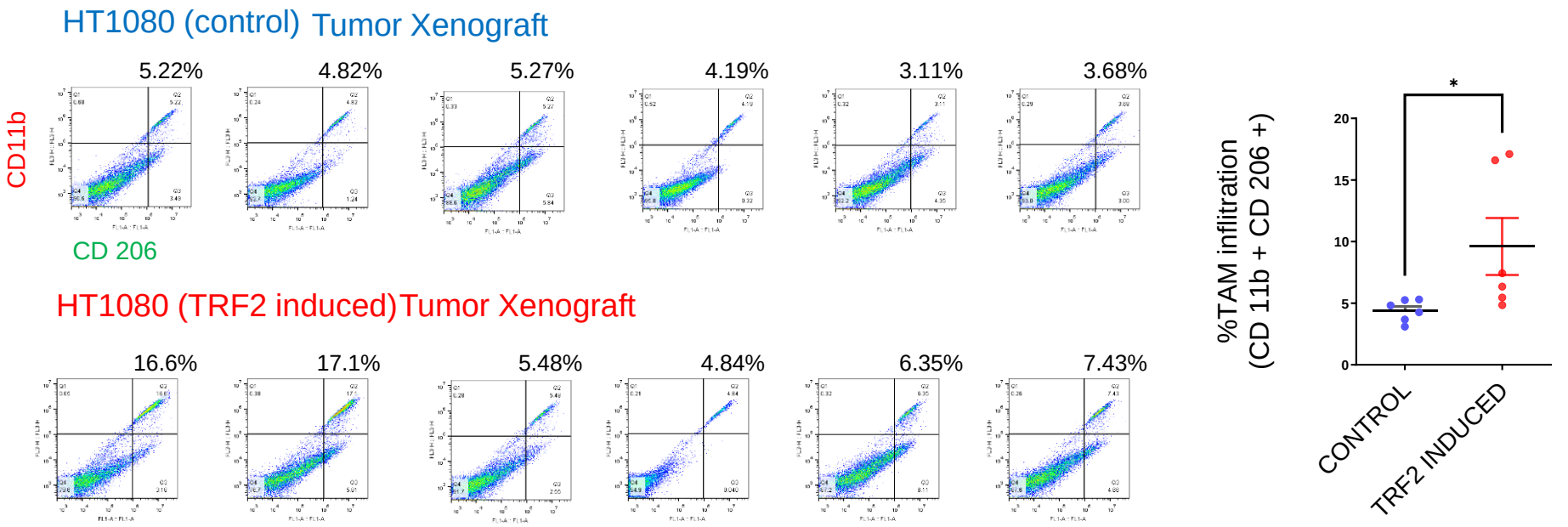

D

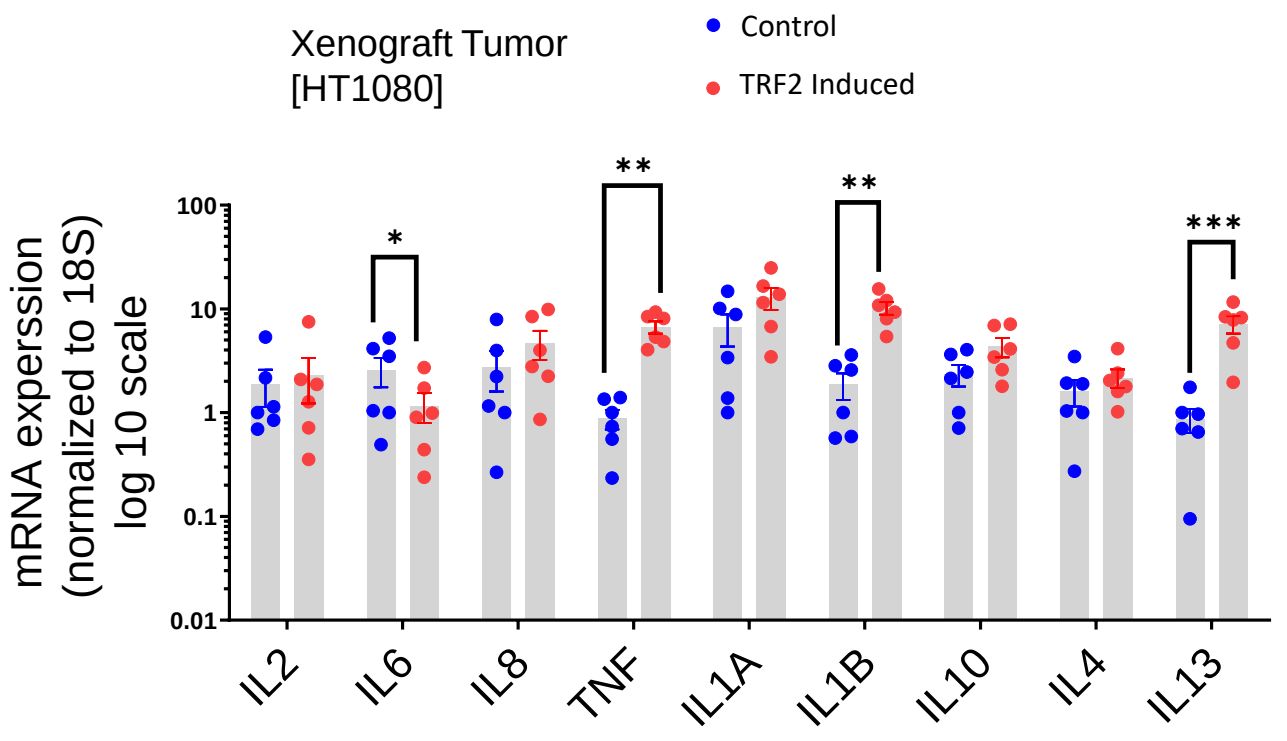

E

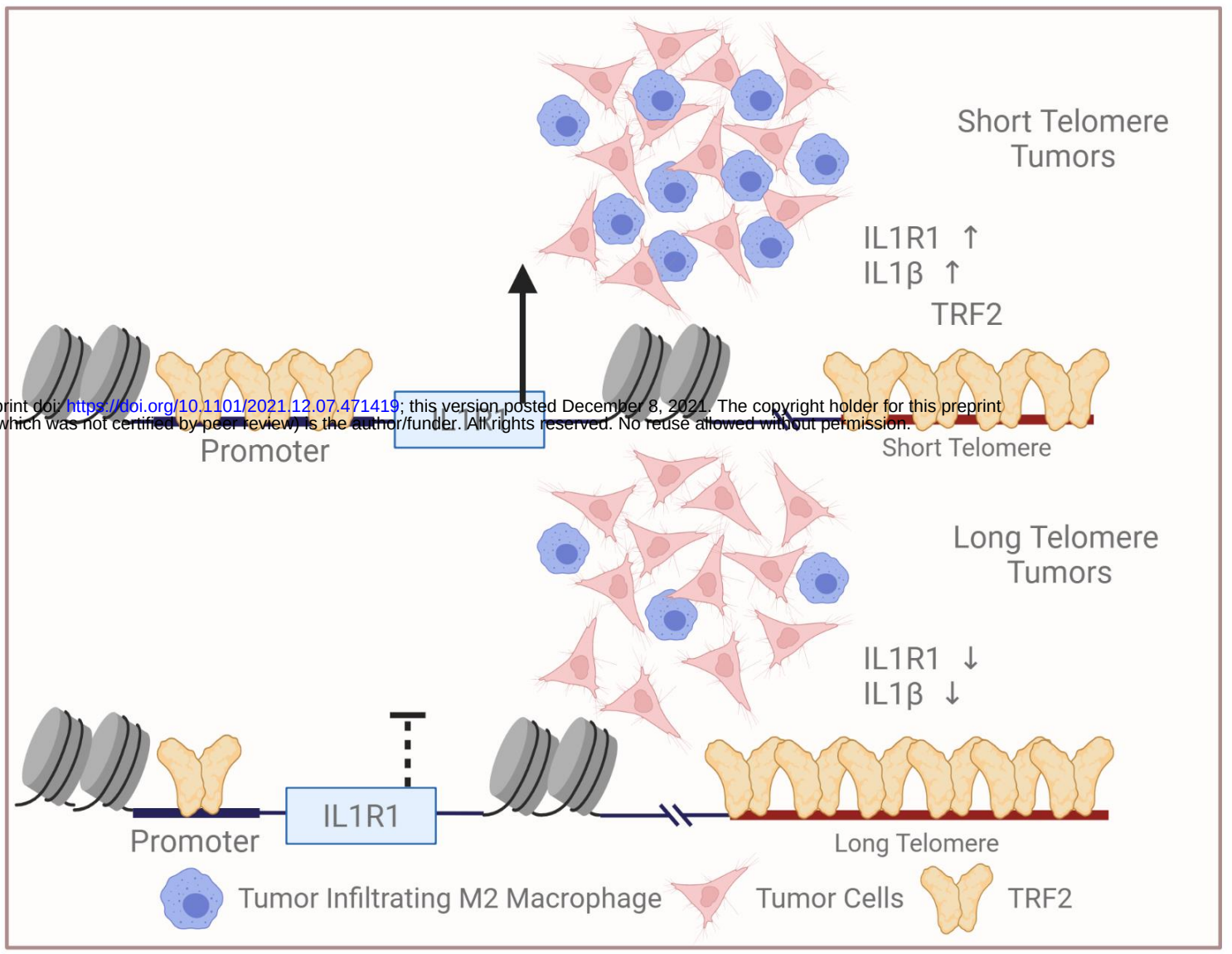

Created with BioRender.com

F

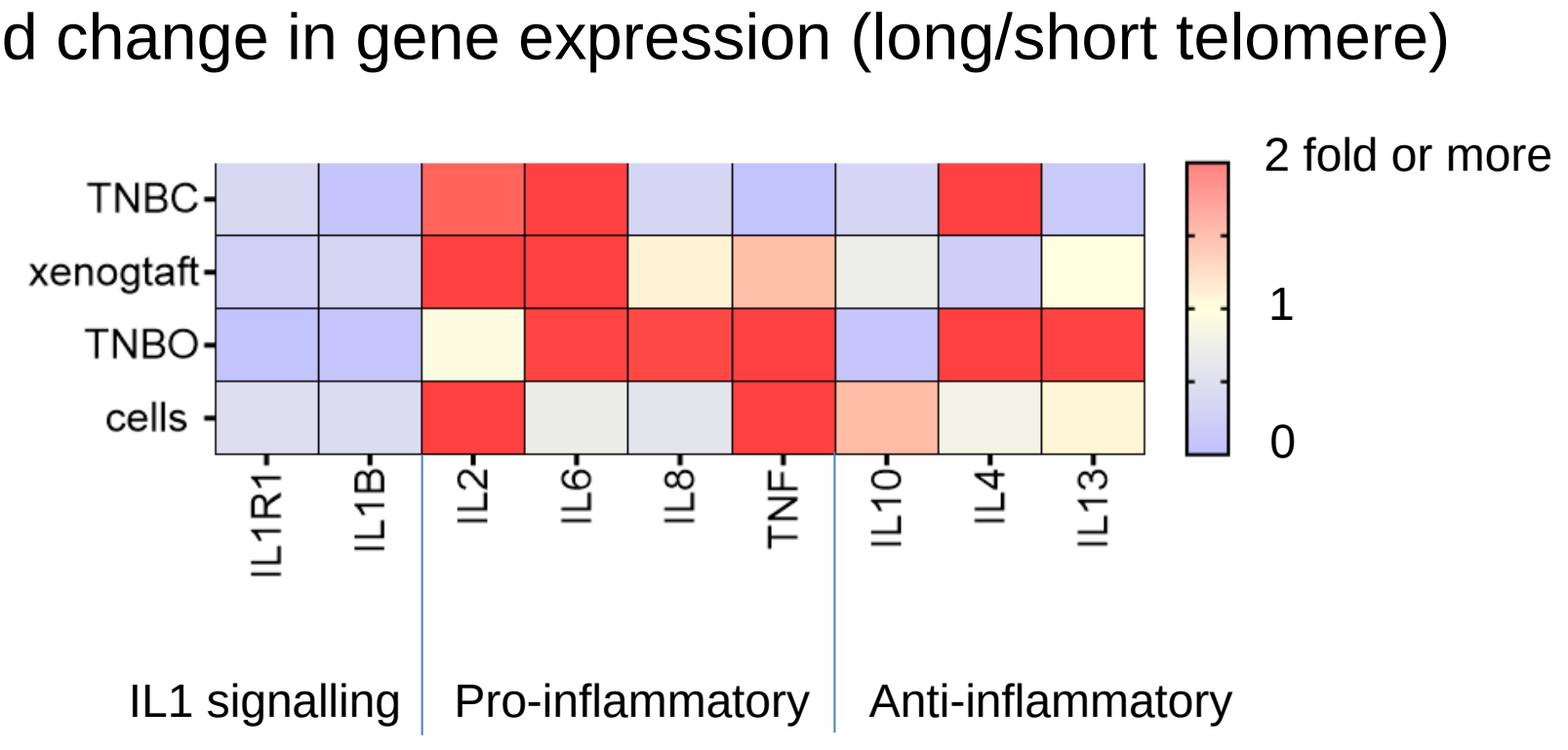

Figure 6 – TRF2 mediated activation of *IL1R1* results in higher TAM in TNBC tumors

A-B. TRF2 and IL1R1 levels in xenograft tumors in NOD SCID mice (see methods; control and TRF2 induced HT1080 cells; N=6) was assessed by immuno-flow cytometry and fluorescence signal for TRF2 and IL1R1 was plotted in the x-axis in log scale. Mean fluorescence signal from individual tumors in control and TRF2 induced tumors have been plotted in adjoining graphs.
C. Percentage of TAM was estimated in xenograft tumors (HT1080 control and HT1080- TRF2 induced) using markers CD11b and CD206. The percentage values HT1080 control and HT1080-TRF2 induced tumors were plotted in the adjoining summary graph.
D. mRNA expression for key cytokines- *IL1A,IL1B, IL2,IL6,IL8* , *TNF, IL10,IL4* and *IL13* were checked in xenograft tumors (HT1080 control and HT1080- TRF2 induced); *18S* was used for normalization.
E. Scheme depicting relatively low infiltration of TAM in tumors with longer telomeres vis-à-vis tumors with short telomeres. Reduced non-telomeric TRF2 binding at the IL1R1 promoter in tumors with long telomeres, and consequent low *IL1R1* activation, attenuated p65-mediated IL1-beta and macrophage infiltration. Figure created with BioRender. Com.

F. Heat map summarizing mRNA expression of key cytokines across the model systems used in the study: TNBC tissue, TNBC derived organoids, xenograft tumors and ex-vivo cells in relation to telomere length. Fold change of gene expression (long/short telomeres) color coded as per the reference legend along y-axis.

Statistical significance has been calculated using Mann-Whitney's non-parametric test for individual graphs (p values : * ≤ 0.05, ** ≤ 0.01, *** ≤ 0.001, **** ≤ 0.0001)

Supplementary Figure 1

Supplementary Figure 1A

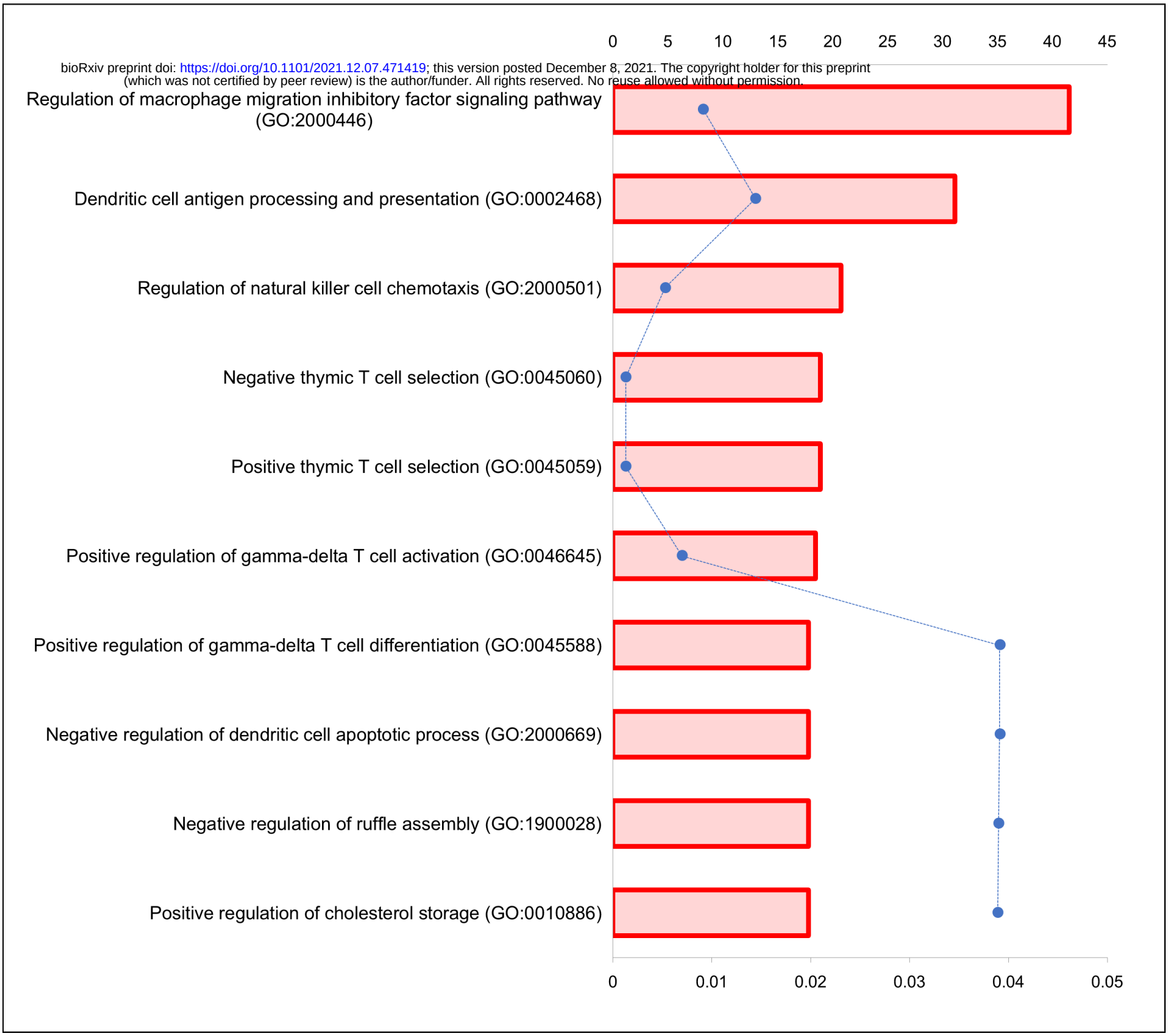

Supplementary Figure 1A:
Gene Ontology analysis of top 500 telomere elongation correlated genes curated across 31 cancer types (see methods). Top 10 hits for 'biological processes' represented in descending order of enrichment. Respective Fold enrichments shown by individual bars (Y-axis – top); the false discovery rate (FDR) shown by blue line.

Supplementary Figure 1B

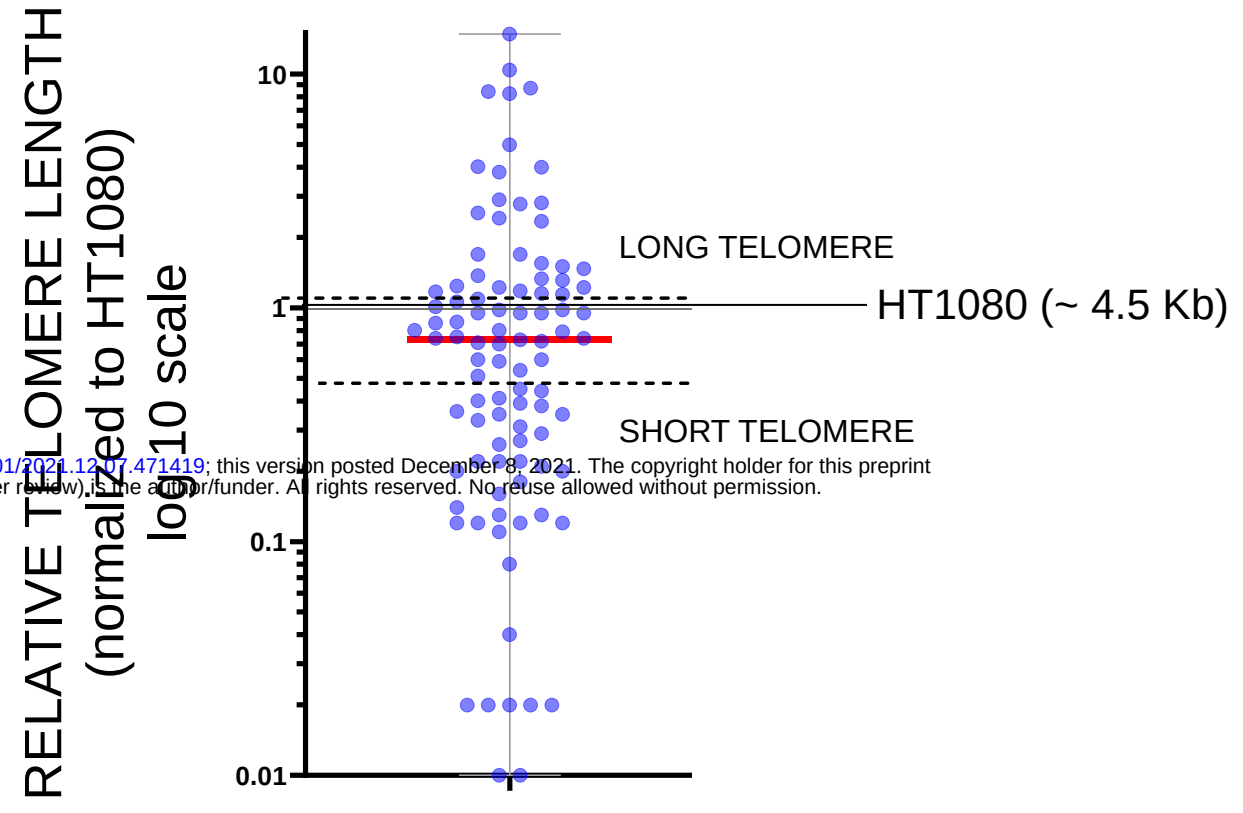

Supplementary Figure 1B:
Relative telomere length of Triple Negative Breast Cancer (TNBC) samples (N=94) by qRT PCR based method wherein signal from telomere specific primers was normalized to single copy number gene 36B4 for individual samples. All samples were run along with HT1080 DNA in the same PCR experiment and telomeric signal from HT1080 was used as a reference (telomere length ~4.5 Kb) to which all TNBC samples were compared. The median telomere length shown by red bar; samples >50% of median were designated as long and <50% of median as short telomere samples (indicated by dotted line).

Supplementary Figure 1C

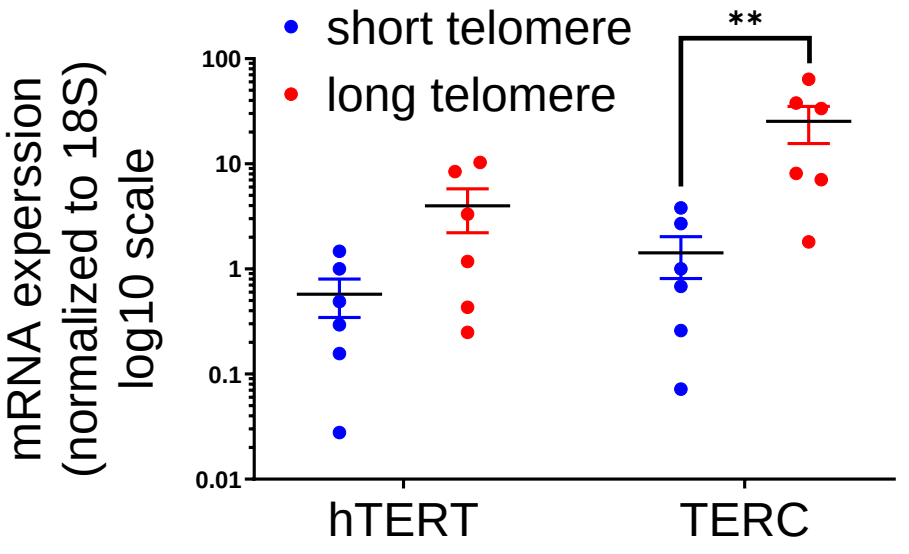

Supplementary Figure 1C:

mRNA expression of *hTERT* and *TERC* in six TNBC samples (long or short telomeres) normalized to the *18S* gene in respective samples. Statistical significance was calculated using Mann-Whitney's non-parametric test (p values : * ≤ 0.05, ** ≤ 0.01, *** ≤ 0.001, **** ≤ 0.0001)

Supplementary Figure 1D

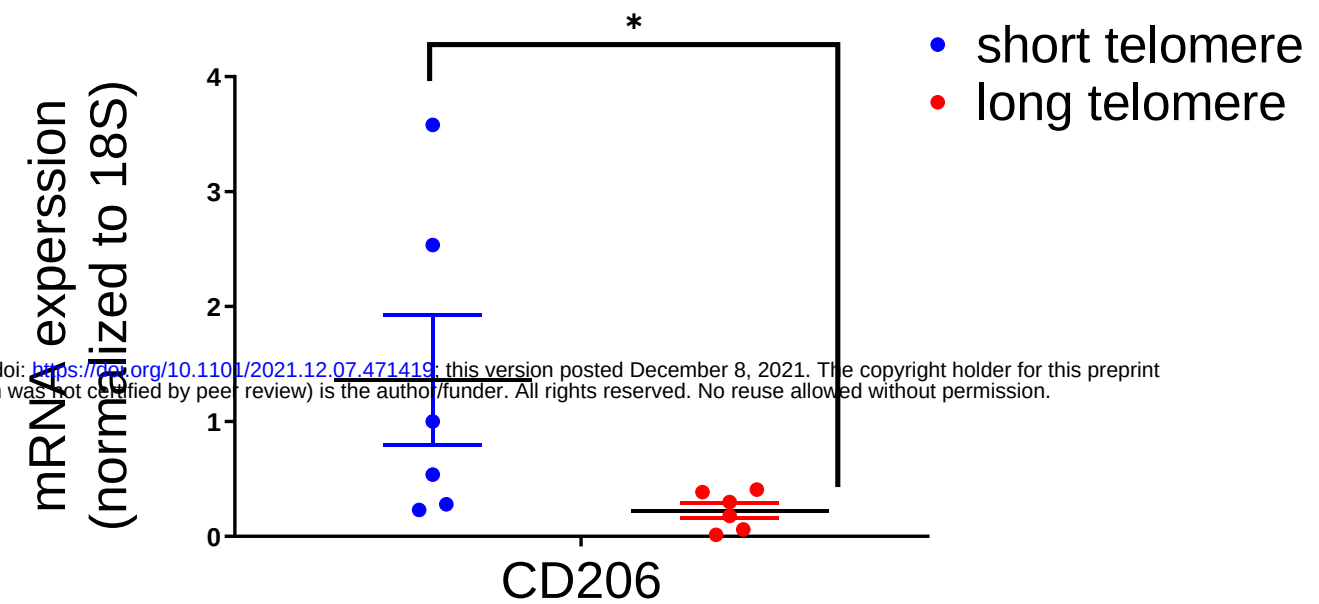

Supplementary Figure 1D:

mRNA expression of M2 macrophage marker *CD206* in six TNBC samples (long or short telomeres) normalized to the *18S* gene in respective cases. Statistical significance was calculated using Mann-Whitney's non-parametric test (p values: * ≤ 0.05).

Supplementary Figure 1E

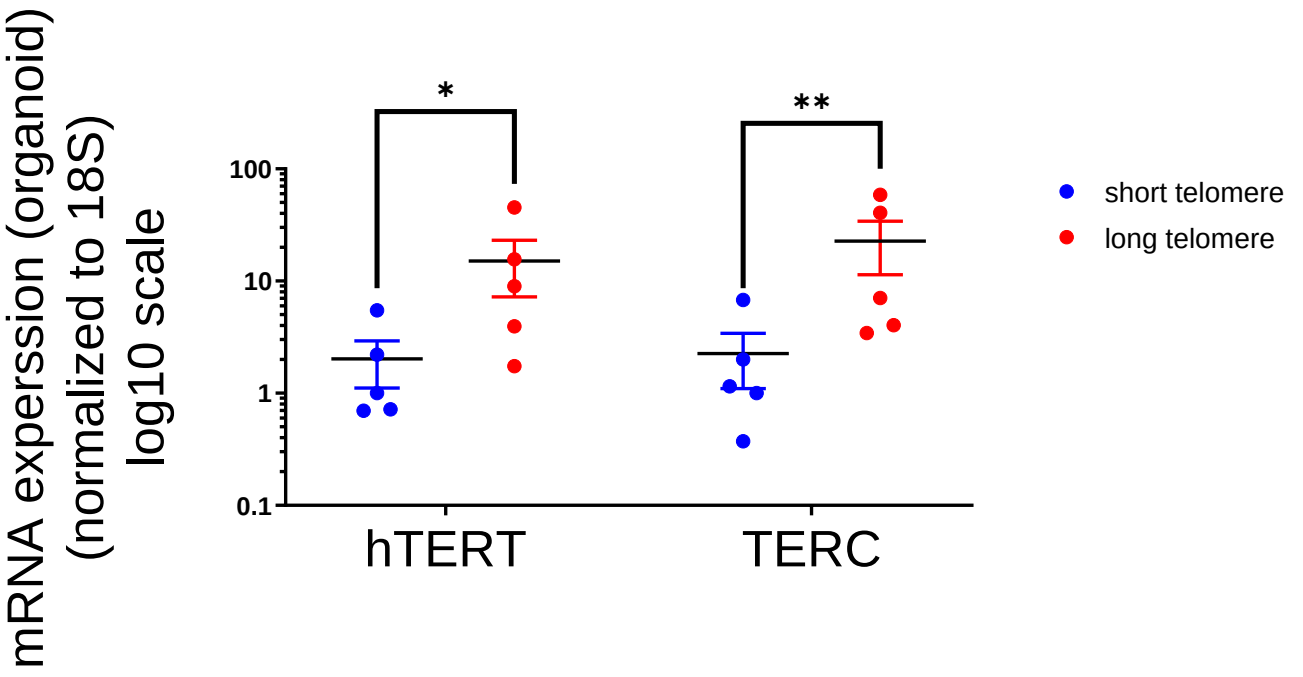

Supplementary Figure 1E:

mRNA expression of *hTERT* and *TERC* in five TNBC organoids (long or short telomeres) normalized to *18S* gene in respective cases. Statistical significance was calculated using Mann-Whitney's non-parametric test (p values : * ≤ 0.05, ** ≤ 0.01).

Supplementary Figure 1F

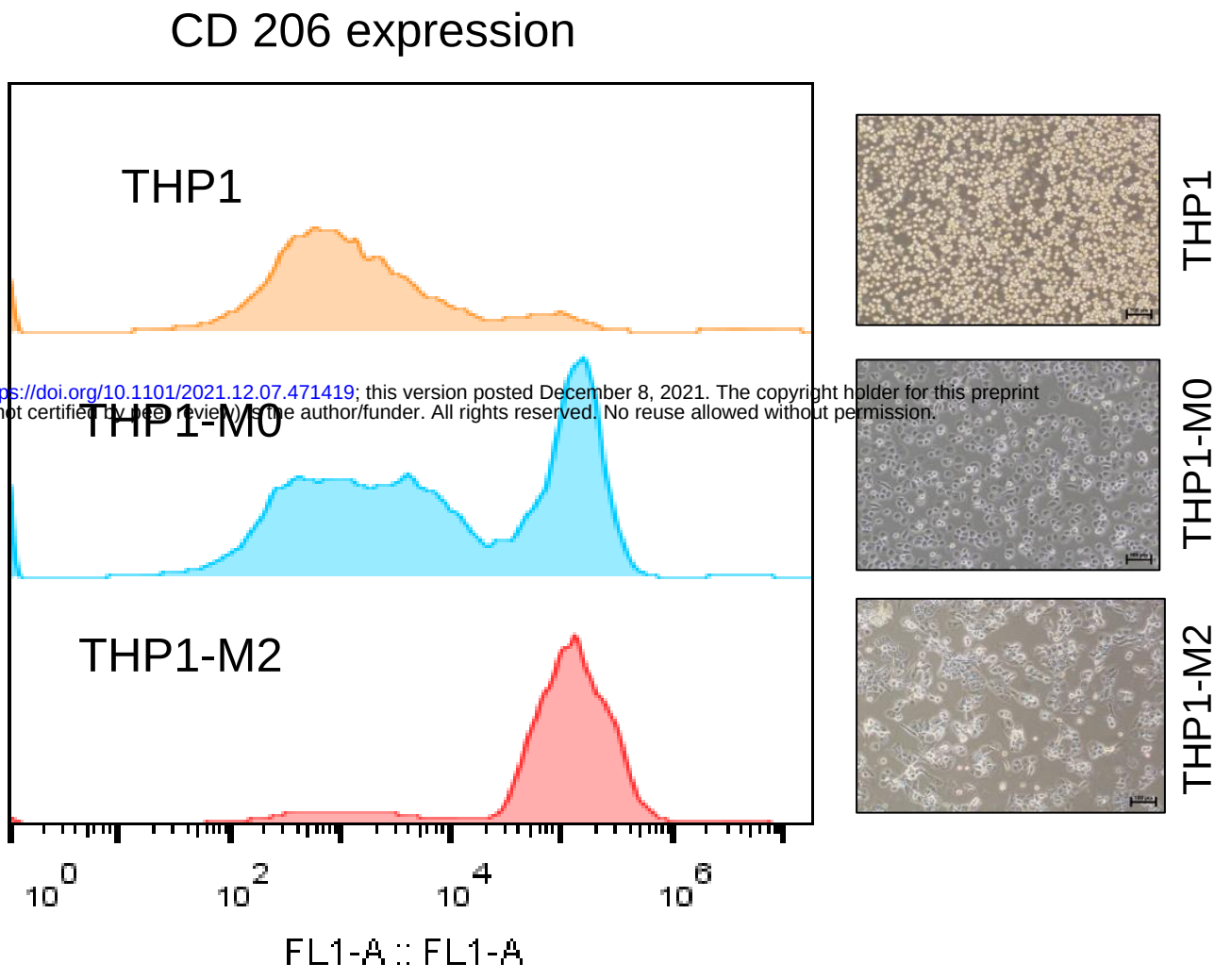

Supplementary Figure 1F:

CD206 expression was checked by immuno-flow cytometry in THP1 cells and macrophages differentiated from THP1 cells into M0 and M2 types (see methods) and plotted along X-axis in log scale . Bright-field images at 10X magnification for each cell stage shown in right panel.

Supplementary Figure 1G

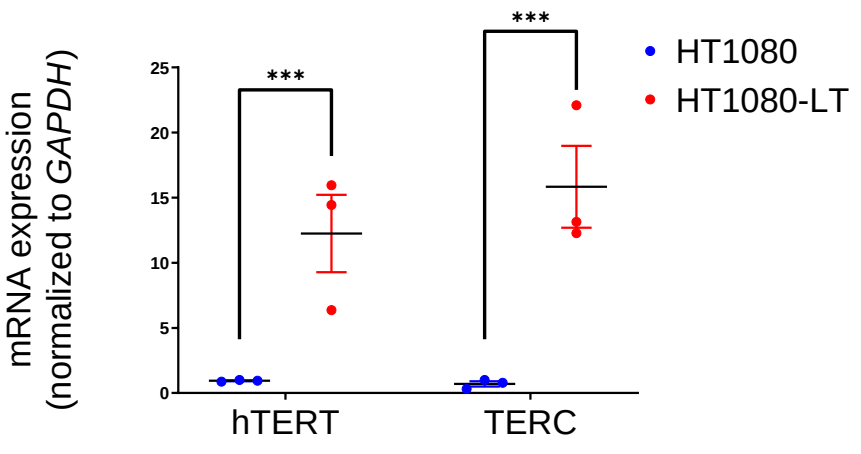

Supplementary Figure 1H

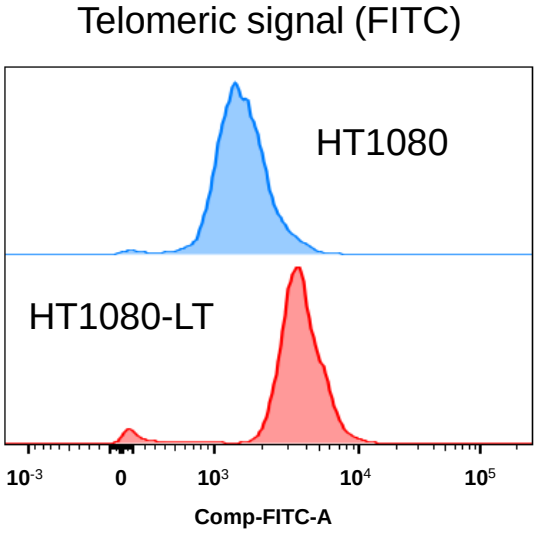

Supplementary Figure 1G-H:

mRNA expression of *hTERT* and *TERC* in HT1080 and HT1080-LT cells (normalized to GAPDH) and relative telomere length was assessed by flow-cytometry analysis of telomeric signal (FITC) plotted along x-axis in log scale. Statistical significance was calculated using t-Test with Welch's correction (p values : * ≤ 0.05, ** ≤ 0.01, *** ≤ 0.001, **** ≤ 0.0001)

Supplementary Figure 1I

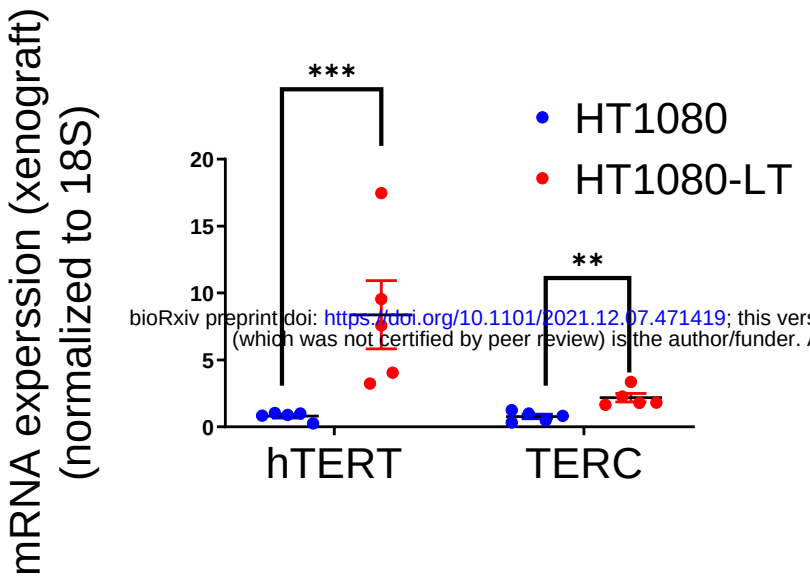

Supplementary Figure 1J

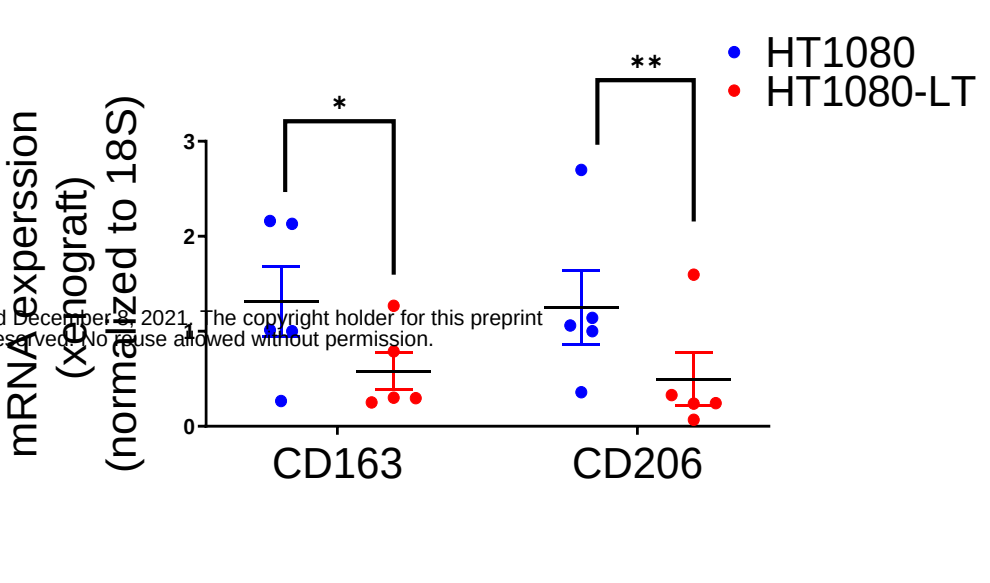

Supplementary Figure 1I-J:

mRNA expression of *hTERT* and *TERC* (normalized to 18S) in xenograft tumors in NOD-SCID mice injected with HT1080 and HT1080-LT cells. Similarly, mouse M2 markers CD163 and CD206 were checked in the xenograft tumors using human 18S for normalization. Statistical significance was calculated using Mann-Whitney's non-parametric test (p values : * ≤ 0.05, ** ≤ 0.01, *** ≤ 0.001, **** ≤ 0.0001)

Supplementary Figure 1K

HT1080 (short telomere)

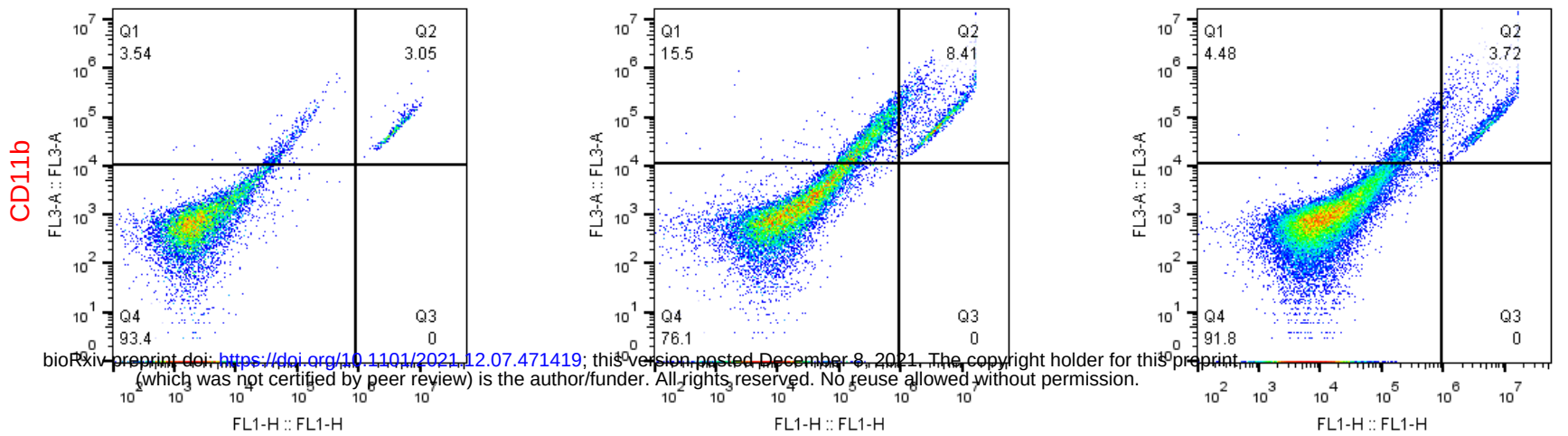

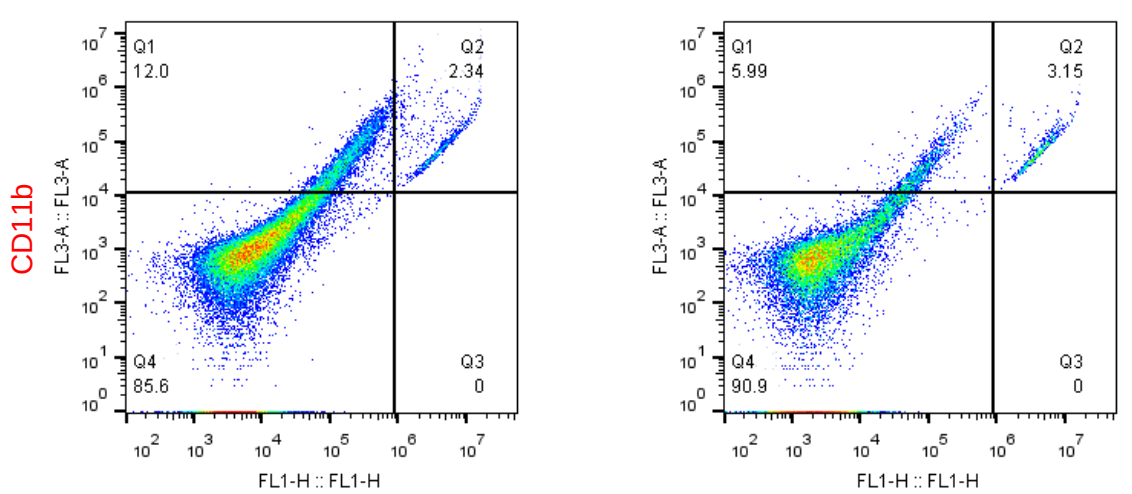

HT1080-LT (long telomere)

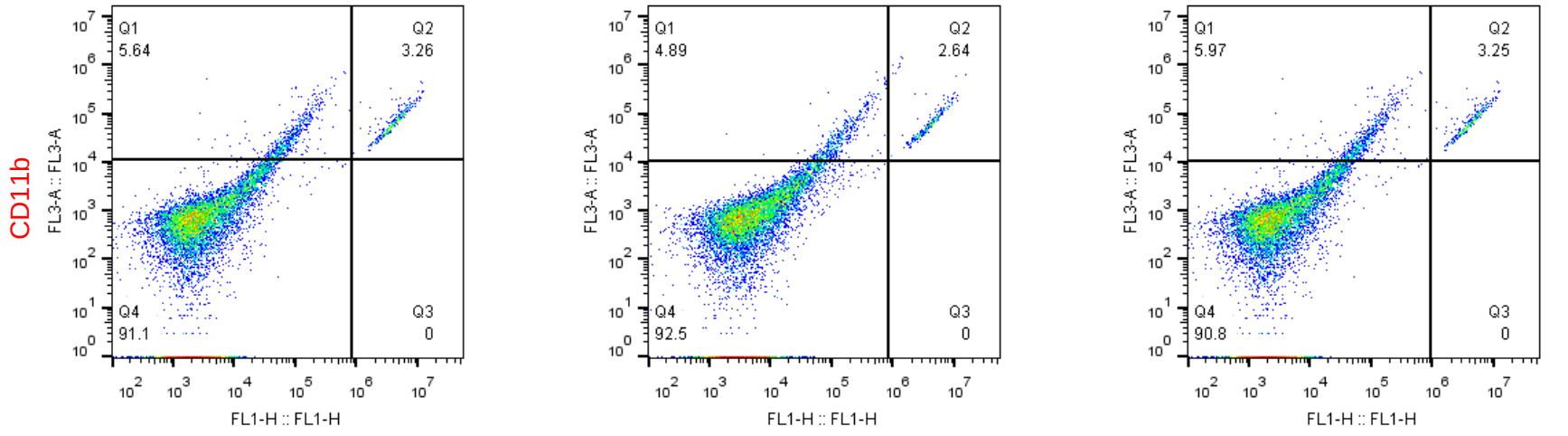

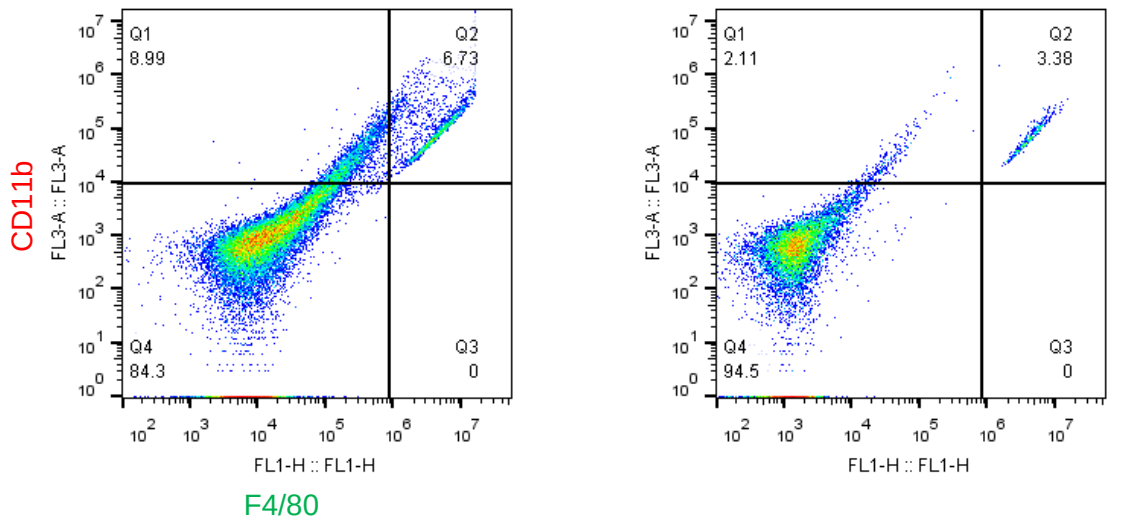

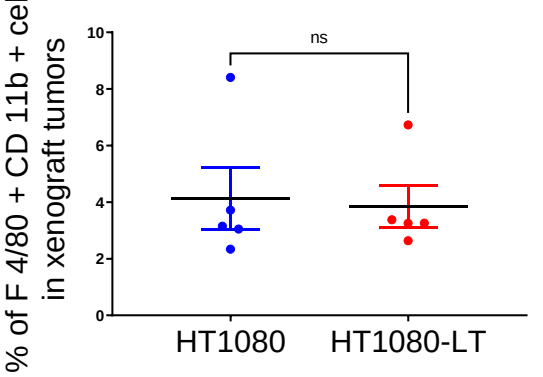

Supplementary Figure 1K:
Percentage of F4/80 positive cells was estimated in xenograft tumors from HT1080 or HT1080-LT cells in top right quadrant. The percentage values for HT1080 and HT1080-LT tumors shown in summary graph – right bottom.

Supplementary Figure 1L

TNBC – CLINICAL TISSUE

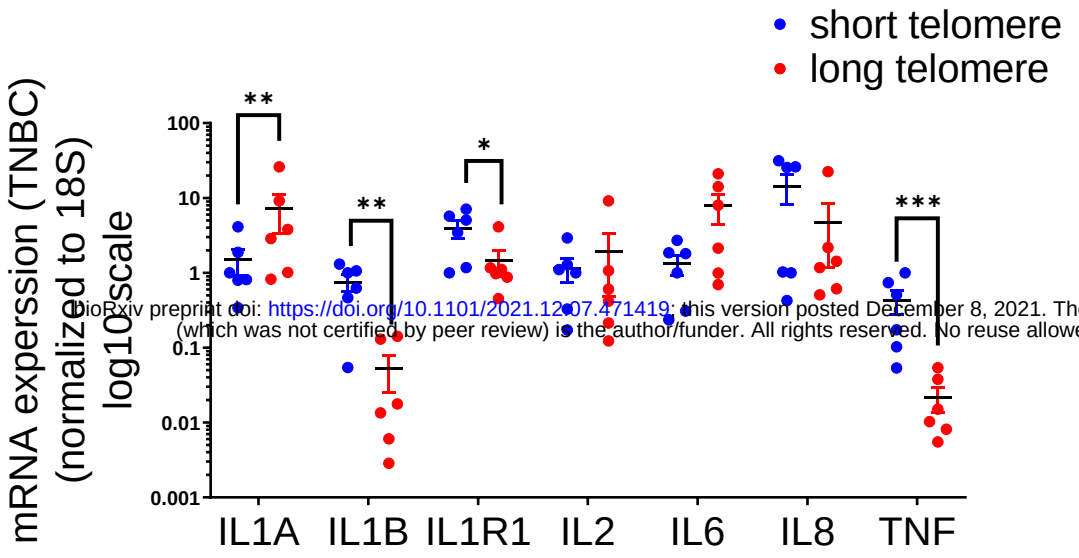

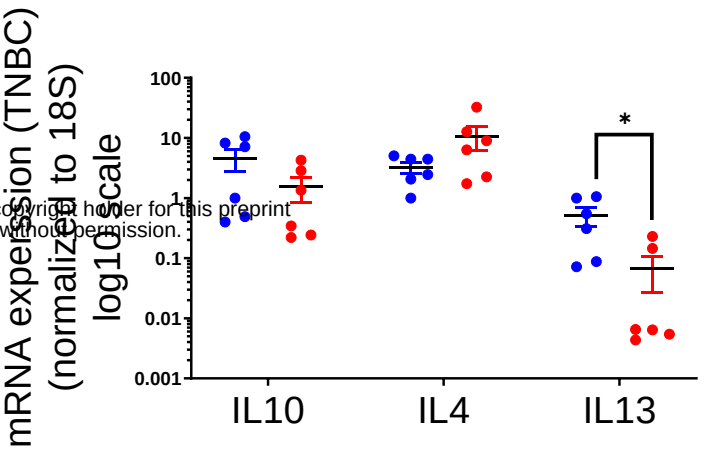

TNBC – ORGANOID

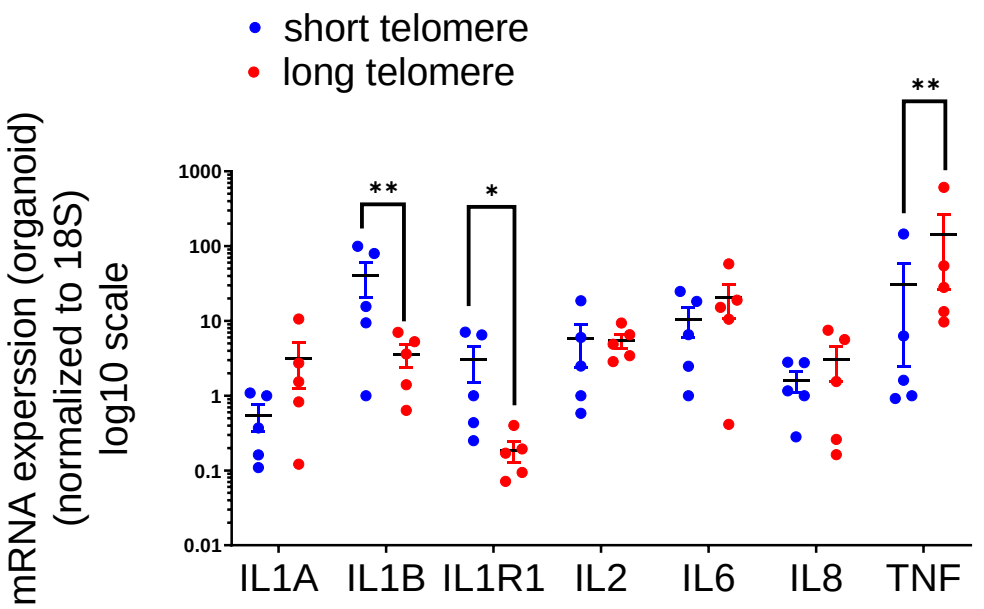

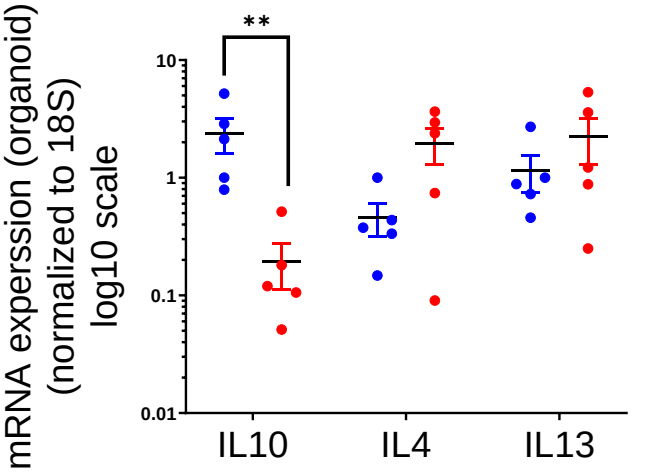

XENOGRAFT

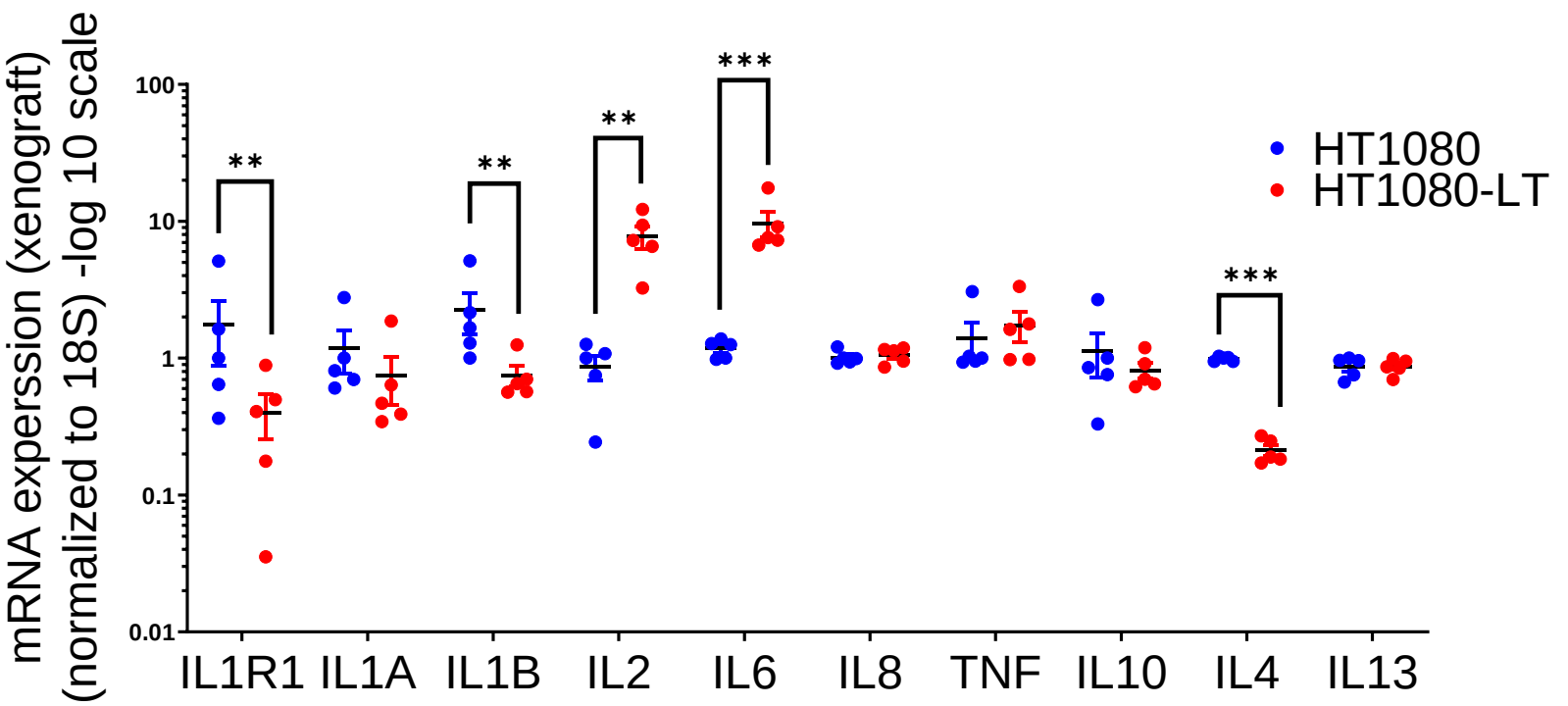

Supplementary Figure 1L:

mRNA expression of *IL1R1* and other key cytokines: *IL1A, IL1B, IL2, IL6, IL8*, *TNF, IL10, IL4* and *IL13* in long or short telomere cancer cells in TNBC tissue, TNBC derived organoids and xenograft tumors from HT1080 or HT1080-LT cells; the *18S* gene was used for normalization in respective cases.
Statistical significance was calculated using Mann-Whitney's non-parametric test (p values: * ≤ 0.05, ** ≤ 0.01, *** ≤ 0.001, **** ≤ 0.0001)

Supplementary Figure 1M

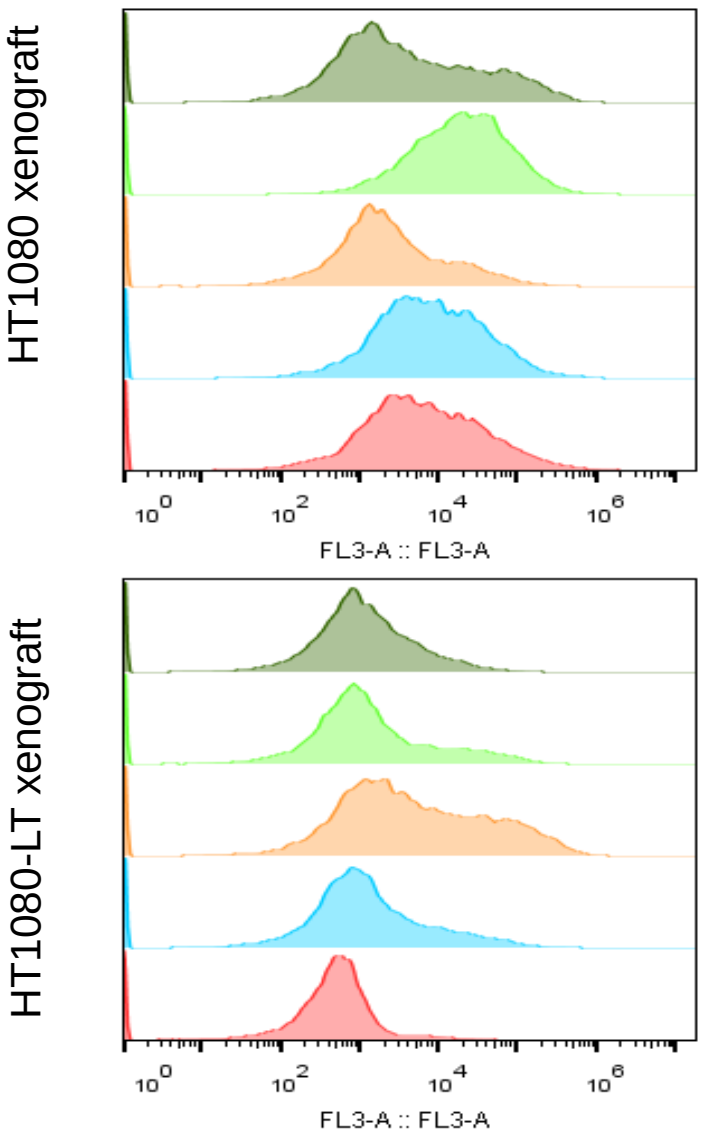

Supplementary Figure 1M:
IL1R1 expression by immuno-flow cytometry in xenograft tumors from NOD-SCID mice injected with HT1080 or HT1080-LT cells (see methods) and plotted along X-axis in log scale.

Supplementary Figure 1N

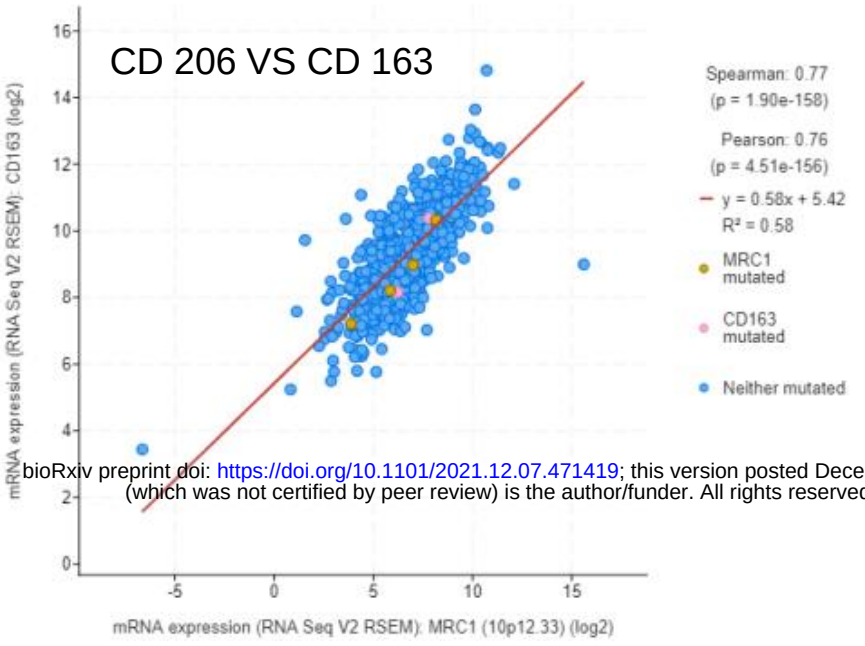

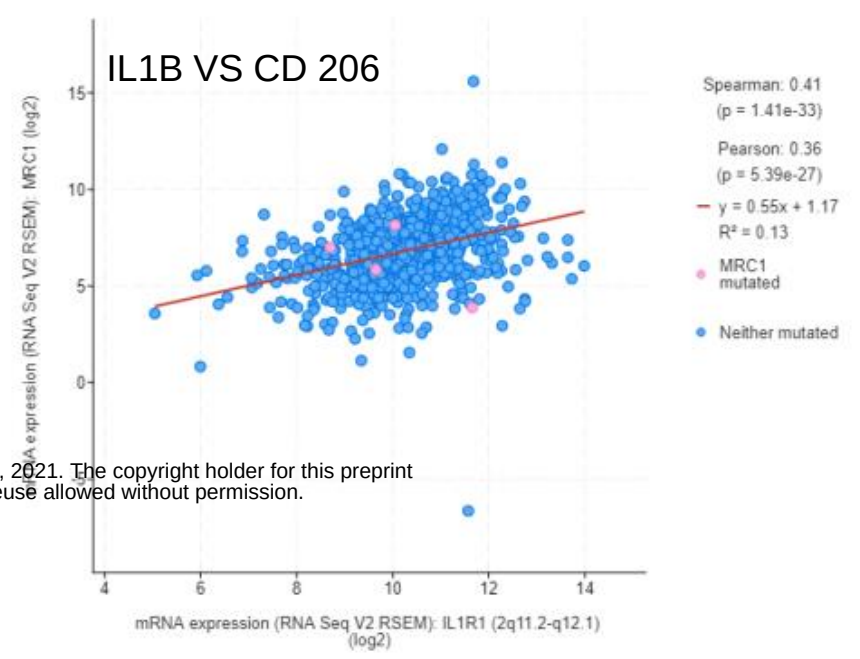

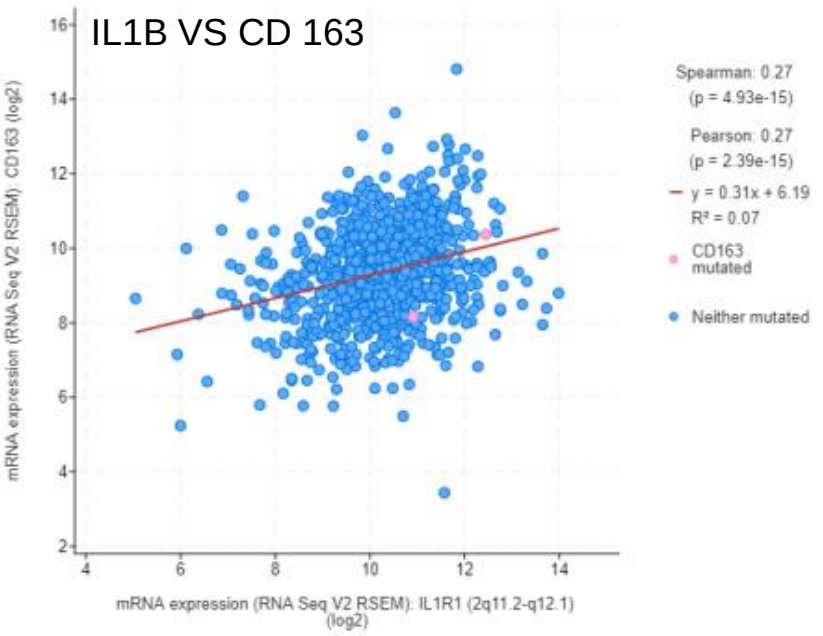

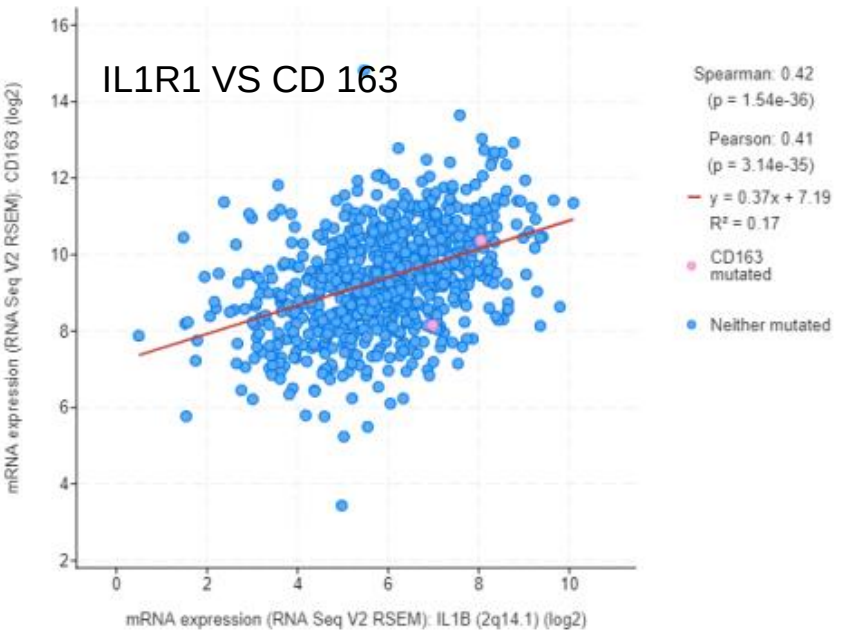

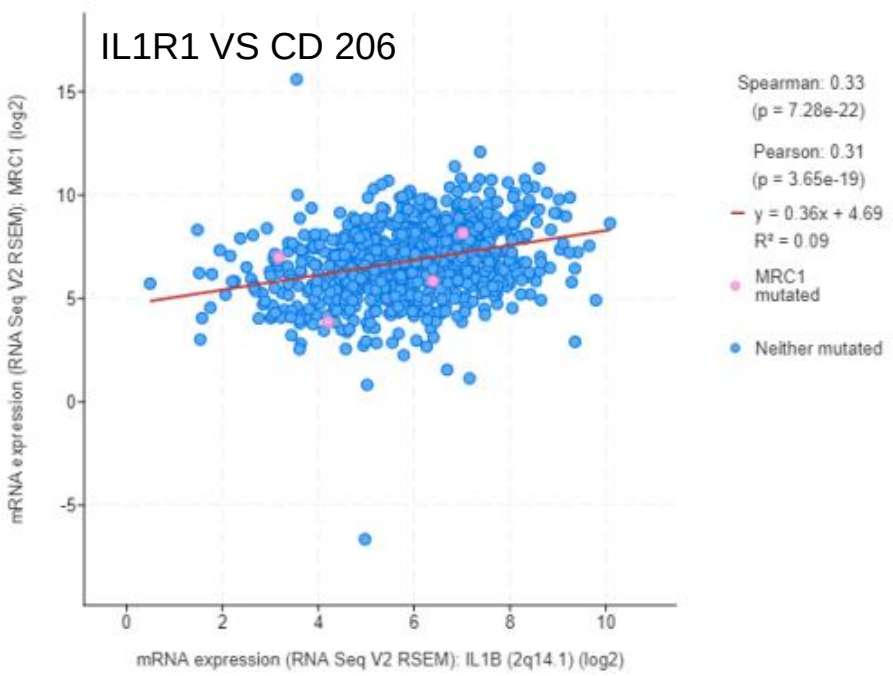

Supplementary Figure 1N:

Correlation of *IL1R1/L1B* with *CD163/CD206* from publicly available breast cancer microarray dataset of 817 TNBC patients (cBIOPORTAL; see methods).

Supplementary Figure 2

Supplementary Figure 2A

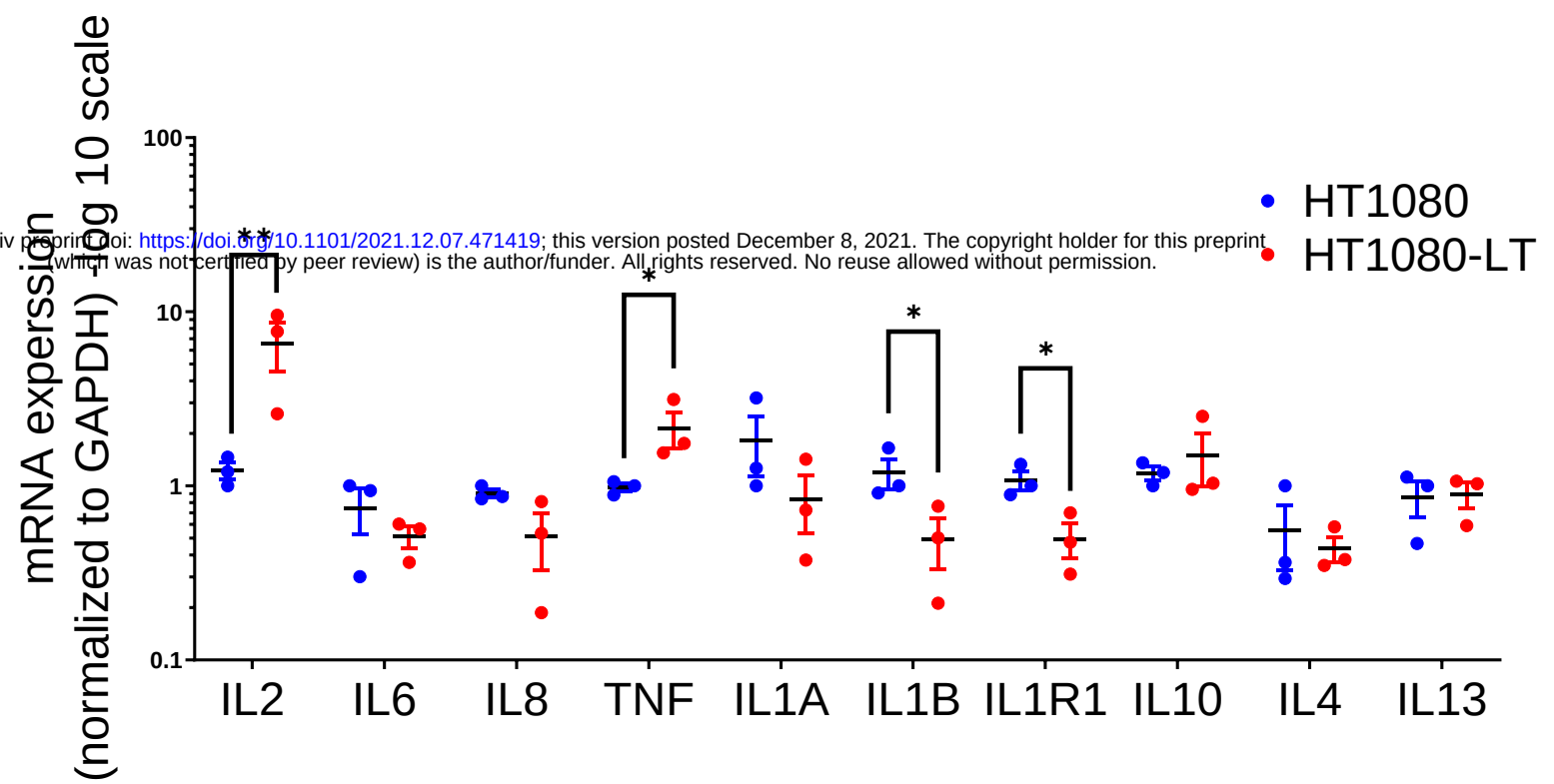

Supplementary Figure 2A:

mRNA expression for *IL1R1* and other key cytokines: *IL1A, IL1B, IL2, IL6, IL8*, *TNF, IL10, IL4* and *IL13* in long or short telomere HT1080 or HT1080-LT cells. *GAPDH* was used for normalization.
Statistical significance was calculated using t-Test with Welch's correction (p values : * ≤ 0.05, ** ≤ 0.01, *** ≤ 0.001, **** ≤ 0.0001)

Supplementary Figure 2B

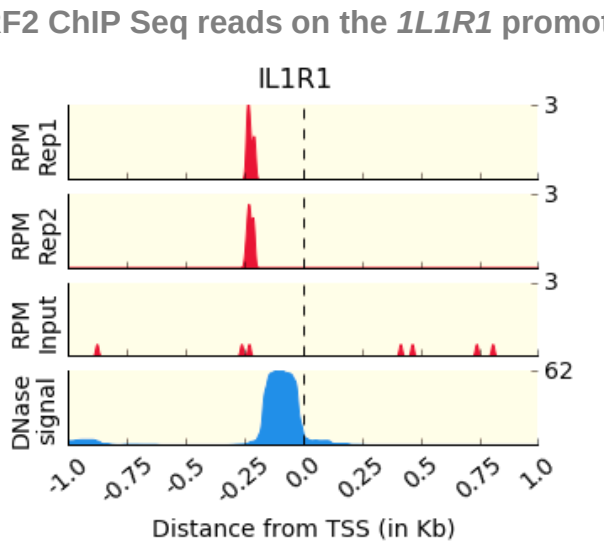

Supplementary Figure 2B:

Mapped reads on the *IL1R1* promoter for TRF2 ChIP-seq (Mukherjee et al, 2019) in HT1080 cells (replicate 1 and 2) and respective inputs for normalization; plotted using publicly available software IGV (Integrated Genomics viewer) with sequence alignment files.

Supplementary Figure 2C

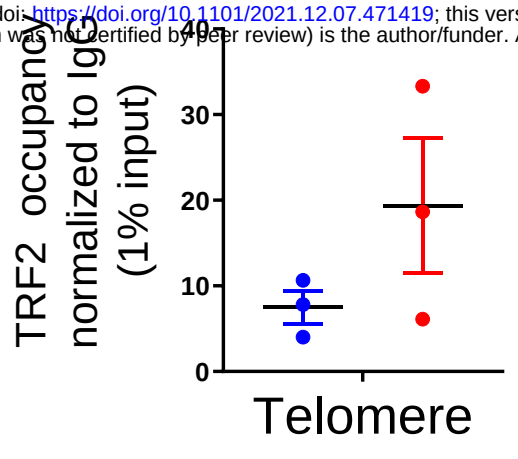

Supplementary Figure 2D

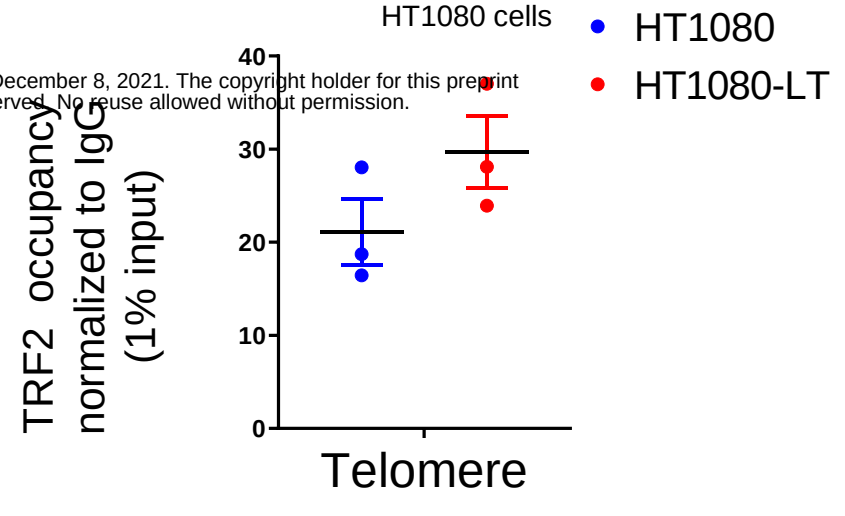

Supplementary Figure 2C-D:

TRF2 occupancy at telomeres following TRF2 ChIP in xenograft tumors (C) and ex-vivo cells in HT1080 or HT1080-LT cells (D).

Supplementary Figure 2E

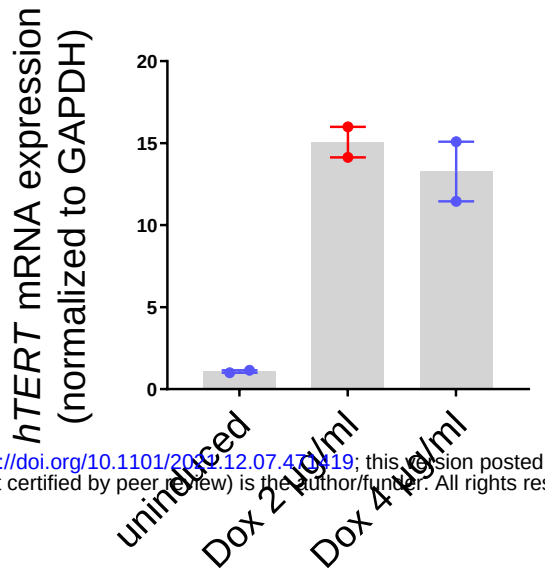

Supplementary Figure 2F

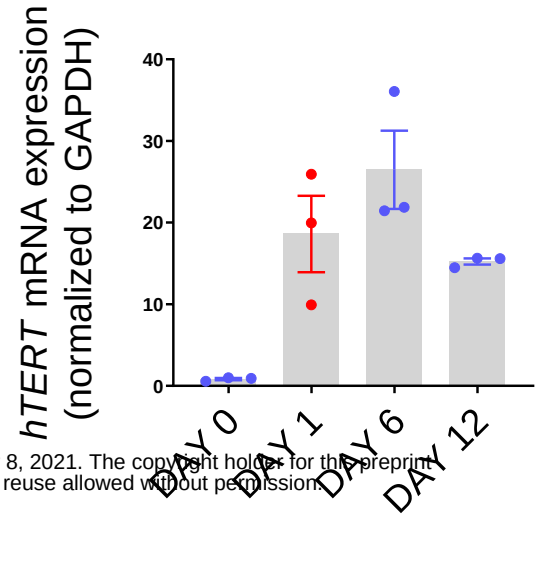

Supplementary Figure 2E-F:

hTERT mRNA expression in TERT-inducible HT1080 cells (see methods) with different concentrations of doxycycline (E) and at different days of induction (F). *GAPDH* was used for normalization.

Supplementary Figure 2G

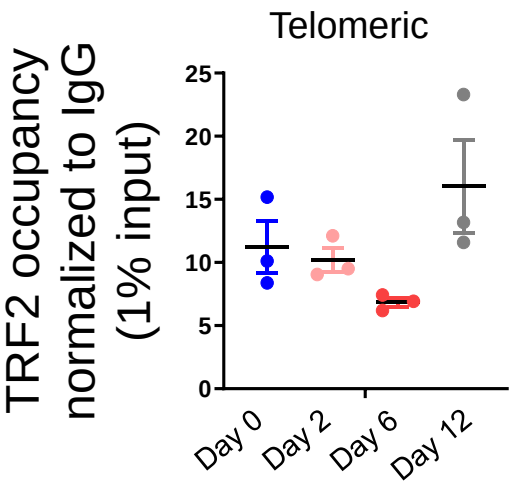

Supplementary Figure 2G:

TRF2 occupancy at telomeres following TRF2 ChIP in TERT-inducible HT1080 cells at different number of days of induction.

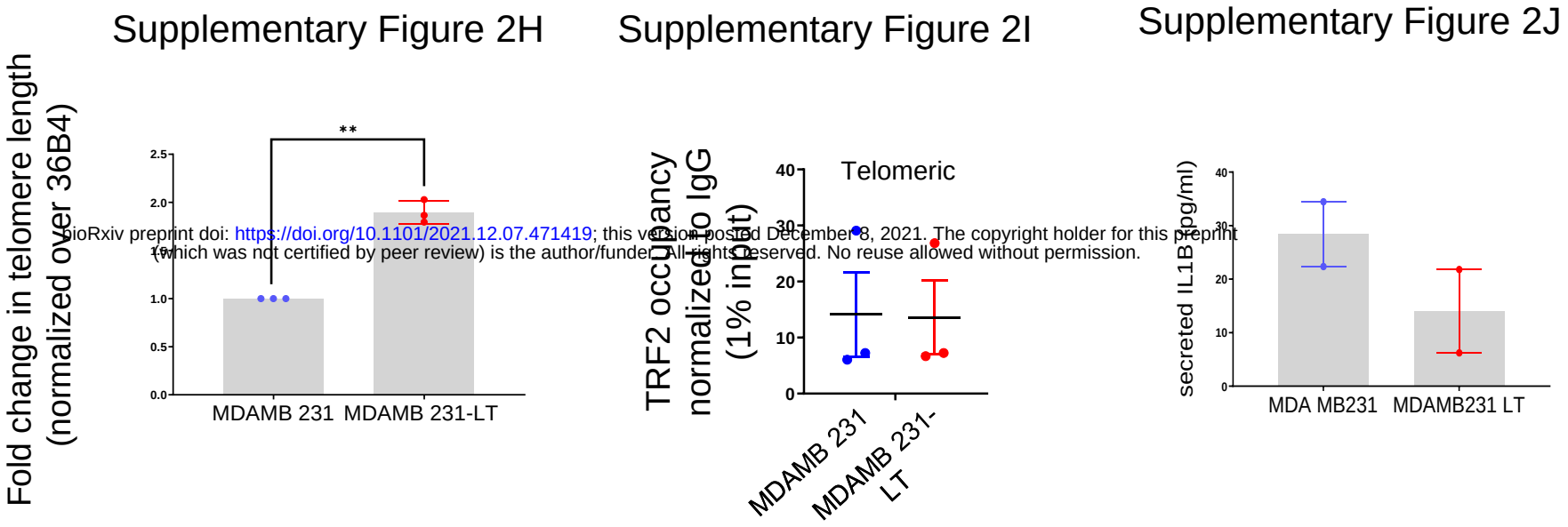

Supplementary Figure 2 H-J:
Relative telomere length by qRT-PCR (H); TRF2 occupancy at telomeres following TRF2 ChIP (I); and, secreted IL1B (ng/ml) (J) in MDAMB 231 or MDAMD231-LT cells in two independent experiments. Statistical significance using t-Test with Welch's correction (p values : * ≤ 0.05, ** ≤ 0.01, *** ≤ 0.001, **** ≤ 0.0001)

Supplementary Figure 3

Supplementary Figure 3A

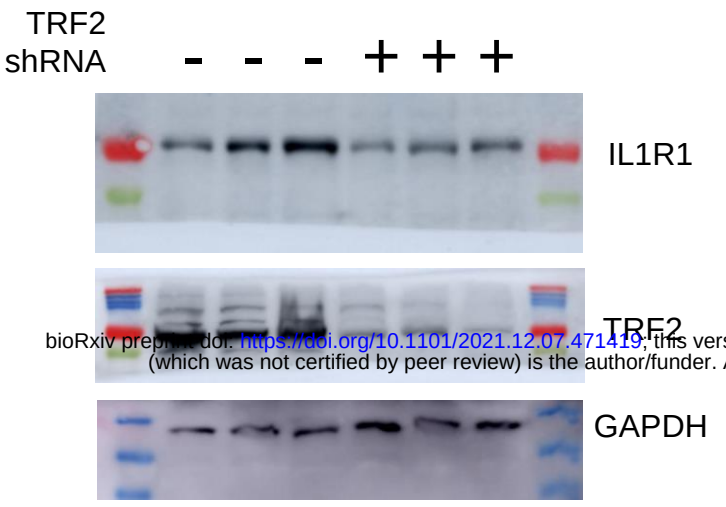

Supplementary Figure 3B

Supplementary Figure 3C

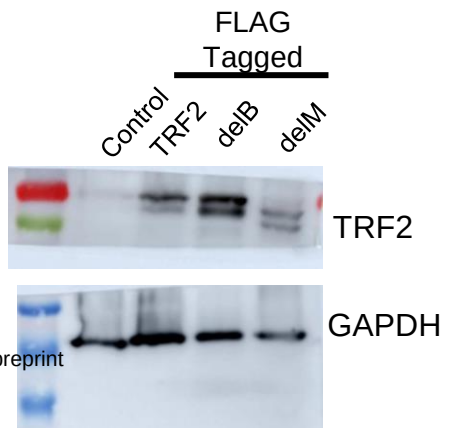

Supplementary Figure 3D

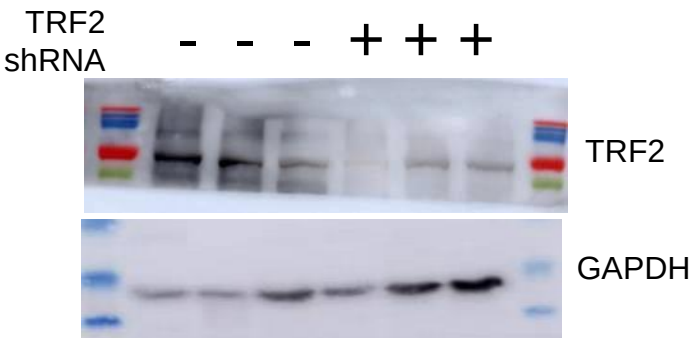

Supplementary Figure 3E

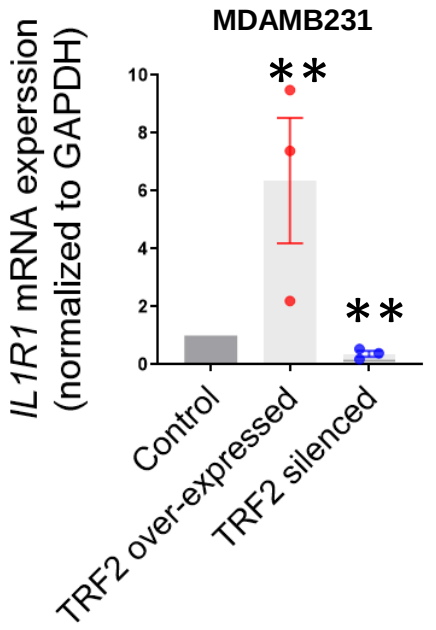

Supplementary Figure 3F

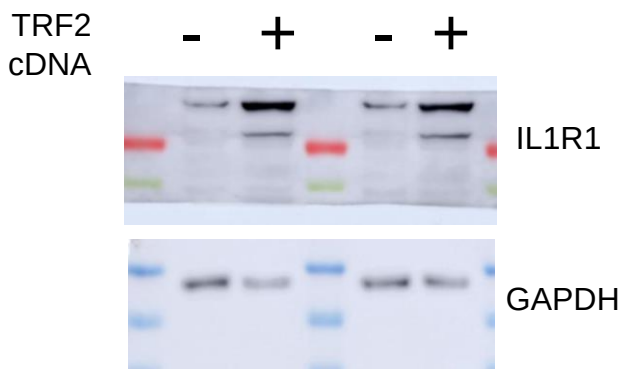

Supplementary Figure 3G

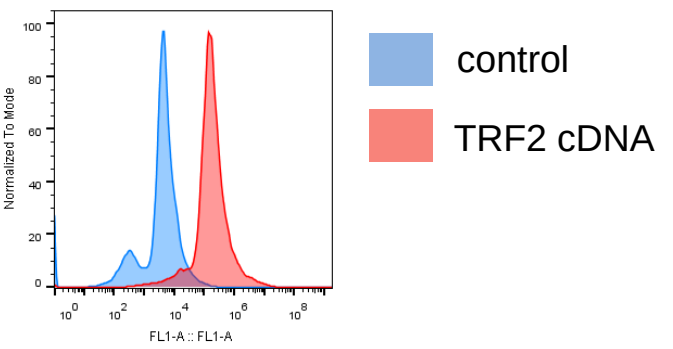

Supplementary Figure 3H

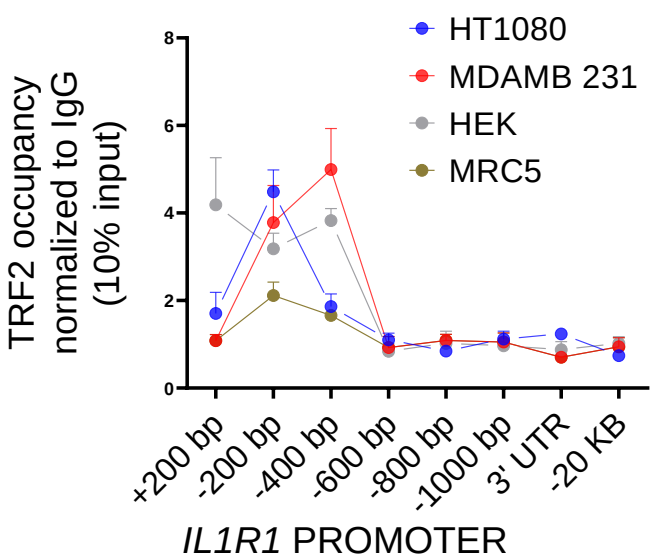

Supplementary Figure 3I

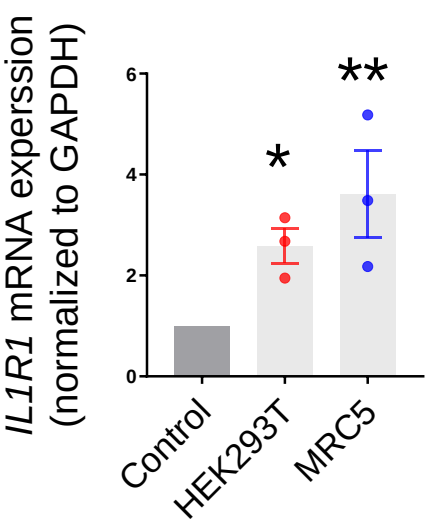

Supplementary Figure 3J

TRF2 ChIP-seq peak
chr2:102686361-102686875

5'-
CCTCCTTAAGTGAAAAATCTGTGAGGAGTTTTC
TATCTTTCTAAGTCTTTGTGGCACACTTATCACA
TGCATAGTACTATTTCTCAAGTTACCCAGGCAC
ACACAGATGTATGGCTTTCAGGAAGCCATACAT
CTGTGTAGCTCTGAGGCCCAGCCTTGTTCAACA
CTTCACTCAGAAGAATTGCTGGCCTGATGACCA
ACAATAATTGTCAACAACTTAAAACTTCATTGAC
GGCTCCTAAAAAAAATCAGTGTGCATGTGTGTG
TGTATGTGTGTGTGCGTGTGTGTGTGTGTGTGT
GTATGAGTGTGTGTATAACATTCATTACTGCAAA
CT**GG**AAT**GG**AGT**GGGG**CT**GG**AAGGCAGCCCA
GAAGCAAGGCTCAGAGCCTGGAGCTGCTGACC
TCTTGGGGACACTGCAGCCCTGGCCTGGCCTA
CTTTTCTCTTCTCCCATATCTGGAAAATGAAAGT
ACGCCTGAGGTATGGCAGCTCTTCACTTGTATCTTT
TCCAGCCATTGGCAGCTCTTCACTTGTATCTTT
CATATCAAAA – 3'

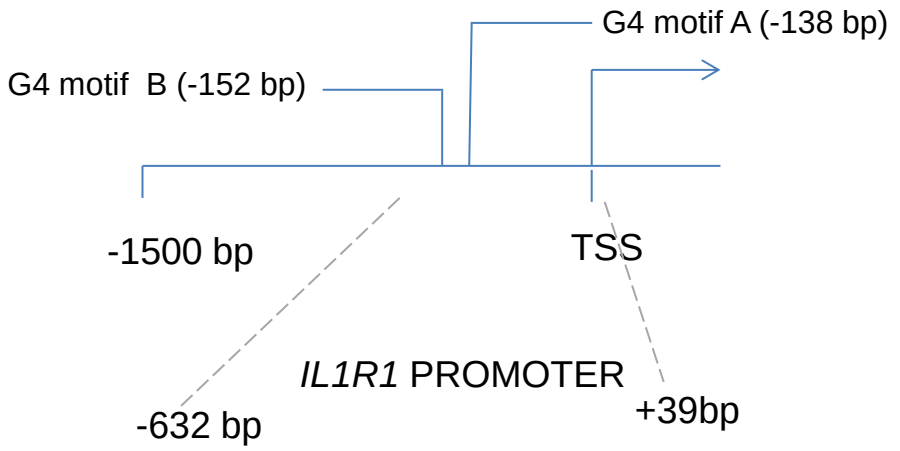

Supplementary Figure 3K

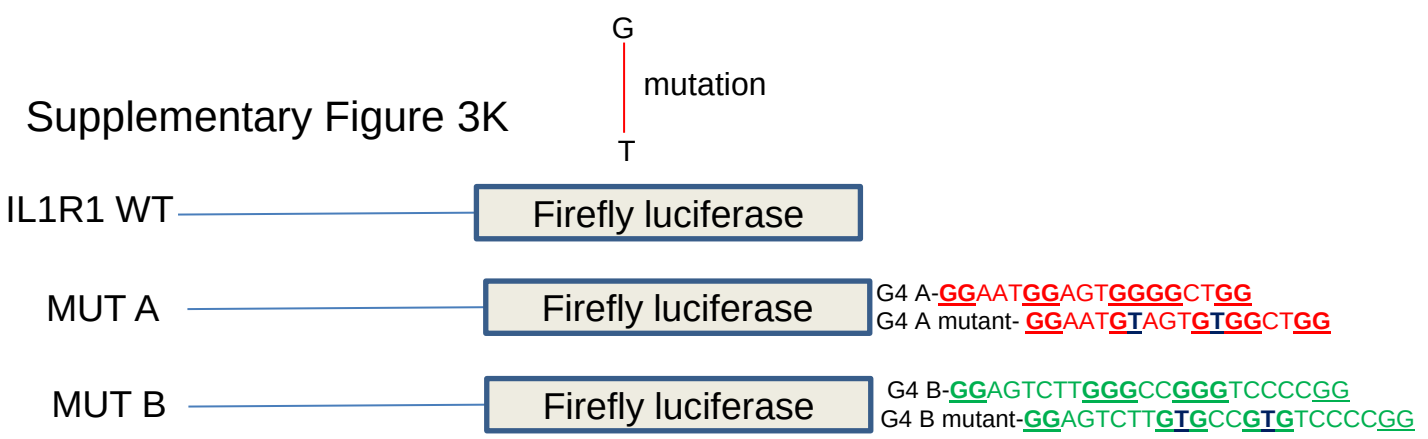

Supplementary Figure 3L

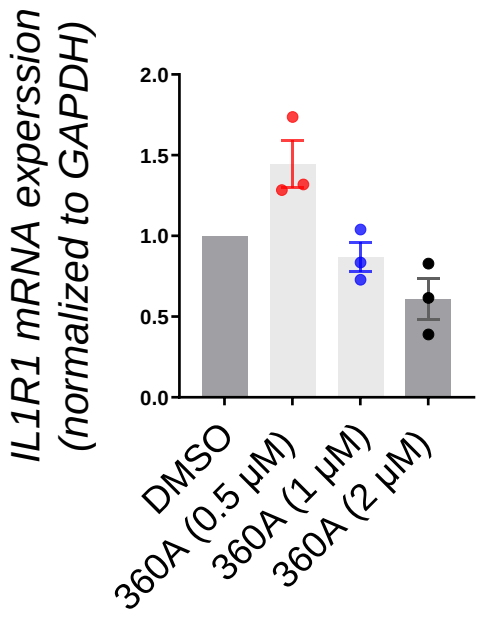

Supplementary Figure 3

A-C. TRF2 knockdown in HT1080 cells using TRF2-specific shRNA (A) and previously reported siRNA (B) following 48 hrs of transfection. Over-expression of TRF2 WT (flag-tag) and DNA-binding mutants, delB and delM in HT1080 cells following 48 hrs of transfection (C).
D. TRF2 knockdown in MDAMB231 cells using TRF2 specific shRNA post 48 hrs of transfection.
E. *IL1R1* mRNA expression in MDAMB231 cells post transfection of TRF2 WT cDNA (over-expression) and TRF2 shRNA (silencing) for 48 hrs. *GAPDH* was used as a normalizing control.
F-G. IL1R1 protein expression in MDAMB231 cells post TRF2 over-expression for 48 hrs by western blot (F) and immuno-flow cytometry (G).

H. TRF2 occupancy on the *IL1R1* promoter in HT1080, MDAMB231, HEK293T and MRC5 immortalized cells by Chromatin immunoprecipitation (ChIP) followed by qPCR. Primers spanning +200 to -1000 bp of TSS were used to check for TRF2 enrichment on the gene promoter. 3'UTR and -20 Kb upstream of TSS used as negative control for TRF2 binding; fold-change of occupancy was calculated over mock IgG after normalizing signal to 1% input.
I. *IL1R1* mRNA expression in HEK293T and MRC5 immortalized cells post transfection of TRF2 WT cDNA (over-expression) for 48 hrs. *GAPDH* was used as normalizing control.
J-K. G4 motifs (A and B) shown on the *IL1R1* promoter upstream of TSS and G4 disrupting mutations marked on the motifs.
L. *IL1R1* mRNA expression (normalized to *GAPDH*) in HT1080 cells following treatment with different concentrations of the G4 binding ligand 360A.

For assessment of statistical significance of independent repetitions of the same experiment , unpaired T test with Welsh's correction was performed for significance (p values : * ≤ 0.05, ** ≤ 0.01, *** ≤ 0.001, **** ≤ 0.0001). Error bar correspond to standard error of mean from three independent experiments unless N is stated otherwise.

Supplementary Figure 4

Supplementary Figure 4A

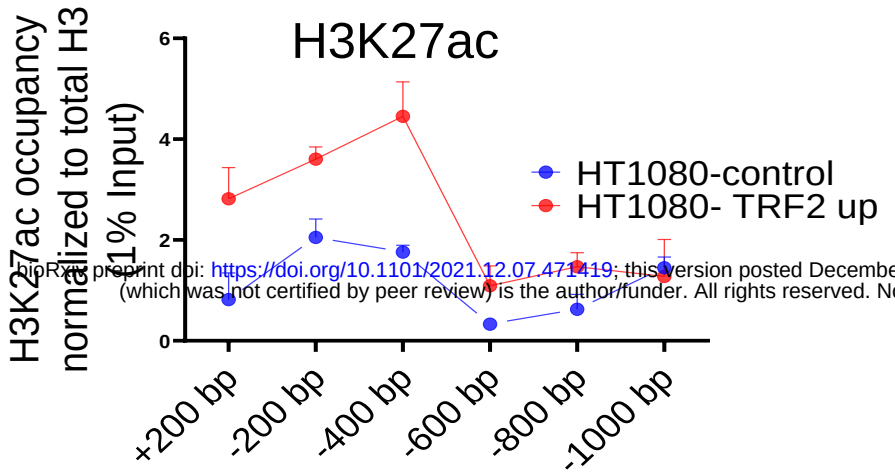

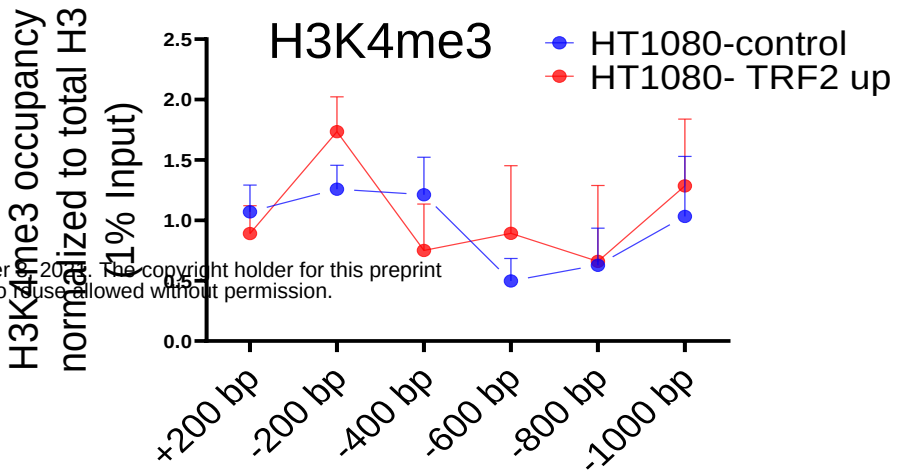

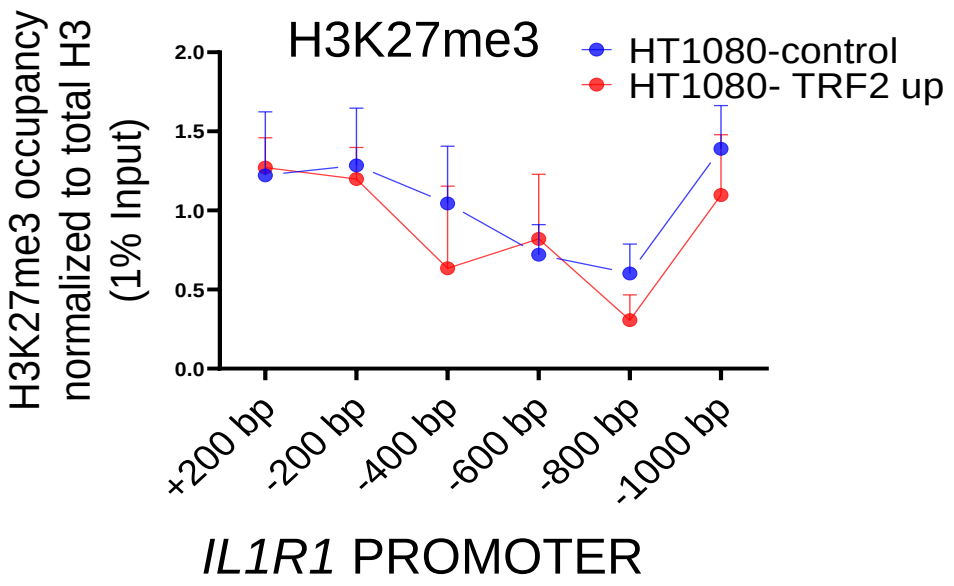

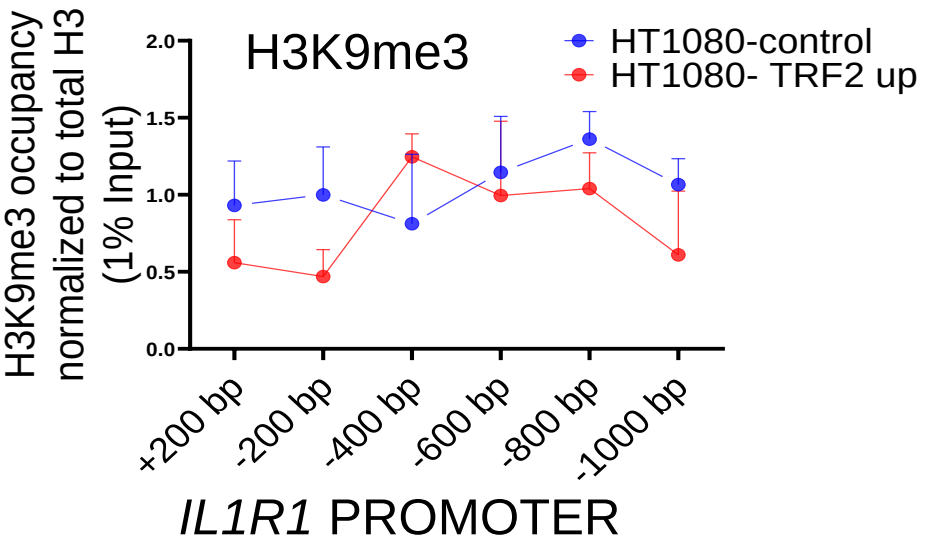

Supplementary Figure 4B

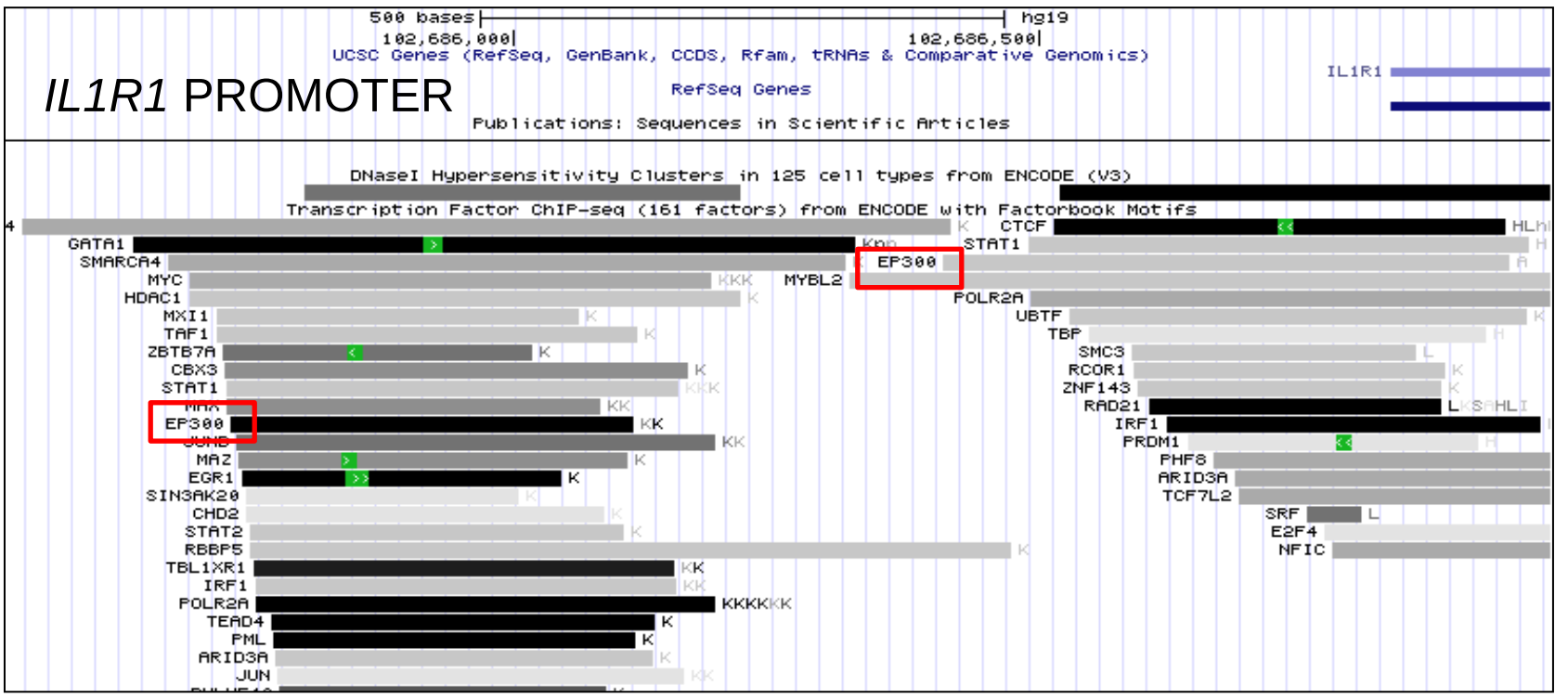

Supplementary Figure 4C

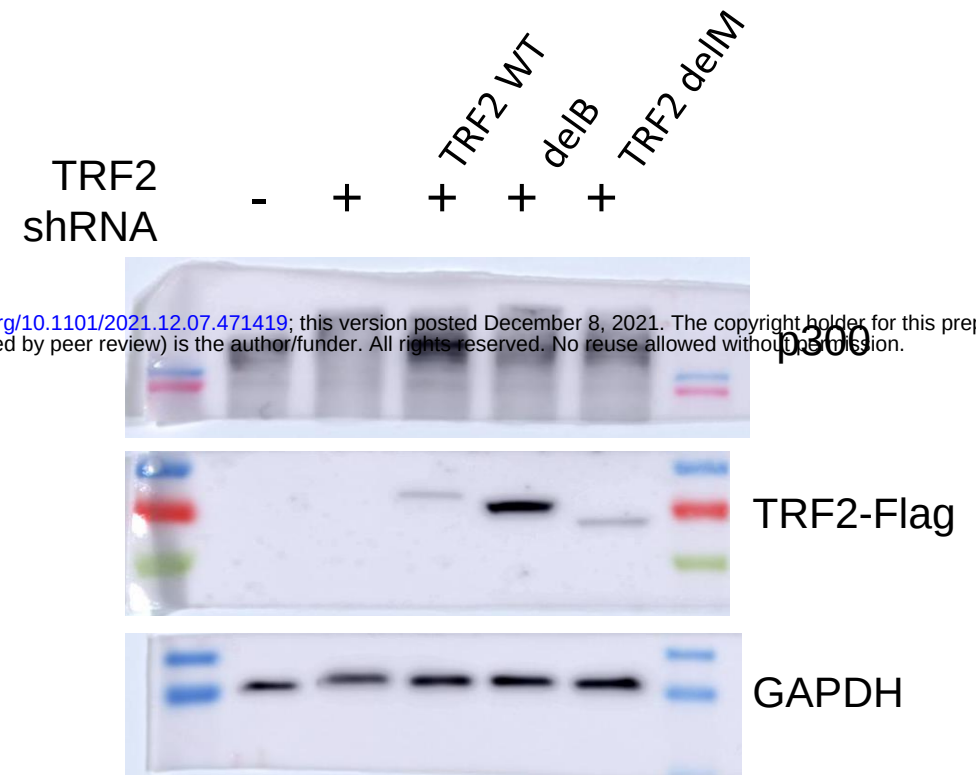

Supplementary Figure 4D

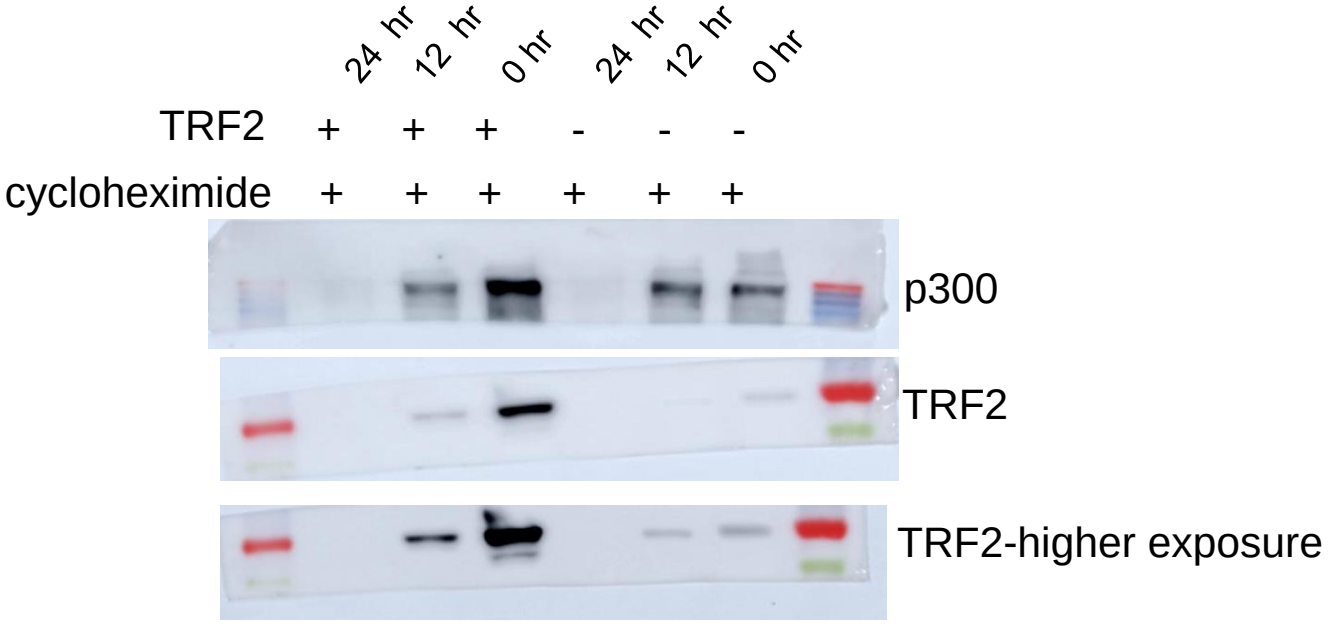

Supplementary Figure 4E

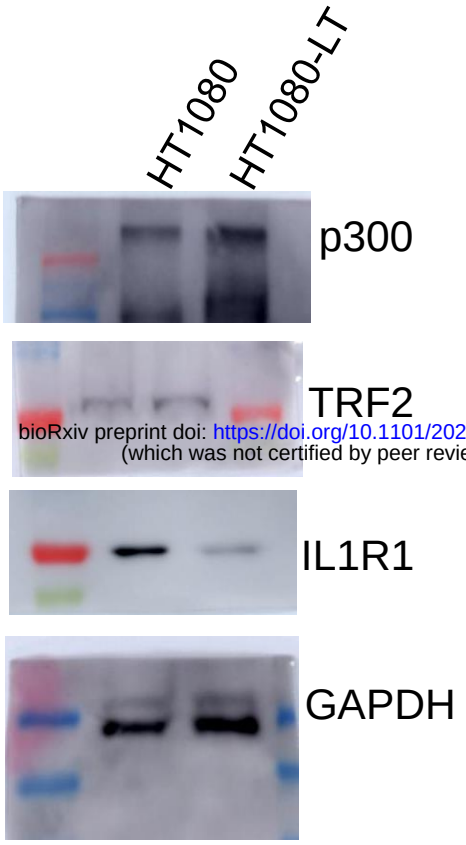

Supplementary Figure 4F

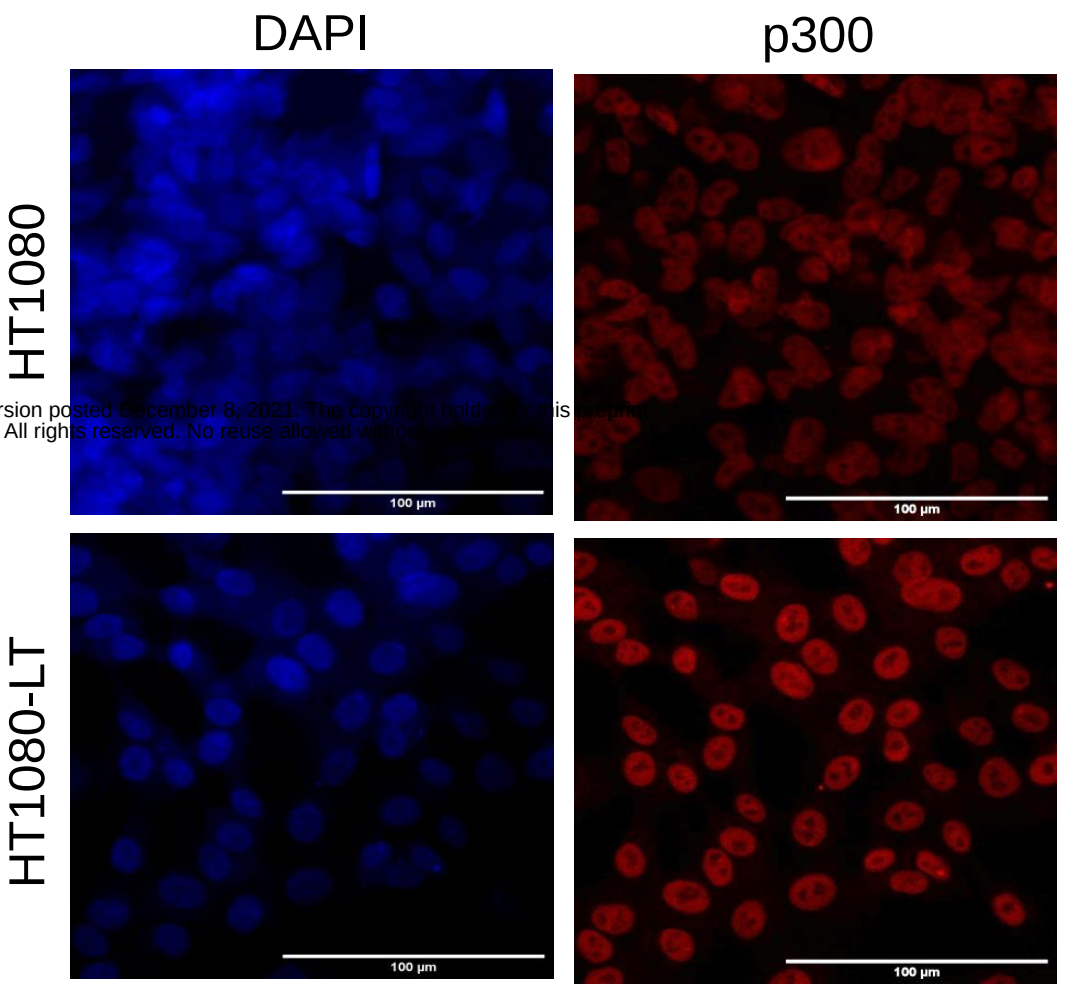

Supplementary Figure 4G

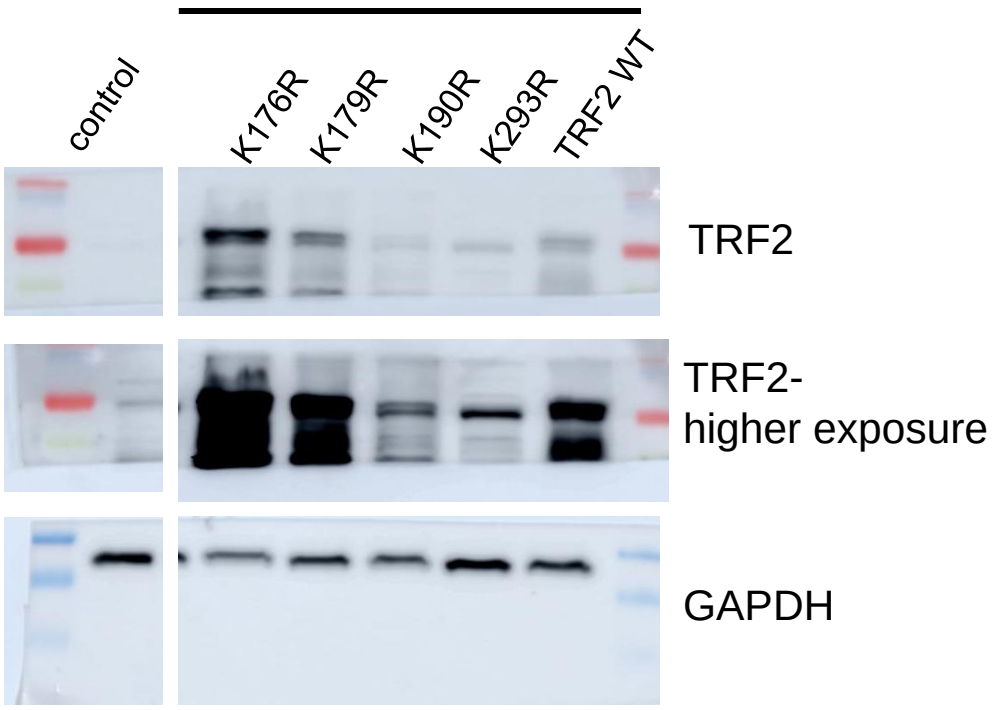

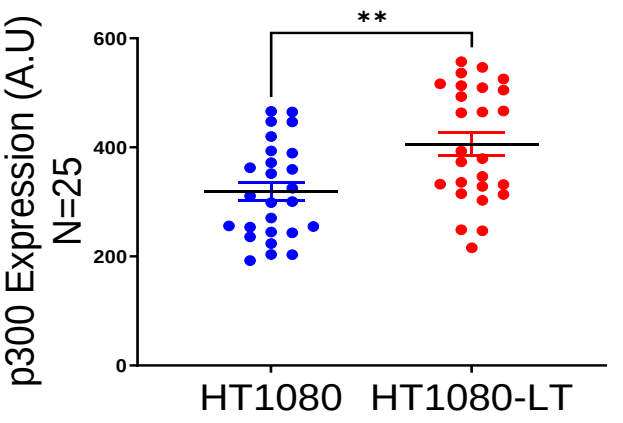

Supplementary Figure 4H

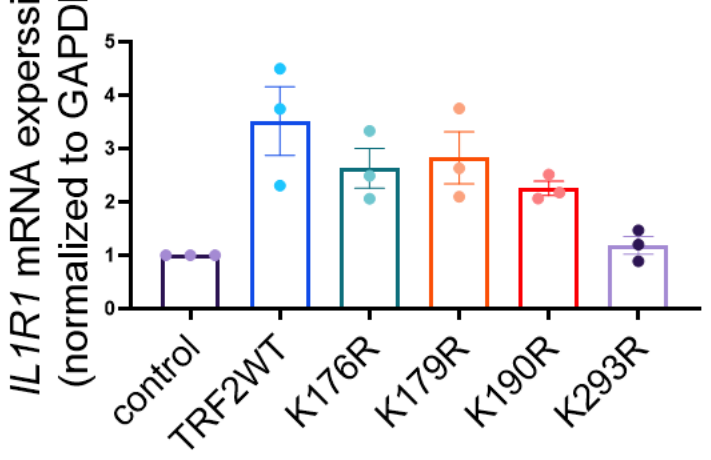

Supplementary Figure 4I

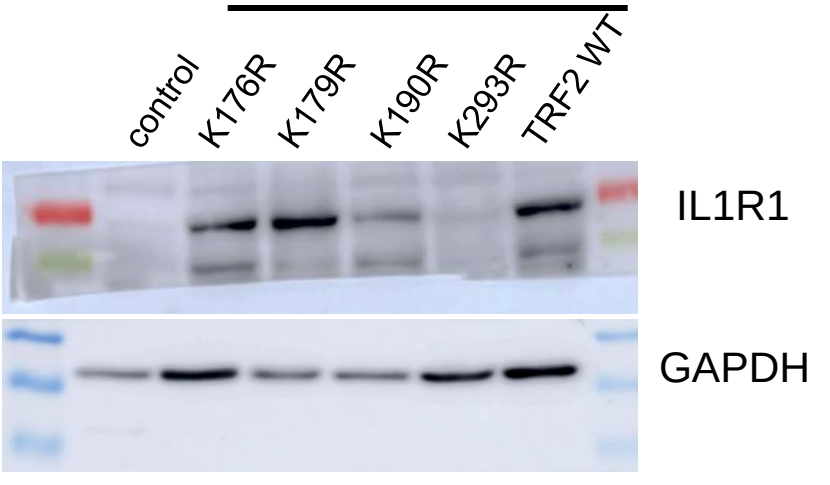

Supplementary Figure 4

A. Enrichment of histone marks H3K27ac, H3K4me3, H3K27me3, H3K9me3 (normalized to total H3) on the *IL1R1* promoter in HT1080 cells in TRF2 high (induced) condition and corresponding control cells.
B. ENCODE curated transcription factors/histone remodelers on the *IL1R1* proximal promoter (up to 1500 bp from TSS) across seven cell lines was plotted using UCSC genome browser hg19 human genome assembly. P300 marked in red box for the two sites of enrichment.
C. TRF2 WT or DNA binding mutants, delB or delM were transiently over-expressed in HT1080 cells in TRF2-silenced background; expression of TRF2 and respective mutants (probed by anti-flag antibody) and p300. GAPDH as used as loading control.
D. p300 levels in control and TRF2 induced condition following cycloheximide treatment at 0, 12 and 24 hrs.
E. p300, IL1R1 and TRF2 protein levels in HT1080 or HT1080-LT cells; GAPDH used as loading control.
F. Immunofluorescence microscopy for p300 in HT1080 or HT1080-LT cells. Mean p300 signal for 25 individual cells plotted in graph below.
G-I. TRF2 PTM mutants (K176R, K179R, K190R, K293R) and TRF2 WT transiently expressed and confirmed by TRF2 western (G); mRNA expression (normalized to *GAPDH*) (H) and protein levels for IL1R1 (I) in HT1080 cells after 48 hrs; GAPDH used as loading control in the western blots.

Statistical significance has been calculated using Mann-Whitney's non-parametric test for individual graphs where N≥5 . For assessment of statistical significance of independent repetitions of the same experiment , unpaired T test with Welsh's correction was performed for significance (p values : * ≤ 0.05, ** ≤ 0.01, *** ≤ 0.001, **** ≤ 0.0001). Error bar correspond to standard error of mean from three independent experiments unless N is stated otherwise.

Supplementary Figure 5

Supplementary Figure 5A

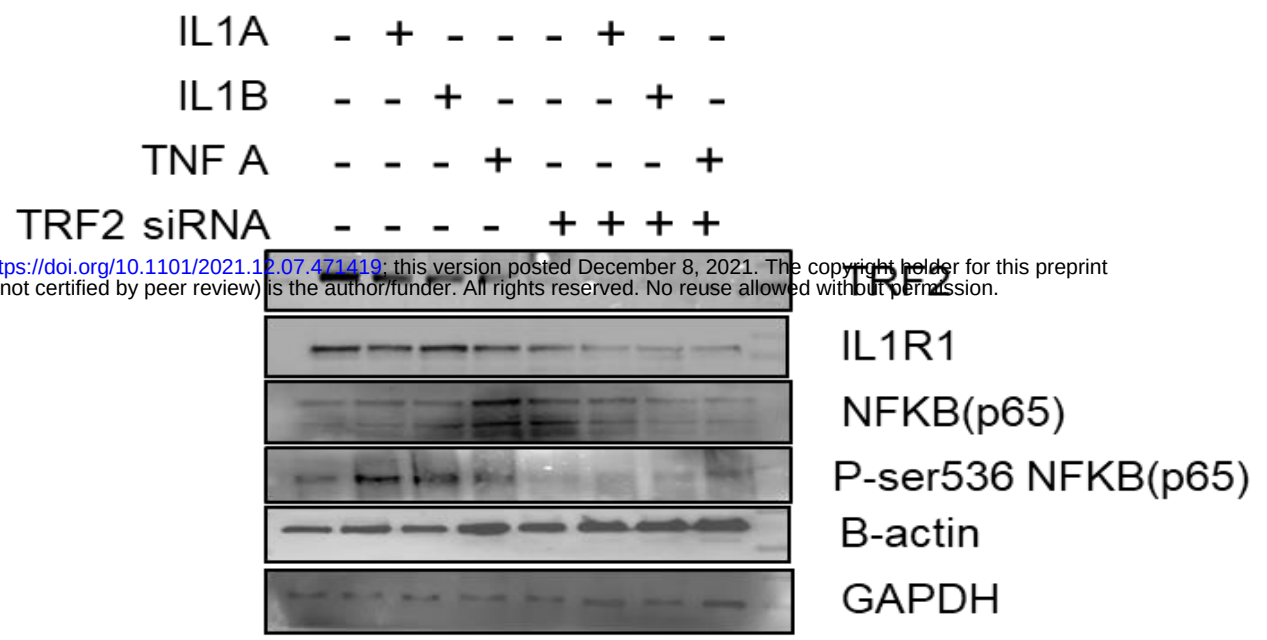

Supplementary Figure 5B

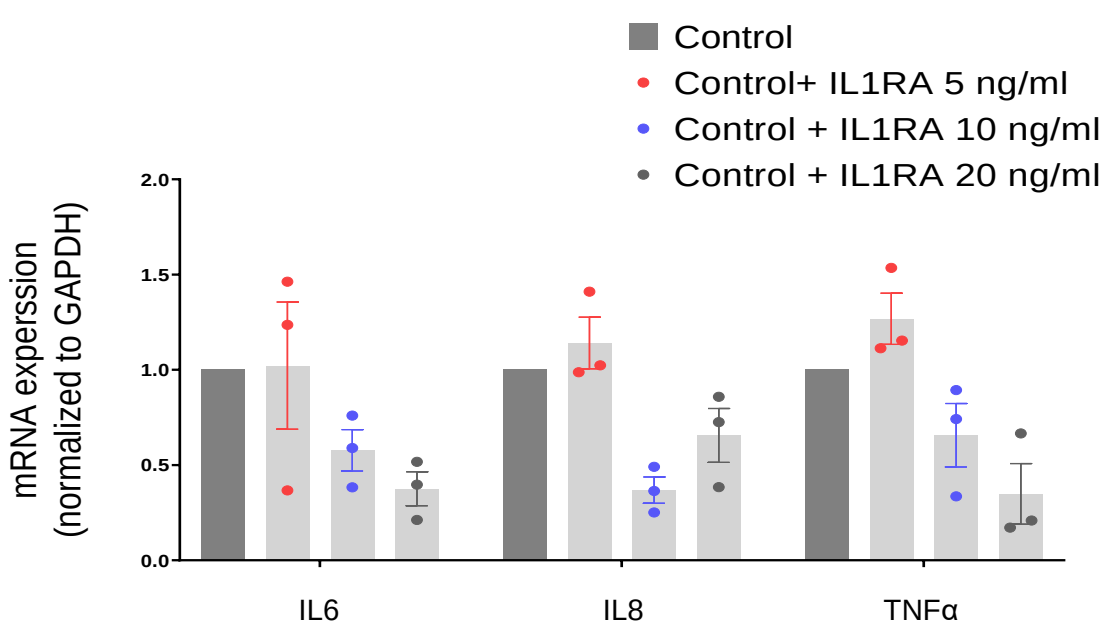

Supplementary Figure 5C

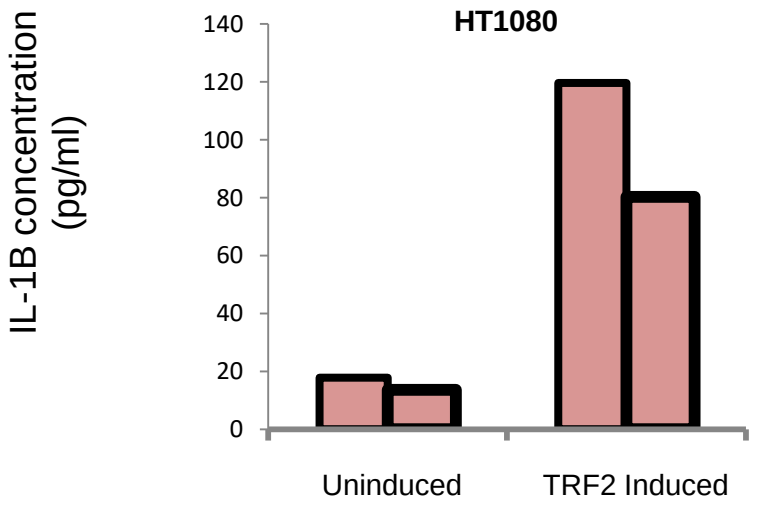

Supplementary Figure 5

A. HT1080 cells transiently transfected with TRF2 siRNA or scrambled control siRNA and treated with IL1A, IL1B or TNF-alpha (10 ng/ml respectively) after 48 hrs of transfection. IL1R1, TRF2, p65-Ser536 phosphorylation, total p65 and GAPDH (as loading control) probed by western blot following 3 hours of cytokine treatment.
B. p65 downstream targets: IL6, IL8 and TNF in HT1080 cells following treatment with IL1RA treatment (5,10 or 20 ng/ml) for 24 hrs. *GAPDH* was used as for normalization.
C. Secreted IL1B (pg/ml) in control or stable TRF2-expressing HT1080 cells in two independent replicates.

Supplementary Figure 6

Supplementary Figure 6A

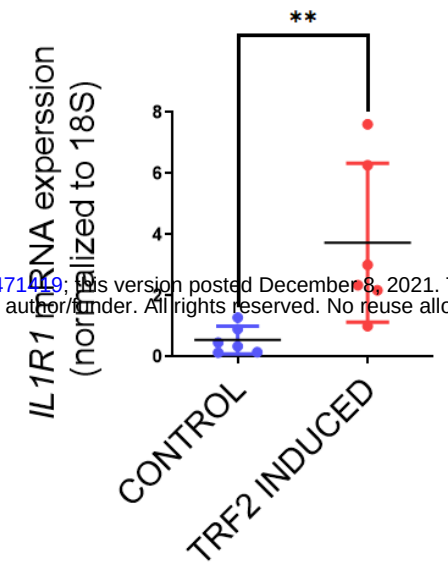

Supplementary Figure 6B

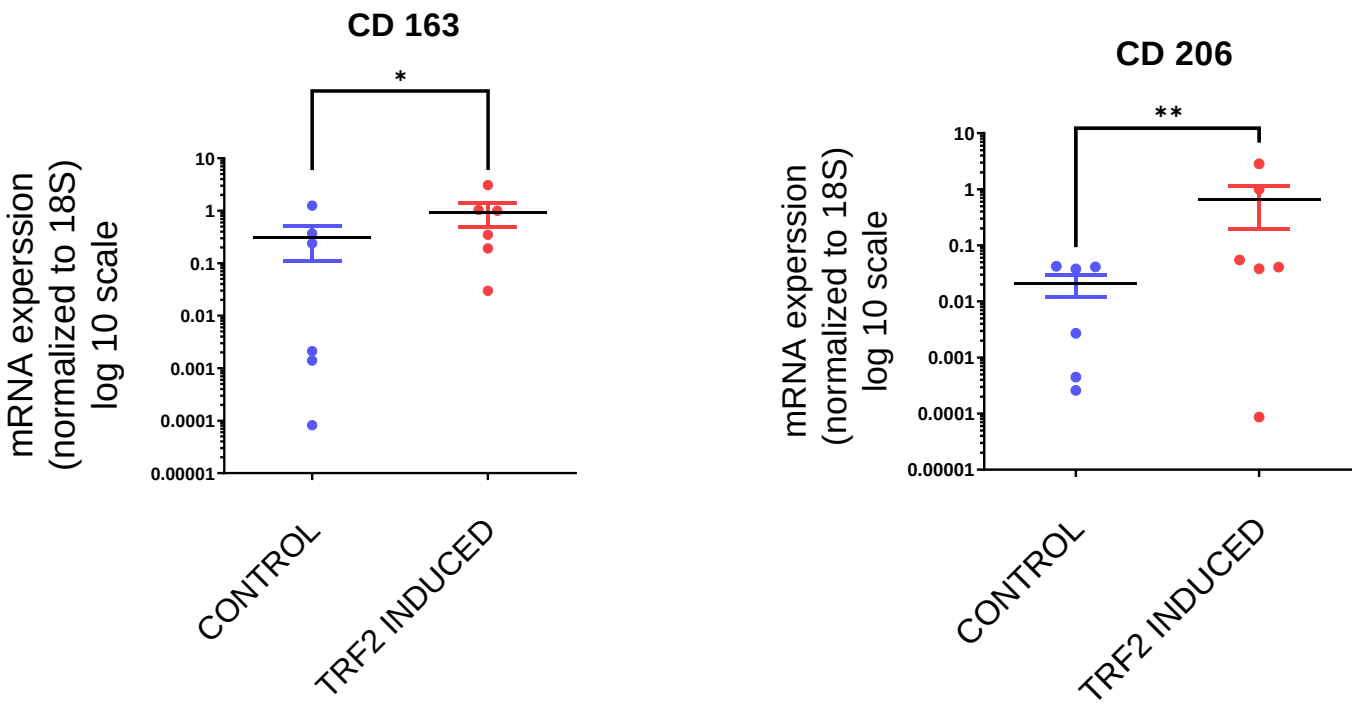

Supplementary Figure 6C

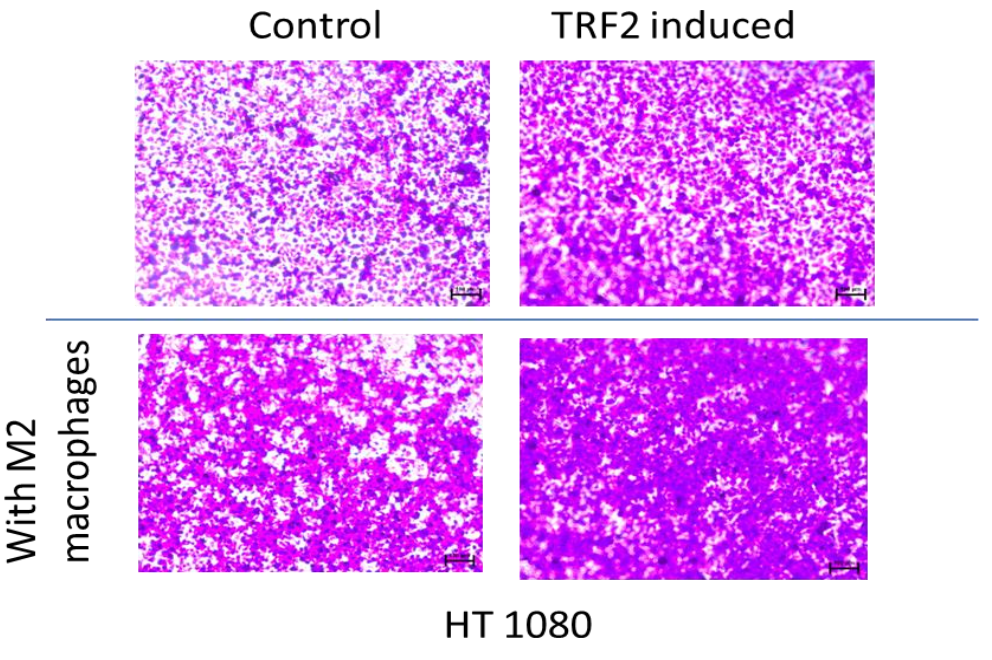

Supplementary Figure 6

A. mRNA expression of *IL1R1* in xenograft tumors (HT1080 control or HT1080-TRF2 induced); human *18S* was used for normalization.
B. mRNA expression of mouse M2 macrophage markers *CD163* and *CD206* in xenograft tumors (HT1080 control or HT1080-TRF2 induced); human *18S* was used for normalization.
C. Invasion assay in HT1080 control or TRF2-induced cells in presence/absence of THP1-derived M2 macrophages. Invaded HT1080 cells were stained for crystal violet stain for visualization.

Statistical significance has been calculated using Mann-Whitney's non-parametric test for individual graphs (p values : * ≤ 0.05, ** ≤ 0.01, *** ≤ 0.001, **** ≤ 0.0001)

Supplementary Figure 7

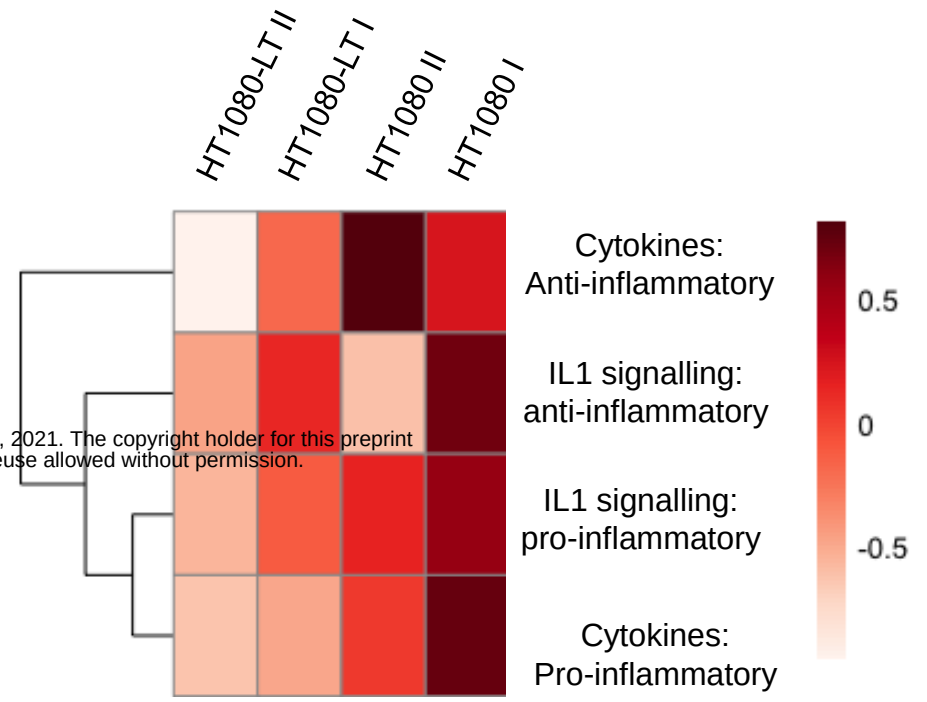

Supplementary Figure 7

Volcano plot for expressed genes in RNA-seq performed in HT1080 or HT1080-LT cells where the x-axis has log-2 fold change for genes and the y-axis represented in log-10 values for adjusted p values. Out of the 4315 differentially expressed genes, 2079 were upregulated in HT1080-LT cells (left). Gene set enrichment analysis on selected key IL1 signalling related (pro and anti-inflammatory) genes and key pro and anti inflammatory cytokines (right). Color key represents fold enrichment.